

STRUCTURAL DESIGN AND EXPERIMENTAL VERIFICATION OF A
FLAPPER MECHANISM COMPRISING PIEZOELECTRIC ACTUATOR

A THESIS SUBMITTED TO
THE GRADUATE SCHOOL OF NATURAL AND APPLIED SCIENCES
OF
MIDDLE EAST TECHNICAL UNIVERSITY

BY

İHSAN BURAK TEMELTÜRK

IN PARTIAL FULFILLMENT OF THE REQUIREMENTS
FOR
THE DEGREE OF MASTER OF SCIENCE
IN
AEROSPACE ENGINEERING

JANUARY 2018

Approval of the thesis:

**STRUCTURAL DESIGN AND EXPERIMENTAL VERIFICATION OF A
FLAPPER MECHANISM COMPRISING PIEZOELECTRIC ACTUATOR**

Submitted by **İHSAN BURAK TEMELTÜRK** in partial fulfillment of the requirements for the degree of **Master of Science in Aerospace Engineering, Middle East Technical University** by,

Prof. Dr. Gülbin Dural ÜNVER _____
Dean, Graduate School of **Natural and Applied Sciences**

Prof. Dr. Ozan TEKİNALP _____
Head of Department, **Aerospace Engineering**

Assoc. Prof. Dr. Melin ŞAHİN _____
Supervisor, **Aerospace Engineering Dept., METU**

Examining Committee Members

Prof. Dr. Yavuz YAMAN _____
Aerospace Engineering Dept., METU

Assoc. Prof. Dr. Melin ŞAHİN _____
Aerospace Engineering Dept., METU

Prof. Dr. Altan KAYRAN _____
Aerospace Engineering Dept., METU

Assist. Prof. Dr. Ali Türker KUTAY _____
Aerospace Engineering Dept., METU

Prof. Dr. Cihangir DURAN _____
Metallurgical and Materials Engineering Dept., YBU

Date: 26.01.2018

I hereby declare that all information in this document has been obtained and presented in accordance with academic rules and ethical conduct. I also declare that, as required by these rules and conduct, I have fully cited and referenced all material and results that are not original to this work.

Name, Last name : İhsan Burak
TEMELTÜRK

Signature :

ABSTRACT

STRUCTURAL DESIGN AND EXPERIMENTAL VERIFICATION OF A FLAPPER MECHANISM COMPRISING PIEZOELECTRIC ACTUATOR

TEMELTÜRK, BURAK İHSAN

M.S., Department of Aerospace Engineering

Supervisor: Assoc. Prof. Dr. Melin ŞAHİN

January 2018, 113 Pages

In this thesis study, torque motor of conventional two stage servovalves is investigated. Possible improvements for the first stage actuation system of servovalve are determined. It is aimed to design a new actuation system for replacing torque motor actuation system. The new system is met the performance criteria of torque motor on the high bandwidth and fast response characteristics. Amplified Piezo Actuator (APA) is designed with a new flapper mechanism to satisfy first stage of servovalve requirements. Subsequently, a new flapper mechanism design is optimized in terms of geometry and stiffness requirements by analyzing through the finite element analysis program.

A mathematical model of APA is developed based on experiments. In order to minimize the hysteresis error, a hysteresis compensator and Proportional-Integral controller is also designed. Controller coefficients and model parameters are then

optimized with the parameter optimization toolbox of MATLAB Simulink®. Moreover, a test structure with data acquisition system is built to measure the displacement of the actuator.

In order to investigate the performance of the system, a simulation is performed in MATLAB Simulink® environment. A prototype of the flapper mechanism test bench is manufactured and sub-systems and components of the system are tested to identify the model parameters. With this prototype, the model is verified by conducting tests on the actuator by open loop hysteresis compensator. A closed loop position test is also performed with the hysteresis compensator.

Various tests are repeated with the flapper mechanism in order to verify the performance of the whole system. A Bouc-Wen compensator and a Proportional-Integral (PI) controller are used to minimize the hysteresis for driving frequencies between 0.1 Hz and 10 Hz. The open loop charge amplifier test is performed to obtain the behavior of system for the driving frequencies higher than 10 Hz. This actuating system is also controlled using different control methods with 1% to 3% displacement hysteresis error.

As a conclusion, this thesis shows that a designed and an experimentally verified actuation system with a flapper mechanism employing a piezo actuator can be used as a torque motor of servovalves.

Keywords: Piezo Actuator, Flapper Mechanism, Position Control, Bouc-Wen Model, Hysteresis Compensator, Hybrid Design

ÖZ

BİR PİEZO EYLEYİCİ KİRİŞ MEKANİZMASININ YAPISAL TASARIMI VE TEST İLE DOĞRULANMASI

TEMELTÜRK, İHSAN BURAK

Yüksek Lisans, Havacılık ve Uzay Mühendisliği Bölümü

Tez Yöneticisi: Doç. Dr. Melin ŞAHİN

Ocak 2018, 113 Sayfa

Bu tez çalışmasında geleneksel iki kademeli tork motorlu servovalfler araştırıldı. Birince kademe eyleyici sisteminin iyileştirmeye açık olan özellikleri belirlendi.

Tork motor eyleyici sistemi yerine geçebilecek yeni bir eyleyici sistemi tasarlanması amaçlanmıştır. Yeni eyleyici sistemi, tork motorunun performans kriterlerini yüksek bant genişliği ve hızlı tepki karakteristiği ile sağlayacaktır. Kiriş kontrol mekanizma tasarımı, mekanik güçlendirilmiş piezo eyleyici (MGPE) ile servovalf birinci kademe gereksinimlerini karşılayacak şekilde yapılmıştır. Sonrasında, yeni kiriş mekanizması sonlu elemanlar analiz programında analiz edilerek geometri ve sertlik isterlerine göre eniyelenmiştir.

Piezo eyleyicinin deneysel tabanlı matematiksel modeli geliştirilmiştir. Histerezis hatasını en aza indirmek için, histerezis kompensatörü ve Orantılı-İntegral kontrolcüsü tasarlanmıştır. Denetleyici katsayıları ve model parametreleri,

MATLAB Simulink®'in parametre eniyileme araç kutusu ile eniyilenmiştir. Ayrıca, bir veri toplama sistemi ile birlikte test düzeneği de, eyleyicinin yer değiştirmesini ölçmek için kurulmuştur.

Sistemin performansını incelemek için MATLAB Simulink® ortamında bir benzetim gerçekleştirilmiştir. Sistemin alt sistemleri ve sistem bileşenleri ile model parametrelerini de tanımlamak için giriş mekanizmasının test prototipi üretilmiştir. Test prototipi ile tasarlanan benzetim, açık çevrimli histeresis kompensatörü ile eyleyicinin testleri gerçekleştirerek doğrulanmıştır. Histeresis kompensatör ve kapalı devre testi voltaj amfisi ile de gerçekleştirilmiştir.

Tüm sistemin performansını gözlemlemek için, testler, giriş mekanizması ile de tekrarlanmıştır. 0.1 Hz ile 10 Hz arasındaki sürücü frekanslarında histeresis etkisini azaltmak için Bouc-Wen kompensatör ve Orantılı-İntegral kontrolcü kullanılmıştır. Sistemin 10 Hz ve üzerindeki sürücü frekanslarında davranışını gözlemlemek için açık devre şarj yükselticisi testleri yapılmıştır. Bu eyleyici sistemi ayrıca değişik kontrol metodları kullanılarak, %1 ila %3 deplasman histeresis hatası ile kontrolde edilmiştir.

Sonuç olarak bu tez ile, tasarımı ve deneysel doğrulaması yapılmış giriş mekanizmalı bir piezo eyleyici sisteminin servovalflerin tork motorlarının yerine kullanılabilceği de gösterilmiştir.

Anahtar Kelimeler: Piezo Eyleyici, Giriş Kontrolü, Bouc-Wen Model, Histeresis Kompensatör Kontrol

to my family...

ACKNOWLEDGMENTS

I would like to express my sincere gratitude to my supervisor Assoc. Prof. Dr. Melin ŞAHİN for his supervision, guidance, advice and help provided throughout this study.

I wish to express to thank to Prof. Dr. Bülent Emre PLATİN for advice and help for this study.

I wish to express to thank to my manager Asli AKGÖZ BİNGÖL for giving me the opportunity to work with piezoelectric materials. I also thanks to my colleagues and friends who contributed this thesis by their understanding, patience and encouragement. I am thankful to K. Okan EYYÜPOĞLU for his efforts in the preparation of test equipment and his help with the test processes. I wish to express my appreciation to ROKETSAN Inc. for all facilities provided.

Mostly, I am grateful to my parents Hanife and Uğur and my dear sister Beyza for their support, confidence and encouragement they provided me not only throughout this thesis but throughout my life.

Finally, I would like to present my deepest thanks to my wife Duygu, for her love, invaluable support and understanding.

TABLE OF CONTENTS

ABSTRACT	v
ÖZ	vii
ACKNOWLEDGMENTS	x
TABLE OF CONTENTS	xi
LIST OF TABLES	xiii
LIST OF FIGURES	xiv
CHAPTERS	
1.INTRODUCTION	1
1.1Background and Motivation.....	1
1.2Objective of the Thesis.....	1
1.3Scope and Outline of the Thesis	2
1.4Assumptions Made and Limitations of the Study	4
2.A LITERATURE REVIEW ON PIEZOELECTRIC ACTUATOR AND CONVENTIONAL SERVOVALVE ACTUATION SYSTEMS	7
2.1Introduction	7
2.2Piezo Actuators	7
2.3Servovalve with Torque Motor Actuation Systems	13
2.4Design of a Flapper Mechanism with a Piezo Actuator.....	19
2.5Conclusion.....	21
3.ACTUATION SYSTEM DESIGN AND MODELING OF A PIEZO ACTUATOR WITH FLAPPER MECHANISM.....	23
3.1Introduction	23
3.2Design Considerations and Performance Criteria of Actuation System	24
3.3System Design of an Actuation System	26
3.4Mathematical Model of Actuation System.....	27
3.4.1 APA Mathematical Modelling.....	27
3.4.2 FEM of the APA	34

3.4.3 Bouc-Wen Hysteresis Model of Actuation System.....	38
3.4.4 System Equation of Actuation System.....	40
3.4.5 Inverse Hysteresis Model of Actuation System	45
3.5 Mechanical Design of Actuation System.....	48
3.5.1 Flapper Design without Flexible Part Assembly.....	49
3.5.2 Flapper Design with Flexible Part Assembly.....	52
3.6 Electrical Design of Data Acquisition System.....	57
3.7 Controller Design of Actuation System.....	61
3.8 Conclusion	67
4. PERFORMANCE TESTS OF PIEZO SYSTEM.....	69
4.1. Introduction.....	69
4.2. Piezo Actuator Characterization Tests.....	69
4.3. Position Test with Flapper Mechanism.....	80
4.4. Step and Chirp Tests	91
4.5. Conclusion	94
5. SUMMARY AND CONCLUSIONS	95
5.1 Summary and Discussions	95
5.2 General Conclusions	96
5.3 Recommendations for Future Work.....	97
REFERENCES	99
APPENDICES	
APPENDIX A.....	105
APPENDIX B.....	107
APPENDIX C.....	111
APPENDIX D.....	113

LIST OF TABLES

TABLES

Table 1: Comparison of PZT Ceramics [8]	10
Table 2: Properties of Piezo active materials [9].....	10
Table 3: Valve Designs in 1955 [21].....	18
Table 4: Comparison APA and Torque Motor	20
Table 5: Design Specifications	24
Table 6: CEDRAT APA 60SM's Standard Properties	25
Table 7: Desired Step and Frequency Response Characteristics.....	26
Table 8: APA60SM Properties	29
Table 9 Parameters of APA	33
Table 10: Finite Element Results.....	38
Table 11: Used Parameters	42
Table 12: Estimated Parameters	45
Table 13: Parameters in Calculation.....	49
Table 14: Parameters of the Designed Flapper.....	52
Table 15: Used Bouc-Wen Parameters.....	72
Table 16: Close Loop Test Scenarios	87
Table 17: Charge Amplifier Test Scenarios	89

LIST OF FIGURES

FIGURES

Figure 1: Examples of Piezo Actuators	12
Figure 2: Comparison of Maximum Displacements and Forces of Some Linear Actuators [15].....	13
Figure 3: Nozzle-Flapper First Stage Components [17]	14
Figure 4: Flapper Nozzle Types of Servovalve [18]	15
Figure 5: Single-nozzle Two-stage Servovalve [18].....	17
Figure 6: APA	25
Figure 7: Basic Sketch of the Flapper Structure.....	27
Figure 8: Piezo Materials [9].....	28
Figure 9: Amplified Mechanism of Actuator	30
Figure 10: Amplified Mechanism Geometry (a) with no Fillet, (b) with Fillet	31
Figure 11: Polarization Direction of the Piezo Materials.....	35
Figure 12: APA's Displacement (mm) Fixed-Free Under Applied 150V	36
Figure 13: APA's Displacement (mm) Fixed-Fixed Under Applied 150V	37
Figure 14: Mode Shape of the APA at its Fundamental Natural Frequency by FEA	37
Figure 15: Simulink® Model of Piezo Actuator	39

Figure 16: Simulink® Model of Bouc-Wen Model.....	40
Figure 17: Simulink® Model of Piezo Actuator	42
Figure 18: Simulink® Model of Estimation Toolbox	43
Figure 19: Trajectories of Parameters.....	44
Figure 20: Parameter Optimization Setting	44
Figure 21: Bouc-Wen Hysteresis Compensator	45
Figure 22: Simulation and Experiment Results	46
Figure 23: Output of Hysteresis Compensator	47
Figure 24: Sub Model of System	47
Figure 25: Section View of Piezo-Flapper Systems	48
Figure 26: One of Flapper Nozzle Type Valve's Flapper	49
Figure 27: Bending Model [26]	50
Figure 28: Linear Model [26]	50
Figure 29: Technical Drawing of the Flapper Mechanism	52
Figure 30: Test Setup.....	54
Figure 31: Flapper Displacement in Actuator by FEA	55
Figure 32: Critical Von Misses on Parts by FEA	56
Figure 34: Flexible Flapper Mechanism Prototype	56
Figure 35: LA75C Specification [13].....	57

Figure 36: The Working Principle of Sensor [30].....	59
Figure 37: National Instruments Compact RIO 9063 Chassis [31].....	60
Figure 38: The Schematic Diagram of the System [13].....	61
Figure 39: Process Flow Diagram	62
Figure 40: Input [V] and Output Signal [μm] Power Spectral Density.....	63
Figure 41: Simulink® Model of the Closed Loop System.....	64
Figure 42: Simulink® Model of the Compensator and Closed Loop Hybrid System	64
Figure 43: The Target Time Response Characteristics	65
Figure 44: Response Optimization Result in Frequency Domain	66
Figure 45: Time Response Result with the Chosen Proportional Controller	67
Figure 46: Simulink® Model of Piezo Actuator	70
Figure 47: Piezo Actuator Test Setup.....	71
Figure 48: Hysteresis by Simulation & Experiment with Sine Input.....	73
Figure 49: The 0.05 Hz Sine Signal Simulation and Experiment Difference	74
Figure 50: The 0.1 Hz Sine Signal Simulation and Experiment Difference	74
Figure 51: The 0.5 Hz Sine Signal Simulation and Experiment Difference	75
Figure 52: The 1 Hz Sine Signal Simulation and Experiment Difference	76
Figure 53: Hysteresis by Simulation & Experiment with Triangle Input	77
Figure 54: The 0.05 Hz Triangle Signal Simulation and Experiment Difference..	78

Figure 55: The 0.1 Hz Triangle Signal Simulation and Experiment Difference ...	78
Figure 56: The 0.5 Hz Triangle Signal Simulation and Experiment Difference ...	79
Figure 57: 1 Hz Triangle Signal Simulation and Experiment Difference	80
Figure 58: Piezo Characterization Test Setup	81
Figure 59: Assembling Structure	82
Figure 60: The Input Signal	83
Figure 61: Displacement of Flapper	84
Figure 62: Displacement of Flapper with PI Controller	85
Figure 63: Displacement of the tip of the Flapper with PI Controller.....	85
Figure 64: Flapper Test Performed at 0.05 Hz	87
Figure 65: Flapper Test Performed at 1 Hz	88
Figure 66: Flapper Test Performed at 10 Hz	88
Figure 67: Flapper Test Performed at 1 Hz via Charge Amplifier	90
Figure 68: Flapper Test Performed at 10 Hz via Charge Amplifier	90
Figure 69: Flapper Test Performed at 100 Hz via Charge Amplifier	91
Figure 70: Step Response of the Prototype with $K_p=250 \text{ V}/\mu\text{m}$	92
Figure 71: Magnitude and Phase Response of the Flapper with APA	93

CHAPTER 1

INTRODUCTION

1.1 Background and Motivation

A servovalve (SV) is a device that is used to control of the fluid flow in hydraulic power systems. There are several types of servovalves which are used as a sub-component in hydraulic systems. Their main function is basically to direct the hydraulic flow with the aid an actuator consuming low power consumption. On the other hand, piezo materials are smart materials and frequently used in several actuation systems. They can be used for different purposes such as actuation, sensing, and energy harvesting. Due to their low weight to size advantage and high natural frequencies, they are also used as the critical parts in space vehicles and aerospace structures. Additionally, piezo actuators are also preferable in aerospace structures in order to get quick reactions in short times and high bandwidth. Therefore, piezo actuators seem to be appropriate for the replacement of the actuation system of a servovalve. They are easy to be supplied and fast response makes them a good candidate for the development and the verification of a flapper mechanism.

1.2 Objective of the Thesis

This study has two main objectives; namely, the development of the flapper mechanism with a piezo actuator and the verification of its model via some experiments.

The development of a flapper mechanism includes manufacturing of the flapper beams with embedded beam with a flexural part. This part allows a bending motion to the flapper. Assembling of a flapper mechanism to a piezo actuator should be performed with several precautions. The development of this system also includes setting up a data acquisition system with laser sensors.

The experimental verification of the developed mathematical model consists of two tests; namely, the position and the ramp responses. Baseline analytical and finite element models (FEM) are created. Through the finite element analyses (FEA), the displacement of actuator along thickness of mechanical flexure is optimized. Then, a full model is developed for the desired displacement concerned for boundary condition with materials properties.

According to the expected displacement obtained from FEA, the accuracy of the displacement of the embedded flapper is checked with respect to the experimental based mathematical model. Mathematical parameters are also optimized to meet design requirements. Therefore, this objective is verified by experiments whether all sensors provide reliable data with acceptable accuracy. If the mathematical model and the experimental results satisfy the design criteria, the system is shown to be working correctly and be appropriate for the replacement of a torque motor of a servovalve.

1.3 Scope and Outline of the Thesis

The thesis is organized as five chapters and their contents are summarized as follows.

In Chapter 2, piezo materials and servovalve are introduced. Firstly, the piezoelectric materials and the conventional concepts of the servovalve systems and its development are discussed. The features of piezo which has strengths and weaknesses and its products that are designed from such sensors and actuators are presented. Also, the areas of usage especially in smart structures are focused on.

Secondly, conventional two stage servovalve with torque motor is also introduced as the literature has lots of applications such as flight control actuation systems. Moreover, the basic information of the hydraulic control techniques with servovalve is presented. Examples of different applications containing servovalve are shown a. A brief comparison is made; the strengths and the weaknesses of piezo actuator with valve regarding open and close control methods are mentioned.

In Chapter 3, the design requirement is provided. The flapper mechanism with the APA is designed regarding given requirements. Final design is modelled both analytically and by using the finite element software. In order to find the FEA of the selected piezo actuator, the parametric FEM is made. The parameters of piezo actuator are tuned to the actuator's producer catalog. The required design parameters of the flapper mechanism is designated according to satisfy the performance criteria of the available torque motor. Mechanical design is optimized by considering the strength of the material and its producibility. These results are illustrated in this chapter as well. Also, system architecture is defined and a detailed description of the mechanical design process of the prototype is given. Selection of the prototype components is explained. Then, the hysteresis which is a nonlinear term is obtained and a simulation model is developed in MATLAB Simulink® environment. The unknown system parameters are experimentally identified and the mathematical model is then validated with the test results. According to the system performance criteria, the piezo actuator's response time and the system bandwidth are important requirements. Therefore a controller namely; a controller in time domain to satisfy the actuator speeds as well as a controller in frequency domain to satisfy the system bandwidth is designed.

In Chapter 4, APA is experimentally verified to mathematical model and then the system prototype is then tested according to requirements. The results are then compared with the ones obtained from simulation.

In Chapter 5, the complete study is summarized. The conclusions of this study and the outcomes of thesis work are declared. Besides, the recommendations for the future work are provided and the similar applications are also discussed.

1.4 Assumptions Made and Limitations of the Study

The list below gives all assumptions made and limitations of the thesis:

- A laser sensor is used to measure displacement of the flapper mechanism. The mechanical mounting of laser sensor to test setup, assembling procedure is important. The sensor has a mechanical mounting direction for collecting the accurate data. For instance, the orientation of the laser must be perpendicular to the measured distance. If the laser beam has some misalignments, output of the measurement has nonlinearities due to mounting inaccuracies. In test set up, the mechanical interface of laser is observed to have production mistakes. Due to the mistake, the orientations misalignment of laser sensor can cause the non-linear behavior during data acquisition. The mounting of sensor is optimized by mechanical shims and it is assumed to be perfect. The difference between manufacturer catalog and experiment is lower than 0.3% and is neglected in all calculations.
- The sampling frequency of the laser sensor is limited to 1000 Hz for the position tests. It is chosen considering the maximum interest of frequency in order to prevent aliasing.
- Position tests are one direction output tests. The twist angle of flapper and the strain data under torsion loading due to the misalignment of mounting actuator is out of concern. Other direction of motion is beyond the scope.
- The experiment is conducted by piezo amplifier which has low current output. The results of the experiment can be developed by using piezo amplifier which supplies the required current output.

- Temperature dependence of the Young's modulus of steel and copper that used is neglected.
- Self-heating effect of piezo actuator which occurs under high dynamic condition for a long time is ignored.
- In FEM, the material properties of the piezo materials are taken as orthotropic.
- It is assumed that the installed embedded strain gauge sensors do not affect the response of piezo actuator and thus FEM does not include the modelling of the embedded strain gauge sensors.
- Mathematical model including nonlinear terms are linearized to get transfer function for the controller optimization.

CHAPTER 2

A LITERATURE REVIEW ON PIEZOELECTRIC ACTUATOR AND CONVENTIONAL SERVOVALVE ACTUATION SYSTEMS

2.1 Introduction

In this chapter, an introduction to piezoelectric materials and control valves are provided through a literature review. The conventional control actuation systems of servovalve such as torque motor actuators are mainly discussed. The innovative control actuation system concept such as a piezo actuation is introduced and forms of mechanic actuation are detailed. The main focus of this research is the presentation of a hydraulic valve with mechanical APA for high bandwidth, fast response and easy installation.

2.2 Piezo Actuators

To begin with the name of piezoelectric is composed of the combination of these two words: piezo means 'press' in Greek and electric comes from electricity. It can be termed as pressure-electric effect. The piezoelectric effect is classified as direct and indirect. In 'the direct piezoelectric effect', strain develops a charge in the piezoelectric material. The indirect piezoelectric effect is explained the development of a charge creates a change in the mechanical dimensions or strain [1].

Piezoelectric has an important role in the development of smart structures while it has a high natural frequency, fast response and reversible applications. Piezoelectric effect was discovered in 1880 by the brothers Pierre Curie and Jacques Curie. Electrification from pressure was correlated with driving force when Pierre Curie observed the relations between pyro electricity and crystal symmetry [2]. Curie brothers continued their works considering the reversibility of electro-elasto-mechanical deformations in piezoelectric crystals [3]. Over the years, piezoelectricity has been improved and used in numerous areas. In 1910 'Lehrbuch der Kristallphysik' was published and accepted as the first standard reference for piezoelectric crystals [4].

The new piezoelectric devices were explored by using natural crystals as sensors which used in underwater applications as hydrophones. Moreover, accelerometers and microphones are the main products of development. As the first engineering application in 1916, Paul Langevin developed an ultrasonic submarine detector. He and his coworkers used quartz crystals and steel sheet to make a piezoelectric effect in transducer of this detector. Then, it has been noticed that these materials have a very high dielectric constants and exhibit dielectric hysteresis. This behavior elucidated that, ferromagnetism has a role in the electric field and named as ferroelectric behavior. Then, the relations between frequency of oscillating crystals at mechanical resonances and electrical properties of materials were discovered by Walter G. Cady. This invention led up controlling the frequency by Quartz crystals. This was named as "crystal frequency control" and these materials were often started to be used in communication industry; radio is the main example for this.

In 1925 at Bell Laboratories, it was understood that piezoelectric crystals could be used in wave filters of multi-channel telephones. Add to this, in the 1930s, microwaves and phonographs were started to be produced using the ferroelectric property of the Rochelle salt resulting from the high piezoelectric effect. In the 1940s, water-soluble piezoelectric "dihydrogen ammonium phosphate" was

discovered. Contribution of this made it possible to produce cheap and simple single crystals for sonar applications [5].

Furthermore, in parallel with development of piezo properties, such as the coupling factor with which known by the symbol “k” is the amount of the effectiveness energy conversion from electrical to mechanical and vice versa, the new areas of use of piezo material are develop. In the same years, Barium titanate (BaTiO_3) which has dielectric constant over than 1000 was discovered by Arthur von Hippel in Massachusetts Institute of Technology in 1940. The polar structure of this polycrystalline Barium titanate can be directed by strong electric field to the desired direction. It was the significant point, with manual operation; a non-piezoelectric material is able to gain a strong piezoelectric property. However, this piezoelectric and ferroelectric property is preserved up to 125°C which is named as Curie temperature. Studies were focused on improving the piezoelectric properties of the material and building man made materials with piezoelectric property. Then, sintered ceramic materials with high dielectric constants and improved piezoelectric properties were developed. In the 1950s, the Curie temperature could be increased to 250°C with invention of the metaniobate (PbNb_2O_6 lead metaniobate) and lead zirconate titanate ($\text{Pb}(\text{TiZr})\text{O}_3$) ceramics. The use of these materials with as sensitive as Rochelle salt and as chemical stability as quartz is common in electro-acoustic and some electrical circuit applications, but is not as efficient as quartz in frequency control and electrical filter applications. Development of Lead Zirconate Titanate (PZT), which is the most commonly used piezoelectric material, was a milestone in the history of smart materials. Around 1965, studies started in Japan which led to the commercialization of piezoelectric material [7].

Piezoelectric ceramics can be categorized into soft and hard types. Soft and hard describes the mobility of the domains and the polarization/depolarization behavior. It is basically categorized according to characteristics in Table 1.

Table 1: Comparison of PZT Ceramics [8]

Characteristic	Piezoelectric type	
	Soft	Hard
Domain wall mobility	High	Low
Piezoelectric coefficients	High	Low
Electromechanical coupling factors	High	Low
Mechanical quality factor	Low	High
Dielectric permittivity	High	Low
Dielectric losses	High	Low
Curie temperature	Low	High
Linearity	Low	High

Nowadays, manufacturers usually used soft types PZT ceramic because of higher strain categorized by their mechanical properties as shown in Table 2.

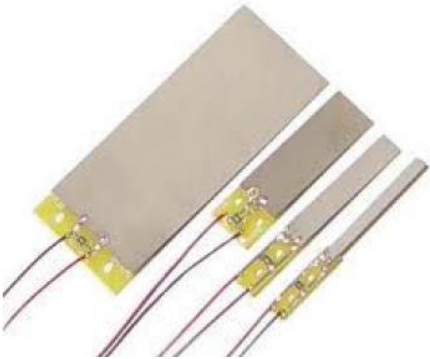
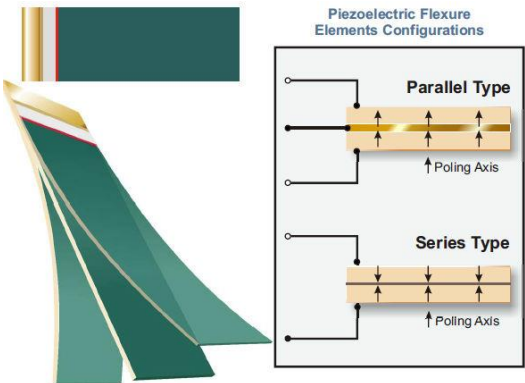
Table 2: Properties of Piezo active materials [9]

MATERIALS	*CONTROL FIELD E ELECTRIC H MAGNETIC*	YOUNG'S MODULUS AT CONSTANT FIELD (GPA)	MECHANICAL QUALITY FACTOR QM	ELECTRO- MECHANICAL COUPLING COEFFICIENT K33 (%)	QUASISTATIC MAXIMUM STRAIN (PPM)
BULK PIEZOELECTRICS					
PZT-8	E	74	1000	64	+/- 110
PZT-7	E	72	600	67	
PZT-4	E	66	500	70	+/- 150
PZT-5	E	48	75	75	+/- 300
Single-crystals (PZN-PT)	E	10	-	90	3000
MULTILAYERED PIEZOELECTRICS (MLAs)					
Soft-type	E	45	25 - 50	70	1250
Hard-type	E	62	200 - 500	60	800
ELECTROACTIVE POLYMERS (EAPs)					
PVDF	E	1	20	30	1000
Dielectric Elastomers	E	1	-	-	3.000.000
MAGNETOSTRICTIVES					
Terfenol-D	H	25	10 - 20	70	1600

Due to the fact that the discovered materials were more effective than the natural piezo materials, these gained piezo character materials were used for different applications. Sensing of mechanical disturbance and affected by electric field are two major usage areas of piezo material. For instance, piezoelectric actuators have

been used in many applications such as atomic force microscopy (Binnig, Quate et al. 1986), inkjet printers (Maeda 1983), fuel injectors in diesel engines (MacLachlan, Elvin et al. 2004), loudspeakers (Kompanek 1965) and many other applications.

Moreover, new types of piezo actuators have been developed for the last decades. There have been existed many forms of piezoelectric actuators which is explained in details [10,11,12,13,14], such as patch actuators, bimorph actuators, stack actuators, mechanically amplified stack actuators, MFC (Macro Fiber Composite) actuators, piezo tube actuators, piezo motors and special design type actuators which are shown in Figure 1.

<p>a</p> 	<p>Piezoelectric patch actuator [10]</p>
<p>b</p> 	<p>Bimorph bender actuators [11]</p>

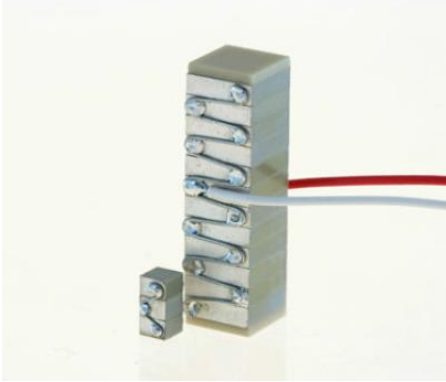
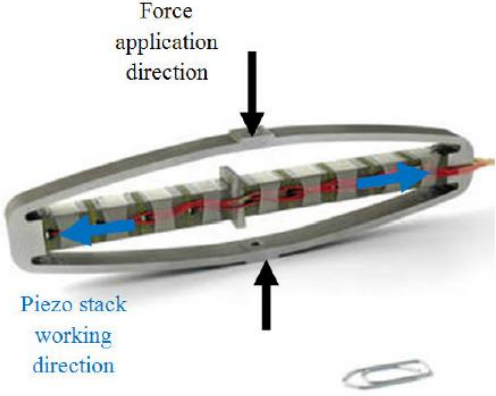
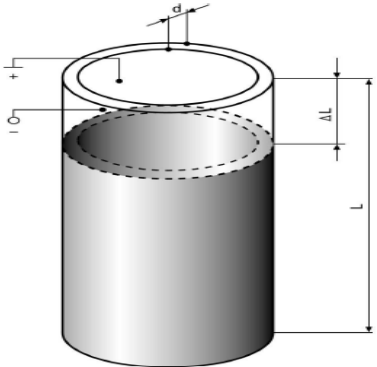
<p>c</p> 	<p>Piezo stack actuator [12]</p>
<p>d</p> 	<p>Mechanically amplified stack actuator [9]</p>
<p>e</p> 	<p>Piezo tube actuators [14]</p>

Figure 1: Examples of Piezo Actuators

The appropriate type of actuator is then selected depending on the requirements of the displacement, force and both for different applications [35]. According to typical force and displacement comparison, the summary of piezoelectric actuator types is illustrated at Figure 2.

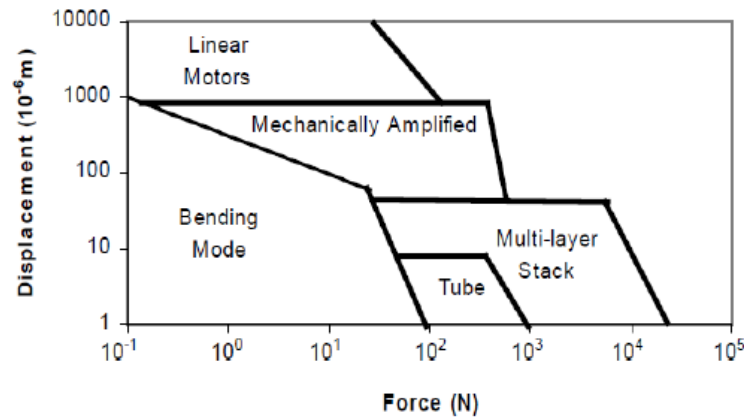


Figure 2: Comparison of Maximum Displacements and Forces of Some Linear Actuators [15]

It can be seen from the Figure 2 that, both force and displacement requirements which is given also given in APPENDIX A, are provided by mechanically Amplified Piezo Actuator (APA). The main aim is to increase the stroke of actuators. The elongated stroke of the actuator is provided through specially designed compliant mechanisms. These mechanisms improve the stroke of the actuator inversely proportional to the force.

Therefore, it may seem to be convenient to investigate the mechanically APA in accordance with the research objective.

2.3 Servovalve with Torque Motor Actuation Systems

Servovalve is a device that basically controls hydraulic flow. There are various kinds of servovalve mechanism and they have been presented in different kinds of disciplines by now. The first contribution in hydraulics came from the early Greek

and Roman civilizations. During the Industrial Revolution, a mean of hydromechanical devices were developed. During World War I, demanding for high pressures brought superior electrohydraulic control systems especially in naval equipment. Electromechanical devices such as large motors and solenoids are another usage of area in which servo motors were used as control devices. The last contribution of servomechanism has come from the field of electronics. The vacuum tube amplifier was developed in the electrohydraulic control system.

Servo valve has a main spool which sets flow that is dependent on the pressure difference. Hydraulic servo valves are classified as ‘Flapper-Nozzle’, ‘Jet-Nozzle’ and ‘Direct Drive’ according to their structures [16]. Flapper-nozzle servo valves are divided into two subgroups: single and double flapper nozzle. Commonly used servo valve is the two-stage nozzle-flapper valve with mechanical feedback consisted of an electro mechanic torque motor, flapper nozzle, spool and feedback shown in Figure 3.

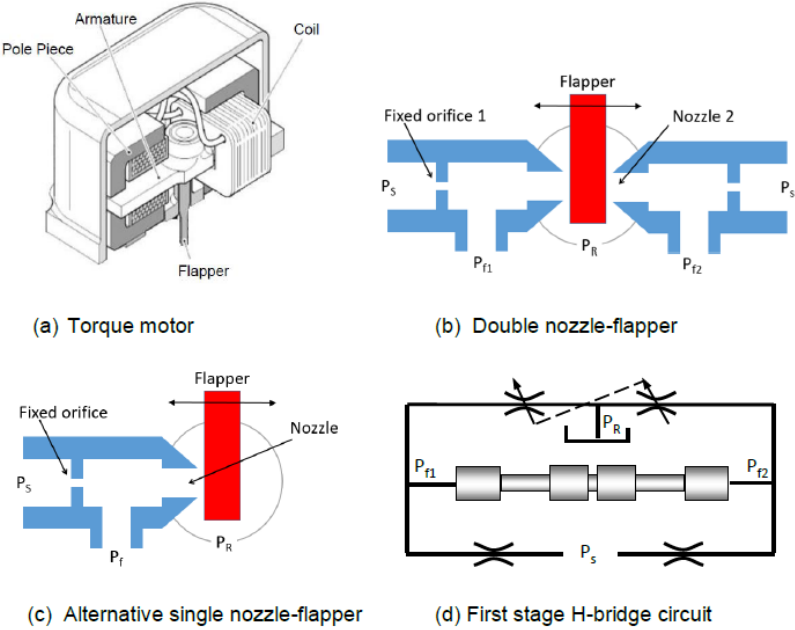


Figure 3: Nozzle-Flapper First Stage Components [17]

An electromagnetic torque motor which is shown in Figure 4 transduces electric to mechanic energy [17]. The flapper nozzle valve is consisted of the flapper, two outlet nozzles, two inlet orifices, backpressure nozzle and a feedback spring. Inlet orifices are controlled by the flapper. The flapper nozzle and the spool valve provide hydraulic force amplification. The amplification is occurred by consuming low power due to using flapper. The flapper controls the flow by the help of torque motor and lead to move the spool part. The torque motor is worked with curren. Positive current affects the motion of flapper and directed to one directions, whereas the negative current is on the reverse. [19].

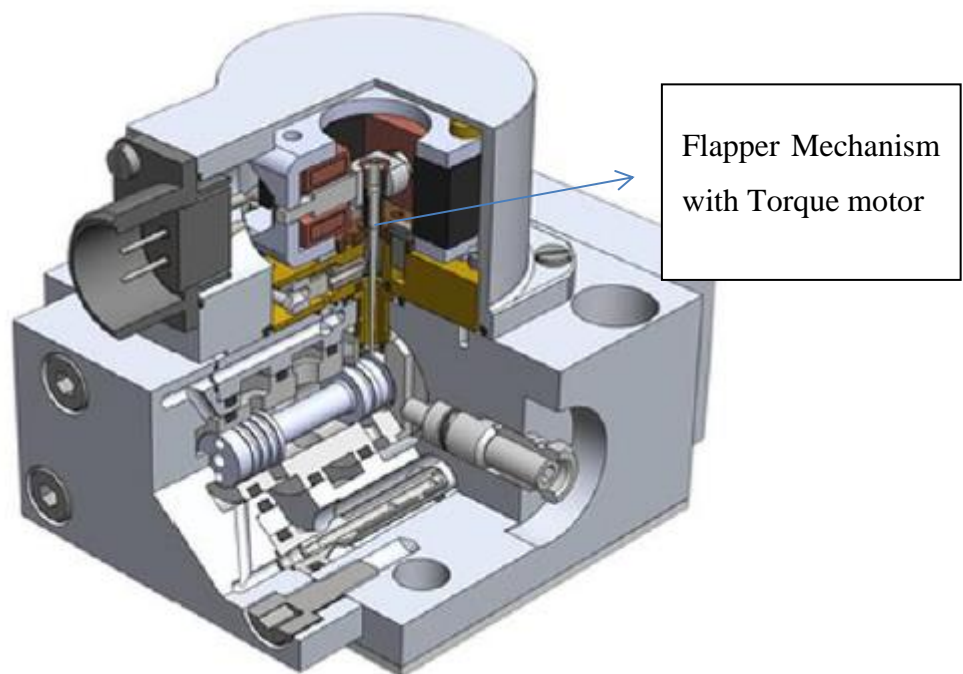


Figure 4: Flapper Nozzle Types of Servovalve [18]

A few types of servovalves are divided into three stages. With these stages, it is aimed to control output easily. Due to complexity of the three stages servovalves, the most used servovalves are consisted of two stages flapper nozzle servovalve. The purpose of the first stage which is known as amplifier part of second stage is to control hydraulic circuit. These kinds of servovalve are controlled by the torque motor flapper that is placed between two sided pressurized liquids. When the

flapper is out of the initial position which is defined as center, the nozzles create a pressure difference across the spool known as 'H-bridge.' Second stage of valve consists of spool valve and feedback wire. The feedback wire which stabilizes force to the flapper and provides to stay neutral position is located between the spool and the flapper.

When the historical development of the servovalve is reviewed, it dates back to the beginning of 19th century. For instance in industry, complex and heavy machinery was necessary in order to overcome that year's problem; therefore the control technology included servovalve is one of the important focuses.

Up to World War II, inventions usually had been made at about control field. Demanding mechanical/pneumatic transducers led to developments of servo mechanism. In Germany, a dual input (mechanical and electrical) valve was patented and used in aircraft automatic flight controls. During the World War II, the important development in electrohydraulic servomechanism occurred owing to the increase velocity of hardware development. It paved the way for automatic control theory. The first two-stage valve was patented in order to provide high force levels and better hysteresis in England in the year of 1946. Servovalve development started at a tremendous rate through the 1950's, largely driven by the needs of the aerospace industry (particularly missiles). After that, two stage valves with feedback were improved by Raytheon and Bell Aircraft. And then, two innovations were made. One is using of a true torque motor instead of a solenoid in order to save the power. The second one is using electrical feedback with a high gain loop to reduce effect of high friction. [17].

In 1950, W. C. Moog developed the first two-stage servovalve with a frictionless first stage with one nozzle. Single-nozzle two-stage servovalve was comprised of a torque motor, a spool, a flapper and a nozzle shown in Figure 5. The main goal is to transmit the flapper by using torque motor lower threshold and higher response were the advantages of this model [18].

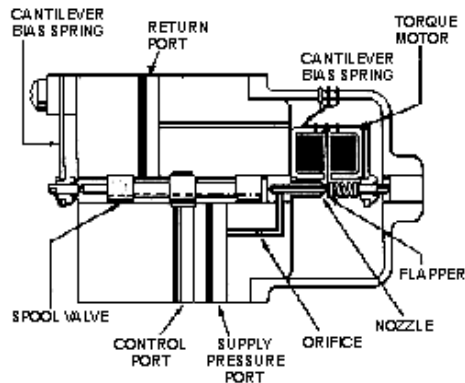


Figure 5: Single-nozzle Two-stage Servovalve [18]

In 1953, T. H. Carson first started the use of mechanical force feedback in two-stage servovalve with the advantage of improving threshold as well as dynamic response, reducing temperature and pressure. Another issue is that, magnetic particles were carried in the oil accumulating in torque motors, but that was solved for the first time in the Moog Series 2000 by isolating the torque motor from the oil [20].

By 1957, a further 17 new different concept valve was designed and had also been presented for the US Air Force, including those manufactured by Boeing, Lear, Dalmo Victor, Robertshaw Fulton, Hydraulic Research, Hagan and National Water. After this year, double nozzle-flapper two-stage valves were starting to dominate other kinds of valves. The highly important advantage of nozzle-flapper arrangements were manufacturing which is cheaper than older type of first stages known as spool and all spool based first-stages need to be overcome friction and overlap using dither signal. Moreover, R. Atchley introduced 'Jet Pipe Servovalve' with the single oil inlet and developed three stage servovalve with electrical feedback [21].

With these developments, servovalves which has two stages has been going on industrial market for many years. Two-stage flow control valves are listed in Table 3.

Table 3: Valve Designs in 1955 [21]

Manufacturer / Type	Electromagnetic driver	First stage	Main stage spool feedback
Bell	torque motor	double nozzle-flapper	no feedback (spring-centered spool)
Moog-	torque motor	double nozzle-flapper	no feedback (spring-centered spool)
Cadillac Gage FC-2	torque motor	single nozzle-flapper	mechanical force feedback
Pegasus	solenoid with spring return	single nozzle-flapper	mechanical position feedback (moving nozzle)
North American	torque motor (PWM)	first stage spool (oscillating)	no feedback (spring-centered spool)
Drayer-Hanson, later made by Lear.	torque motor	first stage spool	mechanical force feedback
Cadillac Gage CG	torque motor (long stroke)	first stage spool	mechanical position feedback (via concentric spools)
Raytheon	antagonistic solenoid pair	first stage spool	mechanical position feedback (via moving bush)
Sanders	torque motor	first stage spool	mechanical position feedback (via moving bush)
Hydraulic Controls	torque motor	first stage spool	electrical position feedback
Bertea	voice coil	first stage spool	electrical position feedback

The main electrohydraulic servovalves were also important in military applications where they were used for radar drives, controls for missile launchers. In aircraft, they were used in flight controls, guidance for missiles and radar antenna positioners [18]. Also there are lots of examples of flight control hydraulic circuit with a servovalves [22].

All in all, the technology is seen to perfect, but it has some issue that should be improved such as bandwidth, null-shift, bulky (caused by torque motor magnet), nozzle and flapper fault, torque motor non-linearity if designed to use very small

currents, and high frequency instability (squeal). To develop an open section for torque motor valves, piezo actuator should be good approach to get fast response and easy producibility. Also, the natural frequency of first stage can be increased with new flapper design and this allows getting ability of controlling higher bandwidths. As a result, actuation system of the valves can be changed with new generation piezo stack actuator. Due to innovation, the system performance such as hysteresis error and response time can be improved and manufacturing process can be easier than torque motor.

2.4 Design of a Flapper Mechanism with a Piezo Actuator

The advancement of piezo technology allows not only low dynamic operations, but also precision operations such as humanlike robotic actuators and microrobotics. The reasons why piezo actuators are widely preferred in various types of applications are in their having,

- Comparatively small final actuator size,
- High force output to mass ratio,
- The capability of high dynamic applications,
- Fast response to input.

As well as the advantages, there are some weaknesses needed to be considered:

- Hysteresis and creep effect on displacement control,
- Change of piezo constant with temperature difference,
- Decomposition at the Curie temperature.

Among control actuation systems, hydraulic actuation system is a very mature technology due to vast utilization in earthmovers, agricultural machinery, ships and aircrafts. The conventional two stages hydraulic servovalve, which is a sub system of a hydraulic actuation system, utilizes an amplifier mechanism to adjust amount of fluid by help of a flapper mechanism which is controlled by a torque motor. The torque motor controls the flapper using magnets and coils, and the

flapper varies the flow rate by changing the nozzle clearance. Nowadays with the advancement of alternative actuator technologies, torque motors began to be seen outdated. Also the implementation of magnets in the torque motor manufacturing is not simple and performance characteristic such as response time and bandwidth are lower than piezo actuator. Moreover, procurement of motor magnet materials is not possible in local market. Therefore, a piezo actuator can be used as a new approach to the actuation mechanism with promising benefits instead of a torque motor. Conventional torque motor actuation methods and piezo actuator are compared with each other as shown in Table 4.

Table 4: Comparison between APA and Torque Motor

Torque Motor	Piezo Actuator
Advantages	
Mature technology	Modernist technology
High robustness and reliability	High natural frequency
Environmental cleanliness	Compact size
High durability	Light weight
No power consumption to hold static load	Easy installation
Good for high & static forces	Error monitoring
Disadvantages	
Heavy weight	High simultaneous energy
Complexity	Requires controller and amplifier
Backlash	Thermal dependency
Electrical noise	Hysteresis and creep
	Power consumption to hold static load

The objective of this thesis work is to design and test of a piezo actuated flapper mechanism which includes;

- optimization and selection of a piezo amplifier mechanism,
- modification of the flapper mechanism with FEA for optimizing stiffness of flapper and stress on parts,
- comparison of the results of the mathematical model with that of the experimental ones,
- performance comparison of the open and the close loop controllers.

This flapper mechanism with APA structure may be used for a control actuation system which satisfies performance characteristics of an available servo valve controlled by torque motor. It is aimed that this design has a better dynamic performance than the servo valves in the market and to present it as an alternative to the torque motors.

To see system behavior, mathematical model is created. The mathematical model used Bouc-Wen model which reflects hysteresis nonlinear effects of the APA. The flapper mechanism added to the model to simulate the all structure's behavior and estimate performance characteristics before real time tests. By help of model, controller coefficients are optimized to fulfill performance requirements.

Finally, performance tests of the flapper mechanism with actuator are performed. The hysteresis model compensator and proportional controller that satisfy the performance criteria are designed.

2.5 Conclusion

In this chapter, piezo materials and torque motor of servovalves are explained with their historical developments. Both advantages and disadvantages of piezo materials and their actuation applications are also summarized. Besides, the features of a torque motor embedded servovalve which has flapper nozzle system are explained. This equipment has several areas of usage. The drawbacks and strong sides of torque motor actuation system are also explained. After

introduction of two topics, the idea claims changing the old-fashioned torque motor actuation system with piezo actuator. It creates higher benefits with more responsive systems. For this application, the system requirements are designated and both fast response and displacement requirements are provided by APA. Also, APA has high natural frequency and small size to fit into the desired place. However, APA has hysteresis error and hysteresis is defined as the inconsistency between the input voltage and output displacement related to this actuator. According to literature survey, even though some different actuation systems for valves may be designed, piezo actuator is found to be appropriate. This piezo actuation system of valve is expected to create more convenience in especially high bandwidth requirement applications. Some critical requirements: lightweight design, easy installation and the ability to work in high bandwidths can be satisfied with this new design as well. Furthermore, through design with APA systems, it is possible to make procurement easier (APA systems compared to the torque motor systems) and reduce the complexity in the system design. With this motivation, mechanical and control design according to analytical and finite element analyses is going to be done and then validated through experiments.

CHAPTER 3

ACTUATION SYSTEM DESIGN AND MODELING OF A PIEZO ACTUATOR WITH FLAPPER MECHANISM

3.1 Introduction

In this chapter, detailed design of APA with flapper mechanism is described. At first, the design consideration and performance criteria of the actuation system which includes piezo actuator and flapper mechanism are defined. Then the piezo actuator is selected from CEDRAT company catalog. According to this actuator capabilities and design requirements, a flapper mechanism and its system architecture is clarified.

To begin with mathematical model section, piezo material and its amplifier mechanism is modeled analytically to verify the catalog value of actuator's stiffness and displacement. Also, this actuator is modelled with finite element analysis program namely ABAQUS CAE® parametrically to find the mechanical amplifier stiffness and the actuator displacement. These unknown parametric values are optimized according to the catalog data of producer. At the end, these analytical and FEA results are compared with each other. Also with FEM, the flapper mechanism is modelled and added to actuator model. Stiffness and displacement of the flapper mechanism is optimized by using parametric FEM script to the design requirement. The aim of the parametric model is to specify the design parameters of the piezo actuator such as actuator size, thickness of amplifier mechanism, thickness of flapper and pre-stress on piezo materials. After analyses, the mechanical design is finalized and to verify the system with

prototype, technical drawing for manufacturing is prepared. The next step of the study is the mathematical modeling to investigate the results of the design in simulation. MATLAB Simulink® model is set up including Bouc-Wen model which is used to simulate the piezo actuator’s nonlinearity. This model is based on the experimental results which require experimental data to work with. With this model, inverse model and PI controller is designed and the controller optimization toolbox is used to optimize parameters to reduce hysteresis which is defined as the inconsistency between the input voltage and output displacement. According to the system architecture, mechanical design of the parts, piezo actuator and electrical equipment of data acquisition systems are selected.

3.2 Design Considerations and Performance Criteria of Actuation System

The design and performance requirements of flapper mechanism are shown in Table 5. The product is selected according to these requirements.

Table 5: Design Specifications

Stroke	<±15 μm
Hysteresis	<%3
Fundamental Resonance Frequency of Structure with APA	>500Hz
Geometrical Limitation	<30x50x60mm

The design criteria according to producibility are listed below:

- To overcome given design requirements, mechanical APA is selected as CEDRAT APA 60SM shown in Figure 6. Analytical and experimental verifications are also presented in Section 3.3.

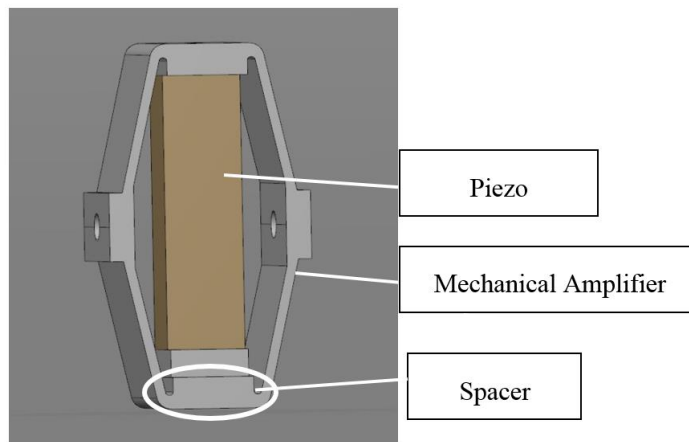


Figure 6: APA

The size and the other related performance properties of this product are convenient for our purpose. It is comprised of amplified mechanism connected to the piezo materials by the help of a spacer which keeps the piezo in compression. Also, it should satisfy the design specifications coming from system performance criteria. The detailed datasheet of the product is presented in Table 6.

Table 6: CEDRAT APA 60SM's Standard Properties

PROPERTIES	Nominal Values
Max. no load displacement	82 μm
Maximum force	105 N
Stiffness	1.287 N/ μm
Resonance frequency (free-free)	10235 Hz
Response time (free-free)	0.05 ms
Resonance frequency (fixed -free)	2802 Hz
Response time (fixed -free)	0.18 ms
Capacitance	1.55 μF
Resolution	1 nm
Mass	10 g
Geometry	Height x Length x Width 13mmx26.9mmx11.5mm

- According to piezo actuator electrical circuit considerations, amplifier supply voltage should be -20 to +150 VDC (Voltage Direct Current) and command input to the amplifier should be analog (-1) to (+7.5)V.
- A feedforward inverse, a closed loop and a hybrid position control models of the piezo actuator are tried and controller performance is described with the criteria that are tabulated at Table 7.

Table 7: Desired Step and Frequency Response Characteristics

Rise Time	<2 ms
Settling Time	<5 ms
Settling Percentage	1 %
Overshoot Percentage	10 %
Undershoot Percentage	1 %
Frequency Response	>150 Hz at -3 dB or 90 deg

The specification of the piezo actuator is defined in this part and the design process of an actuator to fulfill the performance measurements is the focus of this research. Therefore, overall design of the structure is handled relating the mechanical and the electrical perspective which are explained in details in the next chapter.

3.3 System Design of an Actuation System

The APA is composed of piezo material and a mechanical flexure. The flapper actuation system is mainly consisting of the following parts:

- Piezo materials (PZT 5H)
- Mechanical amplified mechanism
- Flapper mechanism

The structure of interest is designed regarding the volume of torque motor in conventional flapper nozzle types of servovalve. In Figure 7, the basic sketch of the flapper mechanism, which is controlled with piezo actuator, is shown. Here, “ d_p ” is the distance of the actuator from the center of rotation, “ d_p ” describes the distance where the displacement is desired and, “ x ” axis illustrates the actuation and moving axis.

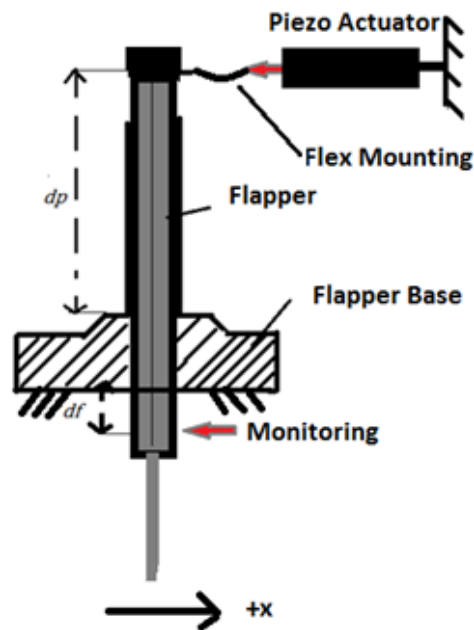


Figure 7: Basic Sketch of the Flapper Structure

3.4 Mathematical Model of Actuation System

The mathematical equations of these parts are explained below by section by section in details here.

3.4.1 APA Mathematical Modelling

APA consists of two parts which are piezo materials and mechanical amplifier mechanism. Piezo material is shown as a sample in Figure 8.



Figure 8: Piezo Materials [9]

The relation between the displacement and the voltage are investigated according to mathematical formula. Electric field, strain and stress features of piezo materials can be explained with equations below [23];

$$S = s^E \cdot T + d_T \cdot E \quad (3.1)$$

$$D = d \cdot T + \varepsilon^T \cdot E \quad (3.2)$$

where,

S	Mechanical strain vector, unit: m/m
s^E	Compliance matrix evaluated at constant electric field, (m^2s/N)
T	Mechanical stress vector, N/m^2
d_T	Piezo Coefficient
E	Electric Field vector (V/m)
D	Electric Displacement, C/m^2
d	Piezo Coefficient matrix for strain/electric field (m/V)
ε^T	Dielectric permittivity matrix evaluated at constant stress (F/m)

The effect of the external force is considered by the equation. The equation is converted to a simplified mechanical variable between force and displacement under a constant electric field,

$$d = -k_1 F_{ext} + k_2 \quad (3.3)$$

where k_1 and k_2 are constant, d is displacement and F_{ext} is external force. The direction of force is opposite to the displacement. This equation illustrated the relation between force and displacement by Hook's law. Displacement of piezo material's formula that is polarized is given in equation (3.4).

$$x_p = n \cdot d_{33} \cdot V \quad (3.4)$$

where,

- x_p Displacement of piezo (m)
- n Number of layers
- d_{33} Piezo Coefficient for polarized strain/electric field (m/V)
- V Voltage (volt)

The parameters of APA60SM are given in Table 8.

Table 8: APA60SM Properties

Number of layers	200
Thickness of one layer	100 μm
d_{33}	5.93×10^{-10} (m/V)

The maximum displacement by piezo at 150V is calculated as below:

$$x_p = 200.593 \times 10^{-10} \cdot 170 = 20.16 \times 10^{-6} \text{m} = 17.78 \mu\text{m}$$

Piezo material has a higher force capability together with a higher natural frequency compared to other smart materials. To obtain optimum displacement and force, piezo actuator is designed with a mechanical amplifier. With this mechanical amplifier, the relation between the displacement and the force may be optimized regarding to requirements. The geometry used in mechanism is illustrated in Figure 9.

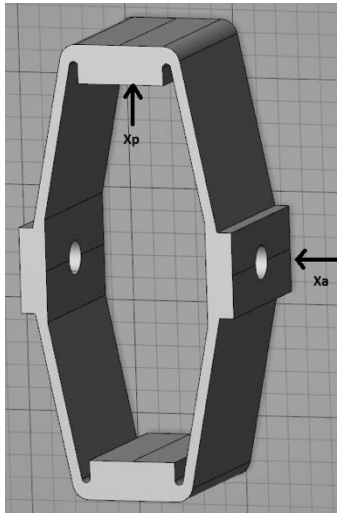


Figure 9: Amplified Mechanism of Actuator

The piezo is embedded in this mechanical parts and analytical sketch is given in Figure 10. The sketch is shown the relation between piezo and mechanical amplification mechanism.

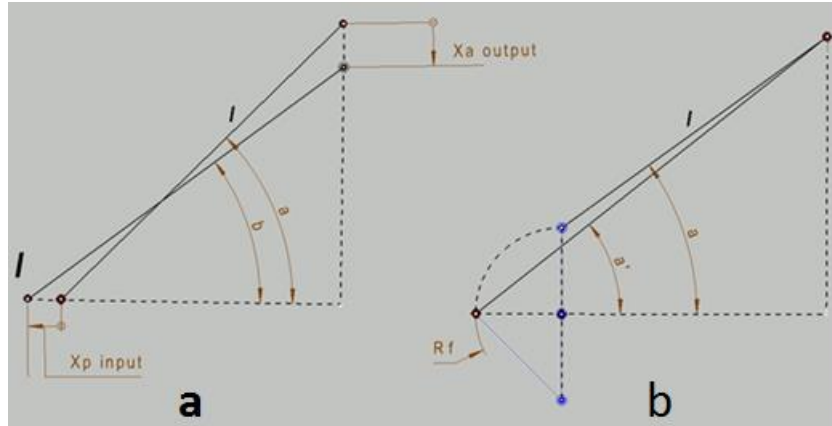


Figure 10: Amplified Mechanism Geometry (a) with no Fillet, (b) with Fillet

where;

- x_a Output displacement of mechanism (μm)
- x_p Input displacement by piezo (μm)
- l Distance between X_a and X_p (μm)
- a Undeformed angle of “ l ” as horizontal ($^\circ$)
- b Deformed angle of “ l ” as horizontal axis ($^\circ$)
- R_f Fillet Radius of “ l ” (μm)
- a^l Undeformed angle of “ l ” as horizontal axis ($^\circ$)

The equation between input and output is given in Figure 10-a and vertical and horizontal displacements are defined in equations (3. 5) and (3. 6) respectively:

$$l \cos(a) + x_p = l \cos(b) \quad (3. 5)$$

$$l \sin(a) - x_a = l \sin(b) \quad (3. 6)$$

The value “ b ” is obtained from equation (3. 5) and placed into equation (3. 6):

$$x_a^2 - 2l \sin(\alpha)x_a + x_p^2 + 2l \cos(\alpha)x_p = 0 \quad (3.7)$$

By solving the equation (3.7), x_a is calculated in equation (3.8):

$$x_a = l \sin(\alpha) - \sqrt{l^2 \sin^2 \alpha - x_p^2 - 2l \cos(\alpha)x_p} \quad (3.8)$$

The relation between X_a and X_p is calculated by mathematical equation analytically. It is called as amplification constant (A) which is the ratio of deflection of piezo and the deflection of mechanism output shown in equation (3.9).

$$A = \frac{l \sin(\alpha) - \sqrt{l^2 \sin^2 \alpha - x_p^2 - 2l \cos(\alpha)x_p}}{x_p} \quad (3.9)$$

Due to the imperfections in the machining processes of the mechanical amplifiers, there is a fillet radius which is shown Figure 10-b. In order to take these imperfections into account during the calculations, the parameter "a'" is used instead of "a" from Figure 10-b sketch. This "a'" parameter is also used in calculation in order to decrease error between finite model and analytic model. This conversion is made according to the Equation (3.10).

$$\alpha' = \alpha + \tan^{-1} \left(\frac{r_f(\cos\alpha - \sin\alpha)}{l + r_f(\cos\alpha + \sin\alpha)} \right) \quad (3.10)$$

The " x_a " can be calculated by using equation (3.11).

$$x_a = A x_p \quad (3. 11)$$

The force related to the mechanical stiffness (F_a) and generated on piezo (F_p) can be calculated by equation (3. 12) and equation (3. 13).

$$F_p = K_p x_p \quad (3. 12)$$

$$F_a = K_a x_a \quad (3. 13)$$

where,

K_a Stiffness of mechanism (N/ μ m)

K_p Stiffness of piezo (N/ μ m)

The efficiency of integrated mechanism(\aleph_m) of actuator can be calculated by (3. 14).

$$\aleph_m = \frac{F_a x_a}{F_p x_p} \quad 3. 14$$

The amplification constant (A) through analytical equation is calculated as shown in Table 9.

Table 9 Parameters of APA

l	10.28 mm
α'	12°
x_p	20.16 μ m

$$A = \frac{10,28 \sin(12) - \sqrt{10,28^2 \sin^2 12 - (20.16 \cdot 10^{-3})^2 - 2 \cdot 10,28 \cos(12) 14,3 \cdot 10^{-3}}}{20.16}$$

$$\cong 4.3$$

The maximum displacement by amplified mechanism is calculated as below;

$$x_a = 4.3 \times 17.78 = 76.5 \mu m$$

3.4.2 FEM of the APA

Piezo material, spacer and amplified mechanism are modelled in ABAQUS/CAE® software using parametric design and parametric code as a script. In order to make a fine tuning with finite element analysis (FEA) and catalog values, the thickness and the height of mechanism are converged to an optimum one. Pre-stress is needed to prevent the tear which can be caused “by the tensile stress of piezo materials [23]. Both 8 MPa and 10 MPa pre-stresses are applied separately to a piezo as a result of reference. These results are compared with each other and a better result obtained from 10 MPa pre-stress is chosen for further analyses.

In these analyses, PZT 5H and stainless steel are used for APA. The material coefficient of piezo, amplified part's that used in analyses and details of analysis are given in APPENDIX B. A static analysis is also performed to find out the static deflection of the actuator upon applying electric potential to the electrodes of piezoelectric materials. The direction of polarization is shown with red arrow in Figure 11.

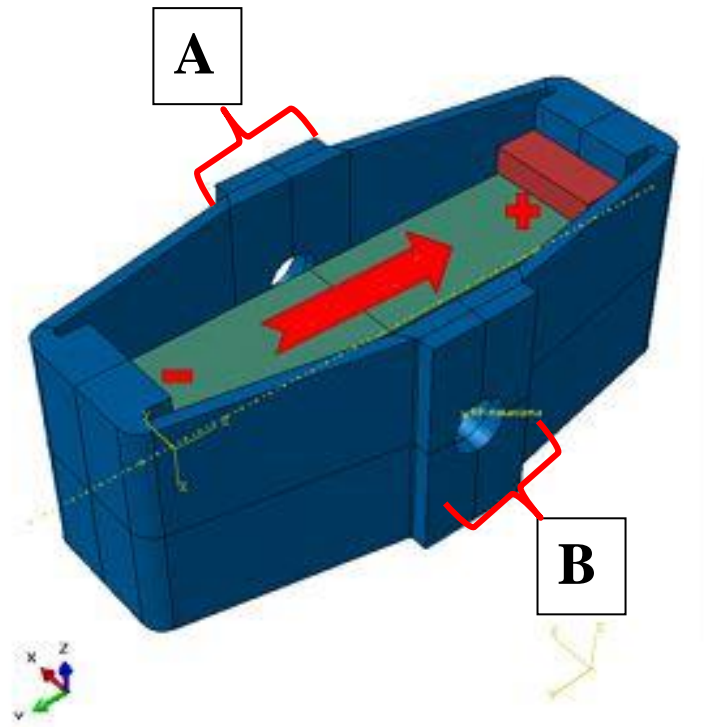


Figure 11: Polarization Direction of the Piezo Materials

The input voltage is applied to negative and positive poles of APA as shown in Figure 11. The maximum potential difference may vary between -20V and +150V.

In this analysis, displacement in “A” side of APA is free in all directions, and displacement in “B” side is fixed in all directions. A voltage load of 150V is applied to the piezoelectric materials and the deflection of the APA is found as 0.0809 mm in the x direction which is seen in Figure 11 and maximum stress is found as 136 MPa in Figure 12.

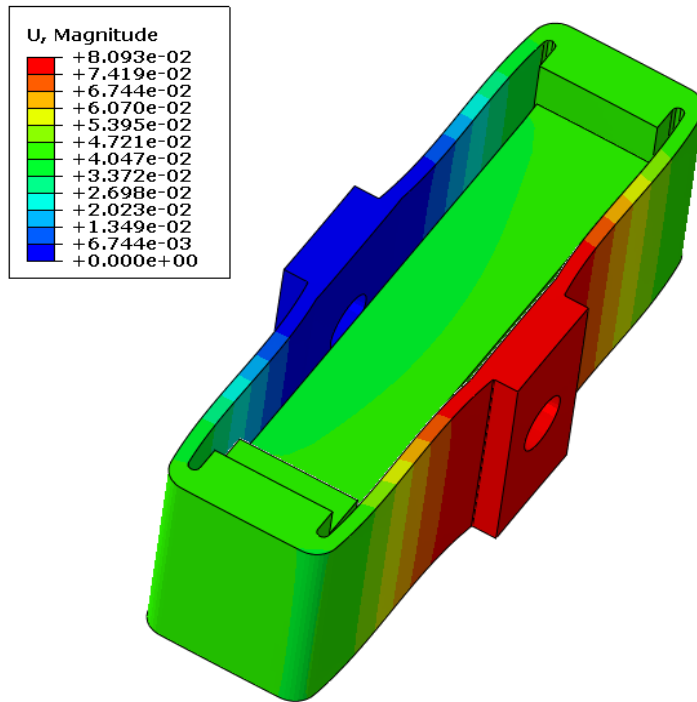


Figure 12: APA's Displacement (mm) Fixed-Free Under Applied 150V

In the second analyses, piezo actuator is fixed by both mounted sided which is defined as fixed-fixed condition. In this condition, 150V is applied to the APA and it is not possible to create displacement. According to fixed-fixed condition, applied voltage causes force generation and deformed shape of actuator is shown in Figure 13. The maximum force in x direction is calculated from stiffness curve as 118 N and the maximum stress is found as 26 MPa.

Fixed-free fundamental natural frequency (2940 Hz) and its associated mode shape obtained from the FEA are given in Figure 14.

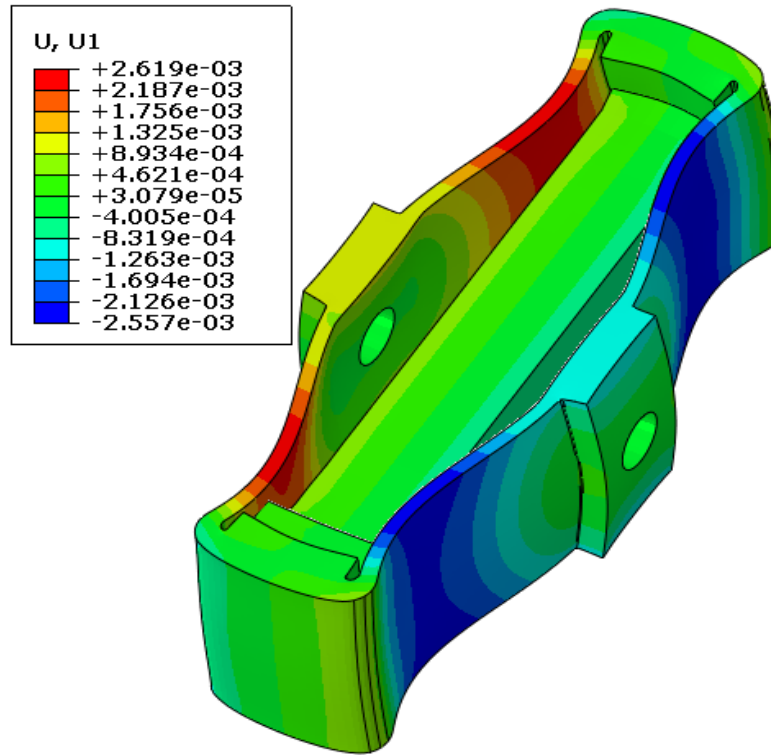


Figure 13: APA's Displacement (mm) Fixed-Fixed Under Applied 150V

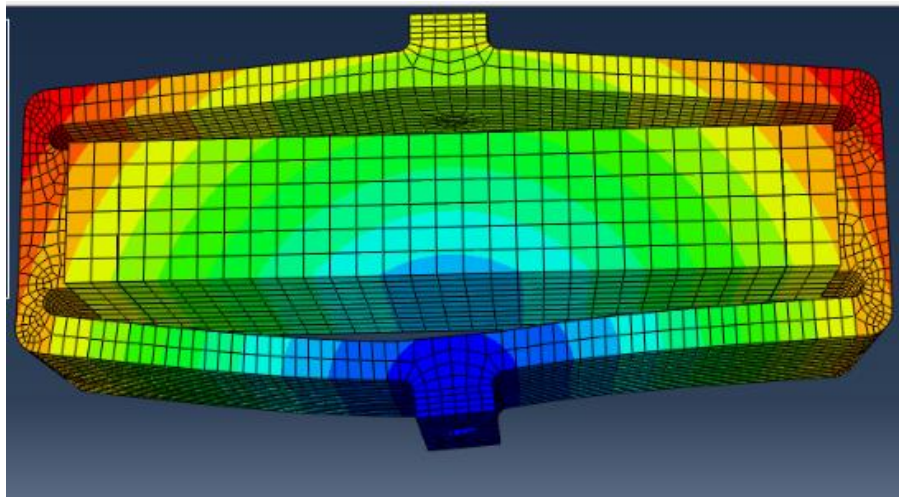


Figure 14: Mode Shape of the APA at its Fundamental Natural Frequency by FEA

All results are summarized in Table 10.

Table 10: Finite Element Results

Maximum Block Force	118 N
Maximum Free Displacement	80.9 μm
Fixed-free fundamental natural frequency (Fixed-Free)	2940 Hz

All in all, the displacement results of FEA and analytical calculation are compared. The displacement result of FEA is 80.9 μm and analytical calculation for the displacement is found as 76.5 μm which are very close.

3.4.3 Bouc-Wen Hysteresis Model of Actuation System

The piezo actuator has hysteresis in displacement. In order to minimize the hysteresis, there are different hysteresis compensators such as the Preisach [37] [38] and the Prandtl-Ishlinskii approaches [39]. In addition to this, the hysteresis effect of piezo actuator is calculated by Bouc-Wen model [32, 33]. Bouc-Wen is an experimental based model and has three parameters to simulate hysteresis of piezo actuator. The input of model is voltage and output is displacement. The hysteresis on the piezo actuator with Bouc-Wen model is shown in Simulink® in Figure 15. The input of simulation is voltage [volt] and the output is displacement [μm] and “dP” is a piezo constant.

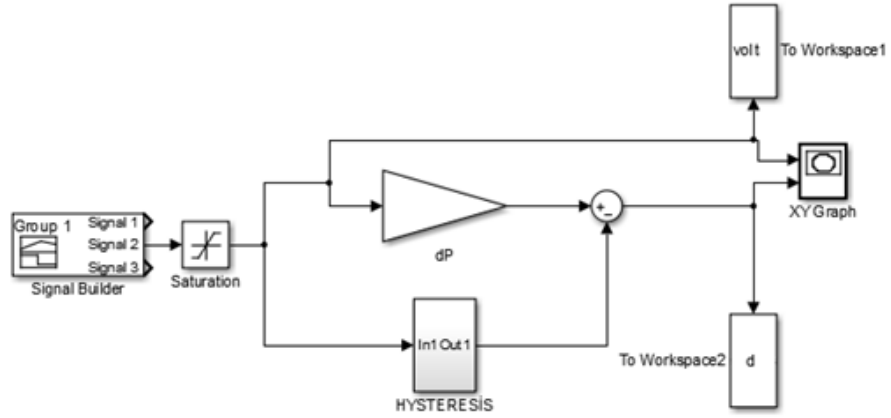


Figure 15: Simulink® Model of Piezo Actuator

This mathematical equation related to Bouc-Wen are shown in equation (3. 15) and (3. 16)

$$y = d.V - h \quad (3. 15)$$

$$\dot{h} = A\dot{V} - B|\dot{V}|h|h|^{n-1} - C\dot{V}|h| \quad (3. 16)$$

where y is the output displacement, d is derivative, V is voltage, h is the hysteresis loop in terms of displacement whose magnitude and shape are determined by parameters A , B and C as shown in Figure 16, n controls the smoothness of the transition from elastic to plastic response. Because of the elasticity of several piezoelectric actuators, it is admitted that $n = 1$ [36]. Bouc-Wen model adds the nonlinearities of hysteresis which is shown in Figure 16.

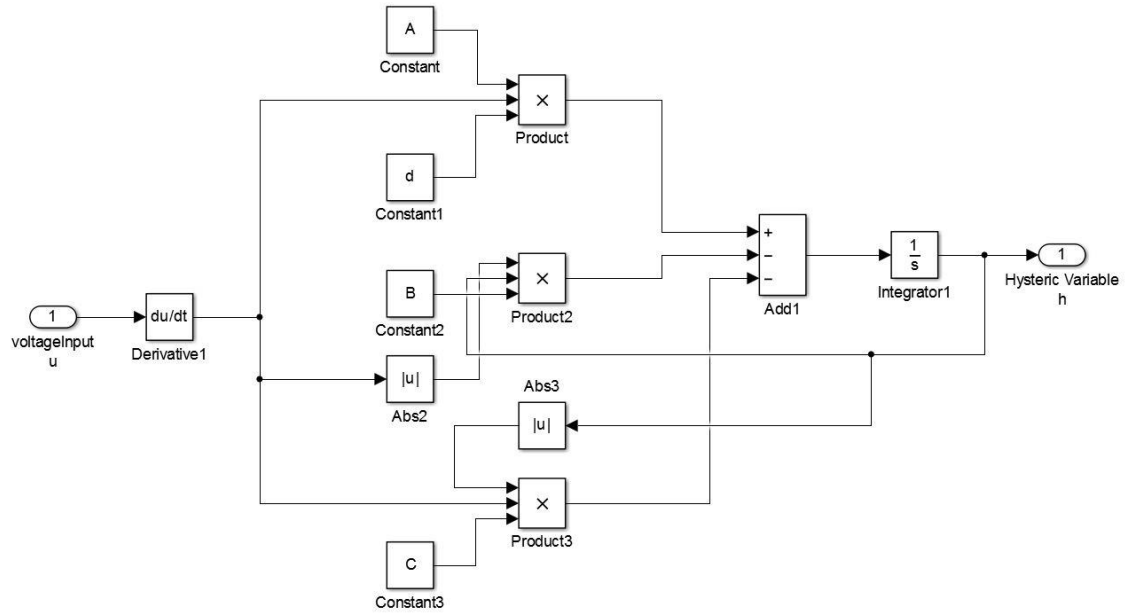


Figure 16: Simulink® Model of Bouc-Wen Model

3.4.4 System Equation of Actuation System

The system which includes piezo actuator and flapper mechanism is simulated in this section. As the first step of the system equation, the force (F_a) developed by multilayer piezo actuator is found. The formula for this step is shown in equation (3. 17).

$$F_a = K_a A n d_{33} V \quad (3. 17)$$

Under dynamic conditions, this developed force of piezo actuator can be correlated with these various forces which are given in (3. 18).

$$F_a = \frac{M_a d^2 x_a}{dt^2} + \frac{B_a dx_a}{dt} + K_a x_a \quad (3.18)$$

where M_a is assumed as the equivalent mass of amplified mechanism and other masses added to the system. B_a is the damping coefficient of the APA (N-s/m)

Balancing two equations of force ((3.17) and (3.18)), (3.19) is found.

$$K_a And_{33} V = \frac{M_a d^2 x_a}{dt^2} + \frac{B_a dx_a}{dt} + K_a x_a \quad (3.19)$$

Taking the Laplace transform of equation (3.19), the displacement is related by voltage as shown below in equation (3.20).

$$X_a(s) = \frac{K_a And_{33}}{M_a s^2 + B_a s + K_a} V(s) \text{ and } K = K_a And_{33} \quad (3.20)$$

$$\Rightarrow X_a(s) = \frac{K}{M_a s^2 + B_a s + K_a} V(s)$$

The piezo equations which are combined together are illustrated in Simulink® block diagram in Figure 17. It defines the relation between the signal input voltage in unit of [V] and the displacement in unit of [μm]. In this particular figure, the coefficients used are provided in Table 11.

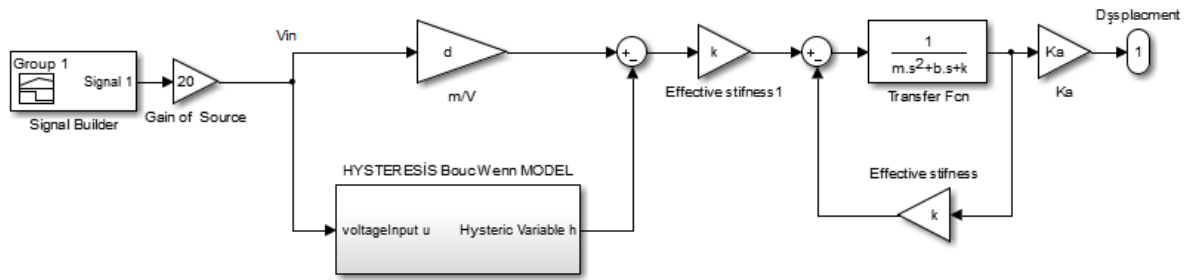


Figure 17: Simulink® Model of Piezo Actuator

Table 11: Used Parameters

d	0.1447	($\mu\text{m}/\text{V}$)
K_1	$1\text{e-}6$	Gain: μm to mm
m	0.0038	Mass (kg)
b	150	(Ns/N)
K_2	50×10^6	N/m
K_a	4.3	Flexure Gain

Bouc-Wen model has parameters which are optimized according to experiment and the overall system dynamic performance is affected by optimization of these. In order to investigate the simulation parameters according to experiment, the Parameter Estimation Toolbox® of the MATLAB Simulink® Software is selected. The model is then prepared for this optimization with these initial parameters and the model is illustrated in Figure 18. The software starts with initial parameters then provides estimated parameters into an optimization problem and solves it to find the best parameter values [24].

The tests are performed without applying any loads. Triangle and sine speed commands are given to the piezo actuator and the displacement measurements are

then obtained from the laser displacement sensor alongside the strain gauge that integrated on piezo. The investigated parameters are specified within a guess range.

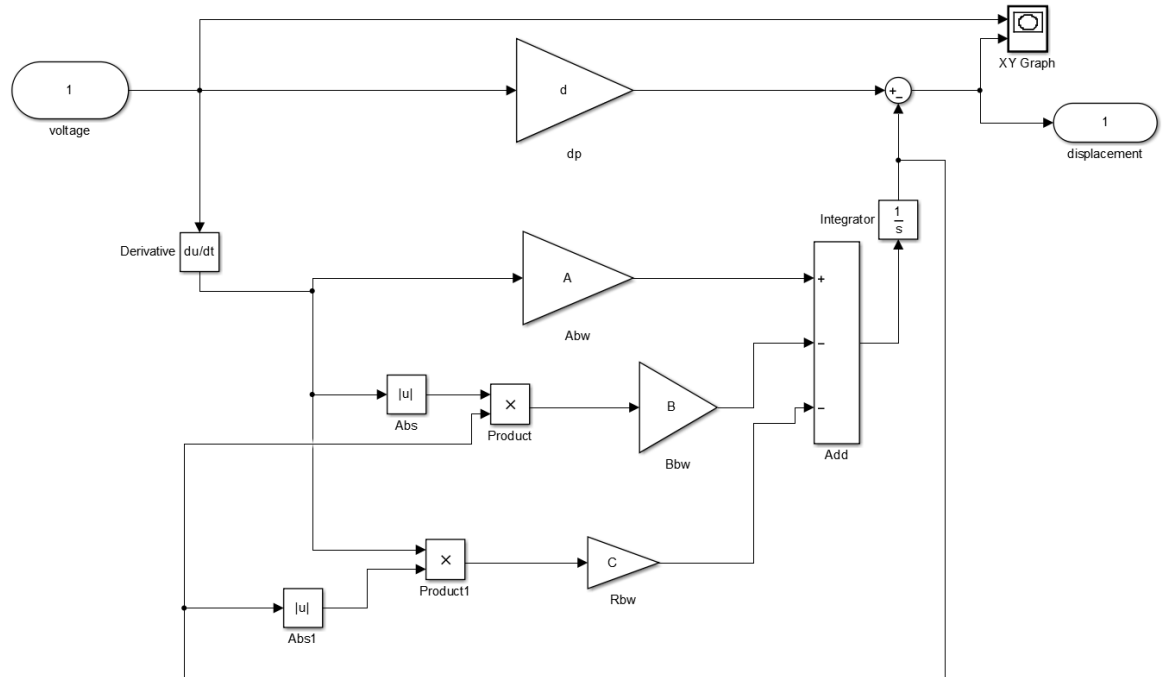


Figure 18: Simulink® Model of Estimation Toolbox

The simulation starts with the rough parameters to have a basis for the optimization. Then, the parameter sensitivity gets higher up to below %1 range. In parameter optimization, the relation of A, B, C parameters is illustrated in Figure 19.

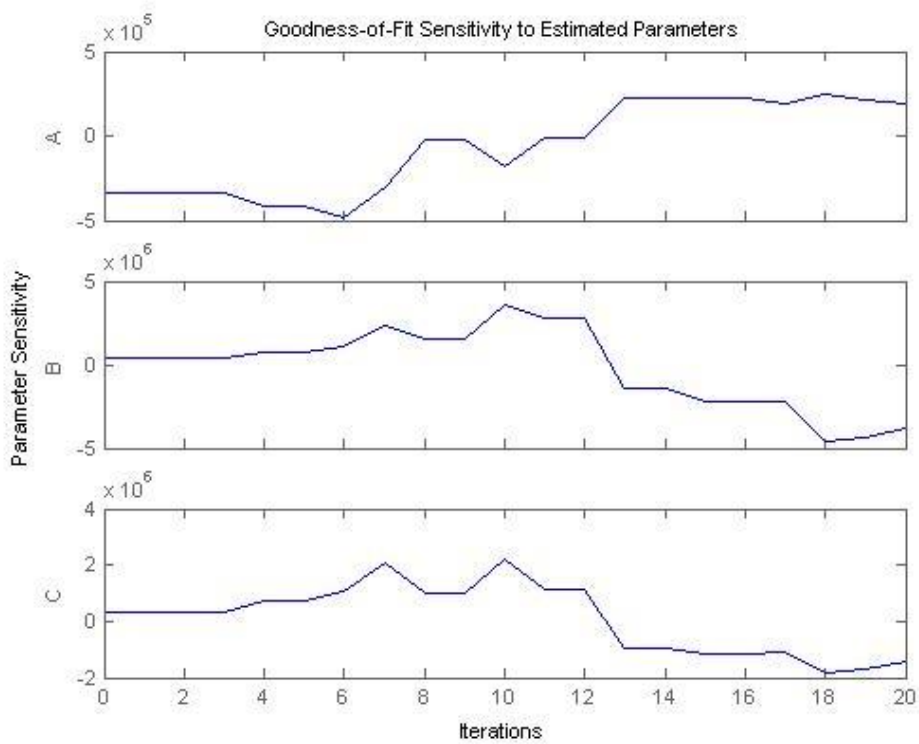


Figure 19: Trajectories of Parameters

After rough estimation, in order to find the more accurate results, simplex method followed by trust-region reflective nonlinear least squares method is used. The solver parameters for this particular case are defined in Figure 20.

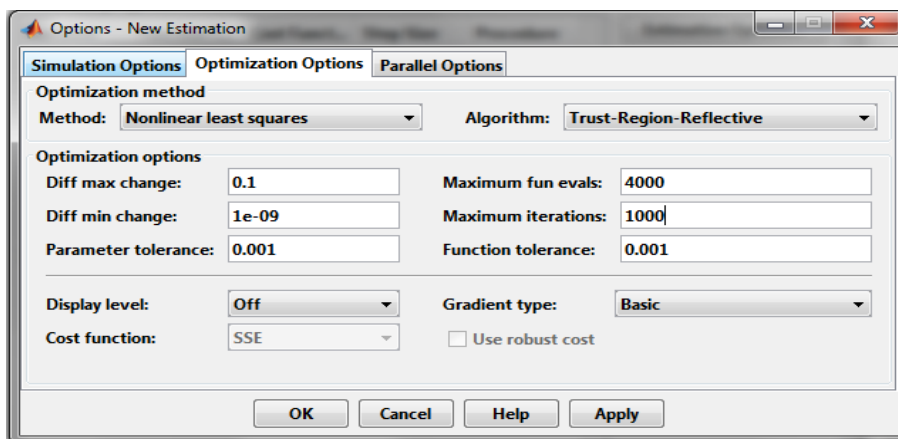


Figure 20: Parameter Optimization Setting

3.4.5 Inverse Hysteresis Model of Actuation System

After the Bouc-Wen model is constructed, the inverse hysteresis compensator is used. This model aims to minimize nonlinearity of piezo and to define nonlinear terms of hysteresis in terms of voltage output. Simulink® model of Inverse Hysteresis Model is shown in Figure 21. Due to control of displacement of piezo actuator, this model is built up with estimated parameters. The main physical parameter which depends on the hysteresis is determined by identification tests and the mathematical model is then verified after finding these parameters.

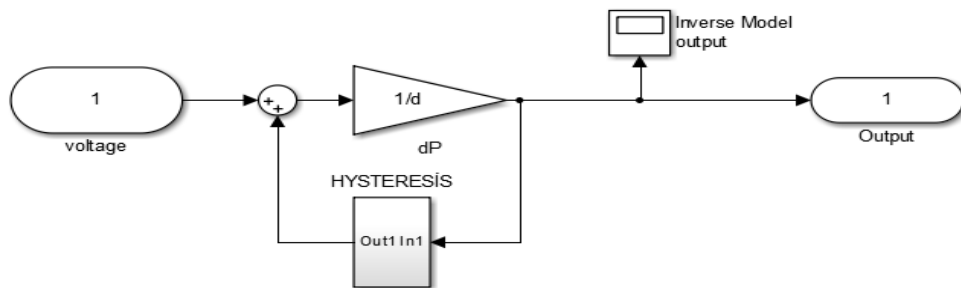


Figure 21: Bouc-Wen Hysteresis Compensator

According to electrical and mechanical design requirements, basic piezo test setup is built up to verify these simulation models. Piezo actuator is used to collect experimental data for compensator. Optimized parameters of the compensator are presented in Table 12. Estimated parameters are investigated iteratively with a cost function, and after a particular iteration, the estimation process is finished.

Table 12: Estimated Parameters

Parameters	
a	$A=0.202306275$
β	$B=0.024332686$
γ	$C=0.002060996$
d	$d=0.602451096$

In Figure 22, the model and experimental result which is the x-label shows the input-voltage signal as volt, and y-label shows the output-displacement in μm is shown. The maximum error between simulation and experiment is reached to 2%. In this particular experiment, the 1 Hz triangle input signal is simulated using Simulink®. The output of the inverse Bouc-Wen model is then illustrated in Figure 23. The x axis of graph is named as time (s), and y axis of graph is named as voltage (V). The Bouc-Wen inverse model is functionalized with APA's nonlinearities and added to Simulink® model which is presented Figure 24.

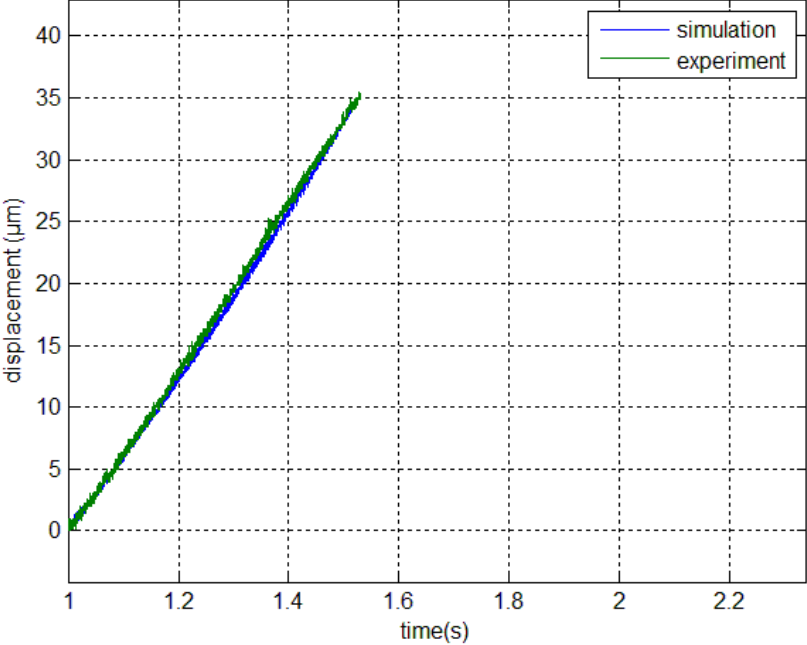


Figure 22: Simulation and Experiment Results

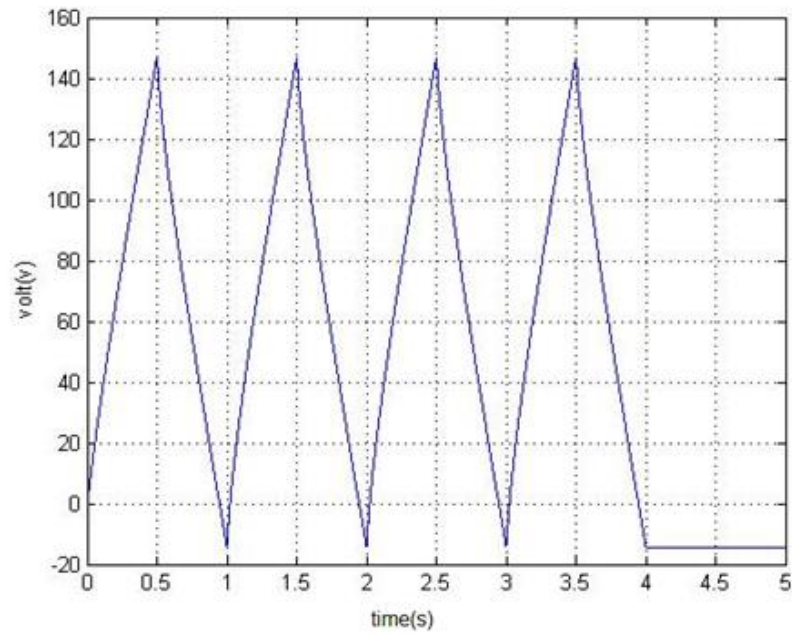


Figure 23: Output of Hysteresis Compensator

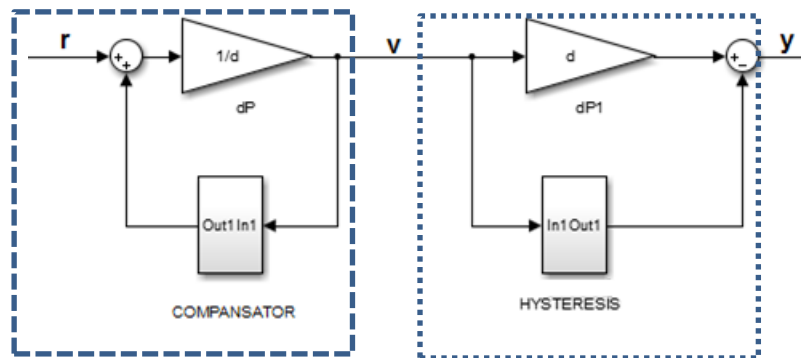


Figure 24: Sub Model of System

As the inverse model parameters are optimized with minimum error, the ideal output of the Simulink® model is going to be linear.

3.5 Mechanical Design of Actuation System

According to the system architecture defined in section 3.3, mechanical part's design process and component selection are described in this section.

Mechanical system design process typically starts with determining nominal operating displacement of the system and selecting an actuator size. After determining nominal displacement in room temperature, other components can be designed with respect to other design requirements.

In Figure 25, the section view of flapper mechanism with APA system is illustrated. The main aim of the design is to drive the flapper through the piezo actuator.

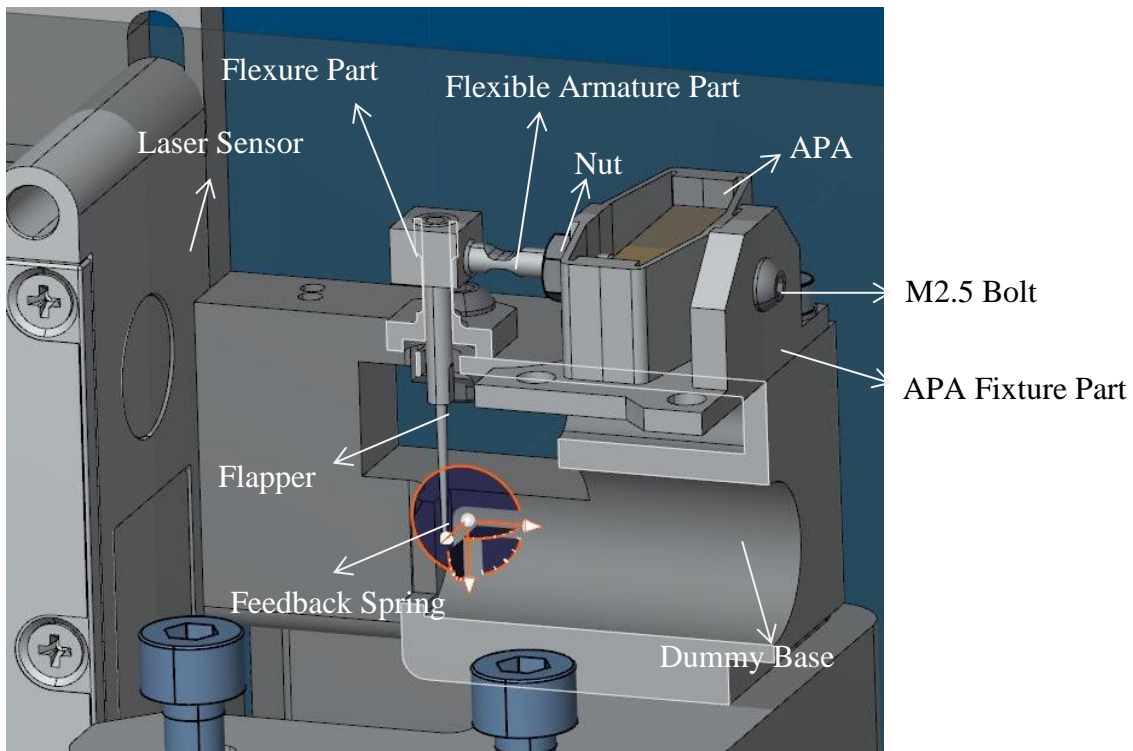


Figure 25: Section View of Piezo-Flapper Systems

3.5.1 Flapper Design without Flexible Part Assembly

The aim of this part is to control flapper with electromagnetic actuator under the influence of armature parts. This assembly consists of four parts which are flapper, flexure, feedback spring and flexible part. In order to hold on main structure, piezo actuator is mounted on armature parts which have convenient interfaces for “M2.5 screw” of piezo actuator. The main assumption is that, the structure allows bending moment on flapper by linear piezo actuator. The assembly is designed as a draft by analytic calculations and then with respect to design requirements the optimum design is verified with finite element method. One of the flappers of two stage flapper nozzle type valve can be seen in Figure 26.

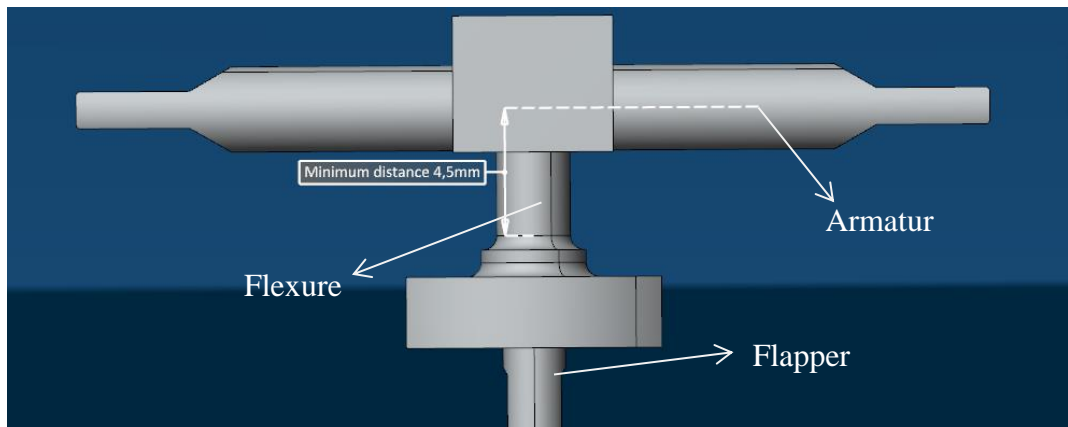


Figure 26: One of Flapper Nozzle Type Valve's Flapper

By having the hydraulic forces at two sides of the flapper, the required torque value on the armature and the other design parameters are given in Table 13.

Table 13: Parameters in Calculation

Name	Value
dp	4.5 mm
df	3.6 mm
M	28.2 mNm

In analytical calculation, flapper mechanism shown in Figure 26 is simplified and modelled like the one provided in Figure 27.

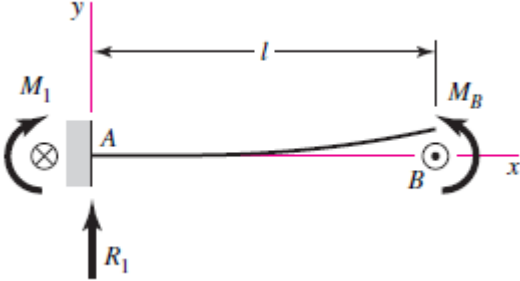


Figure 27: Bending Model [26]

And the new design of the flapper mechanism using piezo actuator is simplified and modelled like the one shown in Figure 28.

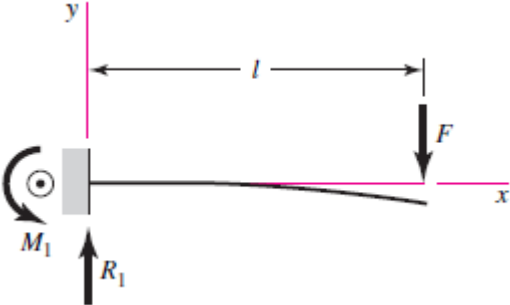


Figure 28: Linear Model [26]

In Eq. (3. 21), bending model is equalized to linear model.

$$\frac{FL^3}{3EI} = \frac{ML^2}{2EI} \Rightarrow 2FL^3 = 3ML^2 \tag{3. 21}$$

where,

- L distance of the actuator from the center of rotation also equal to dp

R_1	Reactive force on point
F	Force of APA
M_B	Moment on flapper

$$F = \frac{3}{2} \left(\frac{M}{d_p} \right)$$

$$F = \left(\frac{28.2mNm}{4.5} * \frac{3}{2} \right) = 9.4 \text{ N}$$

Necessary force to satisfy the given maximum displacement is then calculated as 9.4 N.

The problem here is that, the equivalent force on armature is simulated for maximum torque in a torque motor actuator which is used in a two stage flapper nozzle type valve. In this type, there is no connection between flapper mechanism and torque motor actuator.

The new design has a connection between flapper mechanism and APA, which replaces the torque motor in the previous system. In order to fit into the conditions which are used to calculate the stiffness value of the flapper mechanism, the connection between piezo actuator and the flapper mechanism should be flexible.

In some of industrial applications of flapper mechanism, the material used in the flapper mechanisms is found to be 36NiCrTiAl alloy named as Elinvar. In order to minimize the dependence on the temperature and control the errors introduced by the temperature variation of the elastic modulus, Elinvar is preferred. However, in prototype tests, the environmental condition is out of concern. Therefore, stainless steel which is more popular and readily available is used in the manufacturing. This material has enough yield and ultimate tensile strength for our analyses.

3.5.2 Flapper Design with Flexible Part Assembly

To get necessary displacement on the flapper, flapper stiffness should be low or mounting part should be designed according to the elasticity requirements. In Figure 29, the technical drawing of the designed flapper is demonstrated and the flexible design parameters are listed in Table 14.

Table 14: Parameters of the Designed Flapper

Flapper Diameter	2.6 mm
Flexible Diameter	0.25 mm
Radius of Curvature	1 mm
Length of Curvature	3.8 mm

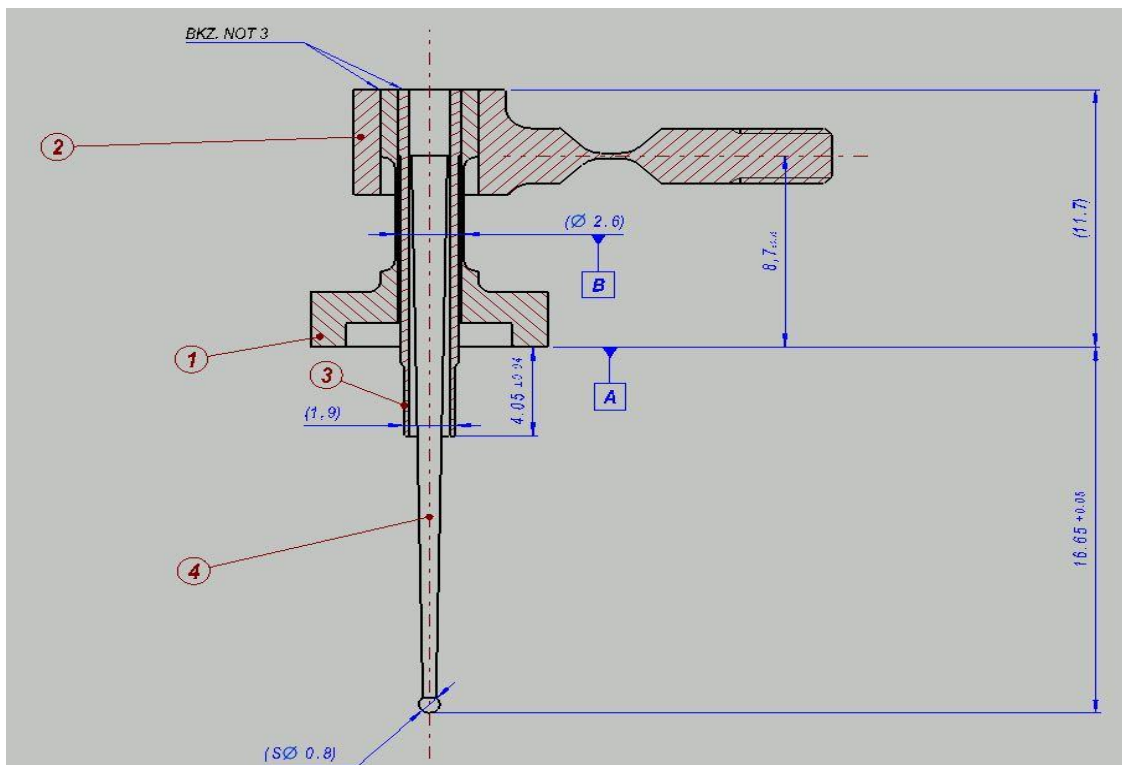


Figure 29: Technical Drawing of the Flapper Mechanism

The curvature size on the flapper, in other words, the amount of elasticity of flapper is chosen according to satisfy the required minimum load and a higher fundamental natural frequency. This also affects the controllability and the bandwidth of the system.

After piezo actuator is built up, the test setup is also modelled in ABAQUS/CAE®. This modelling is made according to the same principles with the model made in Section 3.3.4. It is seen that, the flapper is pushed and pulled by piezo, using one amplifier mechanism which translates the motion in opposite direction according to piezo. In order to get a higher displacement with piezo, the flapper is thinned in a particular region to allow more bending. Proportional to the bending in the flapper, the displacement of the flapper is increased up to mechanical strength of the flapper. Another term that will be affecting the displacement is the flexible part design and in order to optimize the mechanical design of flexible part, thickness and length of curvature are main optimization parameters to be obtained in the FEM analysis. Different thicknesses in designing process are used to get desired displacement in flapper. The thickness that found from analyses is validated with experiment, therefore one prototype is produced. The prototype is seen in Figure 30. All parts are hex meshed according to mesh independency given in APPENDIX B. This mesh size is optimized according to solving time. Also bolts are preloaded according to manufacturer's catalog [28]. The main body assumed to be bounded to the ground.

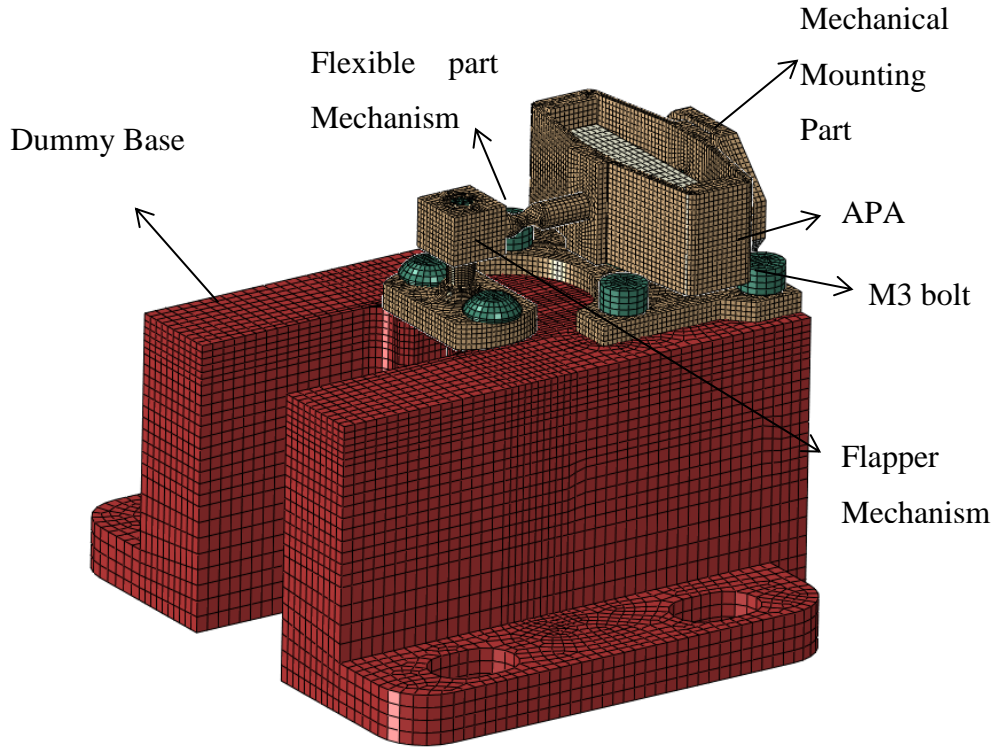


Figure 30: Test Setup

First, the static displacement test under electrical load is performed. The initial electrical voltage is given as 75V and after some iterations, the flapper displacement at desired point is estimated to be 24.2 μm which is shown in Figure 31 with the 85 times exaggeration for graphical purposes. This value verifies our design requirements which are presented in Section 3.2. When resonance occurs at higher frequencies, amplification is typically smaller than at low frequencies. But, long-term vibration where small stresses can cause fatigue failure, the response in the high frequencies may still be worthwhile. This long term fatigue is not our focusing issue.

$$x_{flapper} = \frac{(x_{piezo}) \cdot K_{piezo} \frac{V_{ref}}{150}}{K_{flapper} + K_{piezo}}$$

$$24.2\mu m = \frac{80\mu m \cdot \frac{1.264N}{\mu m} \cdot 75/170V}{(1.264 + K_{flapper_2})N/\mu m}$$

$$K_{flapper_2} = 0.58N/\mu m$$

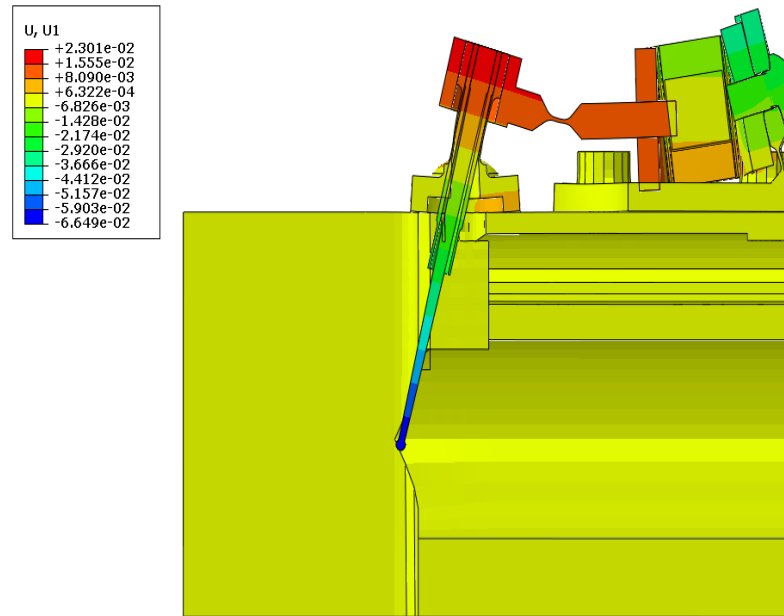


Figure 31: Flapper Displacement in Actuator by FEA

For thickness optimization, the critical Von Misses stresses are given in Figure 32. It is seen that, flexible invar armature has up to 100 MPa and copper flexure has up to 200 MPa stress.

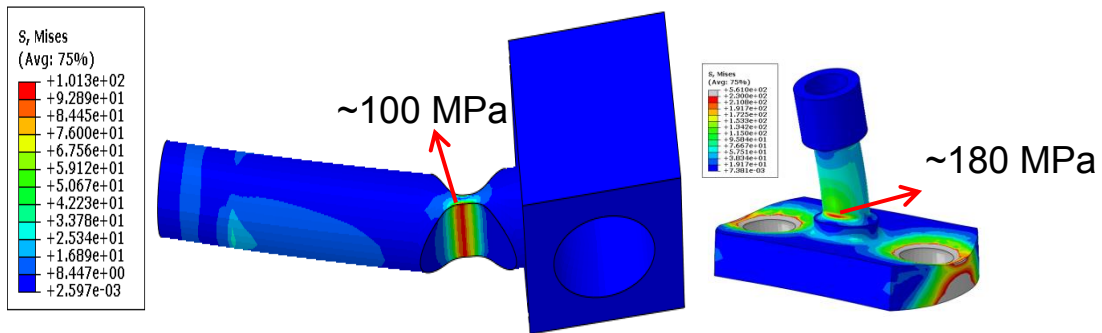


Figure 32: Critical Von Misses on Parts by FEA

This tuned mechanical design is also manufactured with estimated thickness, to be confirmed experimentally. This flexible flapper mechanism prototype is shown in Figure 33.

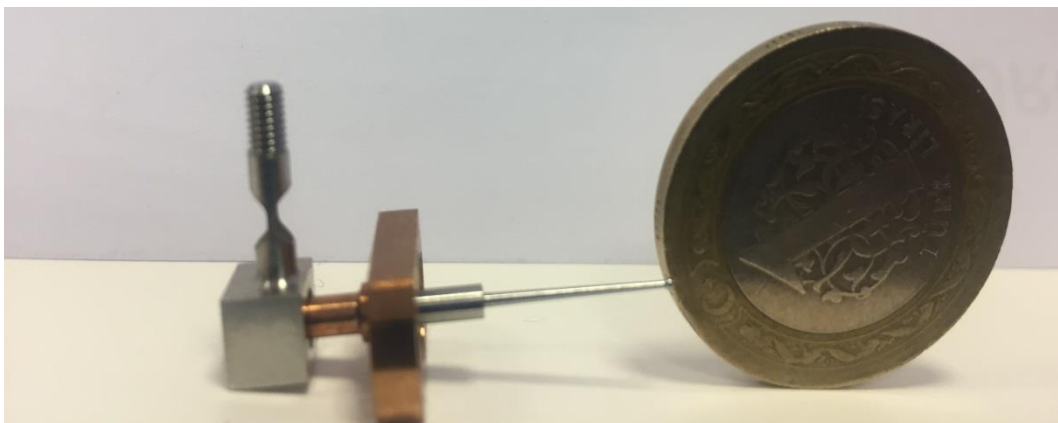


Figure 33: Flexible Flapper Mechanism Prototype

The piezo actuator is capable to work on much more pulling than pushing motion, which means that even though it can be used to move flapper in both directions, it will create a higher pulling displacement. To neutralize this issue, mechanical assembly of the actuator must be calibrated.

3.6 Electrical Design of Data Acquisition System

In electrical design section, components of the electrical system such as the piezo amplifier, sensors, controller and data acquisition system are given in detail.

To control displacement of the piezo actuator, -20V to +150V analog signal is utilized for control input signal. The piezo amplifier and the controller are selected as CEDRAT TECHNOLOGIES LA75C. This product is shown in Figure 34. The amplifier LA75C with its controller (CA45) receives -1 to +7.5VDC and converts it into -20 to +150VDC signal with maximum continuous peak output current of 2400 mA to drive the piezo actuator. The set values of the piezo drive's performance parameters; control mode, input and output type can be reached. These parameters can be adjusted by connection interface of RS232 and CAN bus via software on the computer [13].



Figure 34: LA75C Specification [13]

The connection of piezo actuator is connected through a CEE22 connector which includes an 110V/230V selection. Piezo actuator is driven by high voltage cables using LEMO CTAC22 connectors and banana plugs on different sides. The strain gauges cable has flex connection and SMD 1mm pitch connector in different sides

[13]. Other equipment is a strain gauge's conditioner is selected as CEDRAT TECHNOLOGIES SG75. It uses the signal coming from strain gauges probe which is implemented on piezo actuator. The gain of channel is set according to piezo actuator [13].

Furthermore, there is a laser displacement sensor in the test setup to monitor the flapper position. In case of unexpected position of flapper according to sensor, emergency stop is added to the test software. The laser displacement sensor, ILD2300-2 is a product of Micro-Epsilon GmbH and uses the principle of optical triangulation, that is, a visible, modulated point of light is projected onto the target surface. The sensor measures the distance in the diffuse arrangement, the distance in the direct arrangement or the thickness of a transparent target. As shown in Figure 35, displacement causes voltage change in electrical circuit of in the sensor. The difference creates a voltage output proportional to the distance to target. The diffuse element of the reflection of the light spot is imaged by a receiver optical element positioned at a certain angle to the optical axis of the laser beam onto a high-sensitivity resolution element (CCD), in dependency on displacement. From the output signal of the CCD element, a digital signal processor (DSP) in the sensor calculates the displacement between the light spot on the object being measured and the sensor. The displacement is linearized and then issued via digital interfaces [30]. In our application, the sensor is used to measure the flapper displacement. The mounting orientation of sensor needs to be careful. To get accurate result, the direction of laser which respect to target must be vertical. Therefore mechanical mounting interface should be designed carefully.

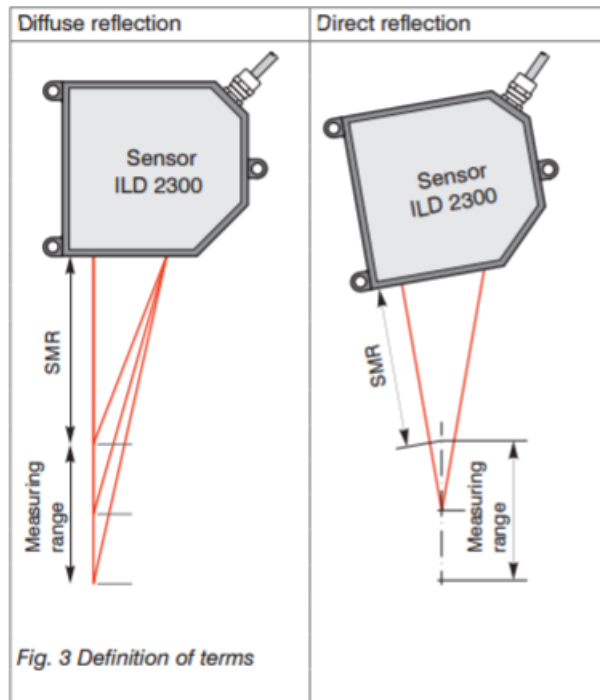


Figure 35: The Working Principle of Sensor [30]

For data acquisition and real time control, National Instruments real-time controller Compact RIO 9063 Chassis and signal input & output modules are used. This is shown in Figure 36. The controller computer specifications are listed below:

- 667 MHz dual-core ARM Cortex-A9 processor
- 512 MB of nonvolatile memory for data logging
- 256 MB of DDR3 memory for embedded operations
- NI Linux Real-Time Operating System
- Artix-7 Field Programmable Gate Array (FPGA) for embedded control and monitoring applications



Figure 36: National Instruments Compact RIO 9063 Chassis [31]

The I/O modules that are used in measurements are listed as below:

- NI 9239 (± 10 V, Simultaneous Analog Input, 50kS/s, 4 Channel Module)
- NI 9264 (± 10 V, Analog Output, 25kS/s per channel, 16 Channel Module)

NI 9239 module is employed to get ± 10 V analog signal of laser sensor for position measurement of the flapper mechanism. It is a channel to channel isolated module which leads elimination of measurement errors caused by ground loops. Also, it protects the measurement from harmful voltage spikes [31].

NI 9264 module is used to send ± 10 V analog output to the piezo actuator driver. According to position error of the actuator, the position controller creates a displacement command to the actuator driver via NI 9264 with ± 10 V analog output.

The electrical connections of circuits between control computer, modules, sensors and power suppliers connection between components is presented in Figure 37.

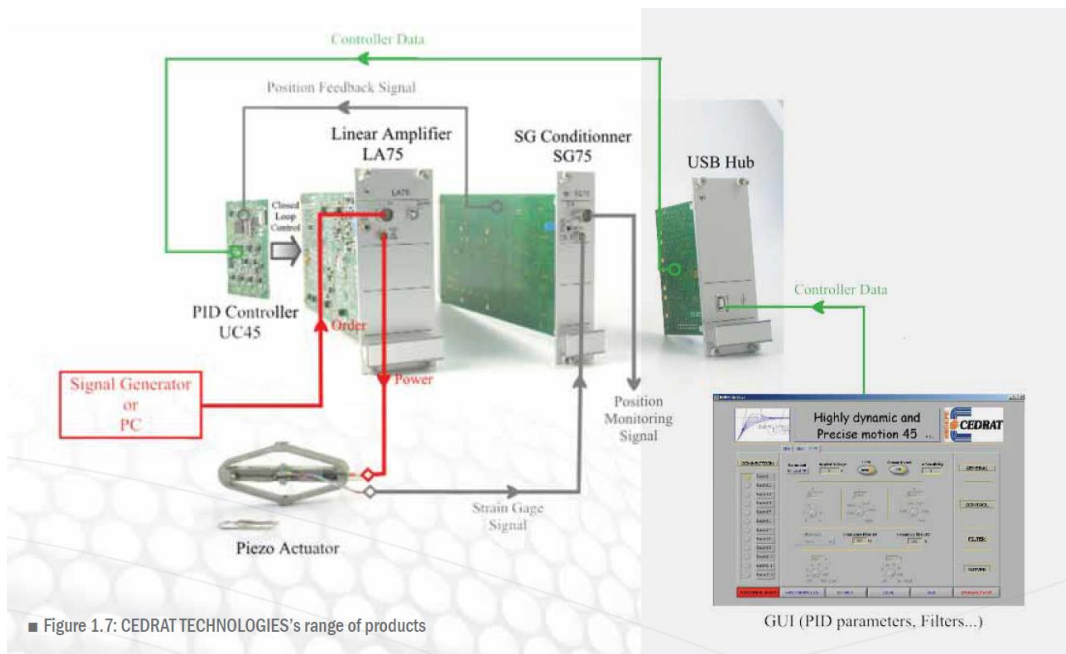


Figure 37: The Schematic Diagram of the System [13]

3.7 Controller Design of Actuation System

Hysteresis is depending on types of amplifier types; voltage or charge amplifier. In case of voltage amplifier, hysteresis is increased with input frequency of signal. In this section, the position of the flapper is controlled d feed forward controller such as Bouc-Wen compensator and proportional controller (PI). Control model of the system has already been shown in Section 3.7 in Figure 17. As illustrated from the Figure 38, reference position signal is sent to mathematical model. Then, the mathematical model sends signals to piezo actuator by NI Module and amplifier. PI controller corrects errors according to difference between the reference and the measured positions of the strain gauge on piezo actuator. The desired voltage command is generated by this flow.

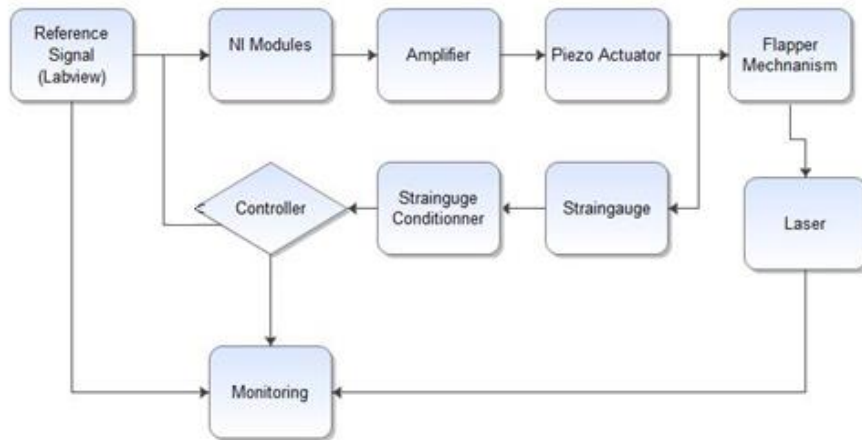


Figure 38: Process Flow Diagram

Before integration of PI controller, position of the piezo is measured with strain gauge and laser, besides the result is read via isolated channel voltage input module that minimizes the measurement noise. This experimental data is compared with the desired signal and generate the error signal to figure out magnitude.

In Figure 39, displacement signal is shown. The noise amplitude in the measurement is in a range of 0.1 microns which is acceptable when the full scale motion of flapper is considered in one way around 18 microns. Moreover, the noise harmonics of position signal are investigated and power spectral density of the signal is obtained. It is seen from Figure 39 that the noise density has no peak at frequency up to 1000 Hz and 1 Hz is peak which is driven signal frequency. The result shows that the electronic component of the system is not affected by the surrounding system.

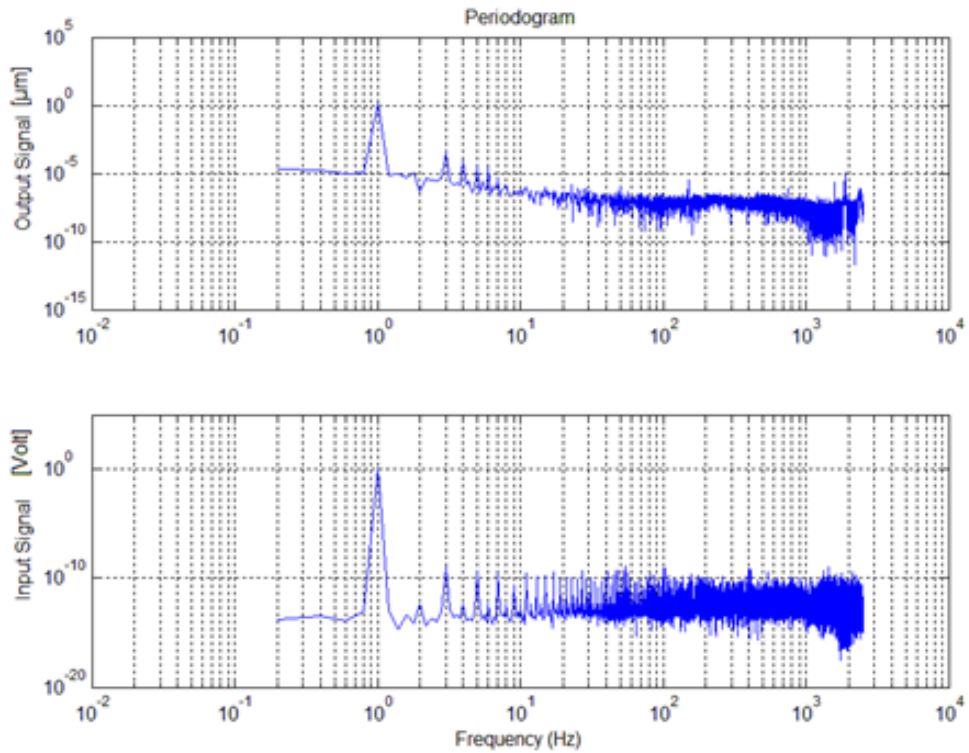


Figure 39: Input [V] and Output Signal [μm] Power Spectral Density

In design process of PI controller, MATLAB Simulink® Check Step Response Characteristics module is used. Simulink® closed loop model of the system is presented in Figure 40. PI controller is optimized by using sub-toolbox of Simulink® Design Optimization which is called Response Optimization according to desired position sensitivity and allowable performance criteria. After desired performance criteria such rise time, proportional and integral gain limitations are considered with respect to time and frequency domains in the software, the parameters create an optimization case. Feedforward control which is Bouc-Wen hysteresis model compensator and PI control are used together in Simulink platform shown in Figure 41.

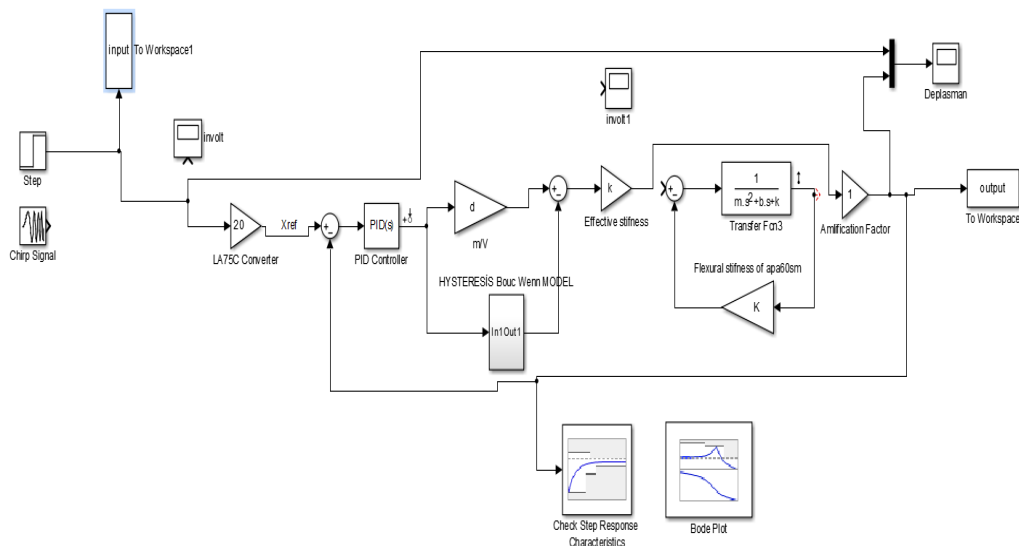


Figure 40: Simulink® Model of the Closed Loop System

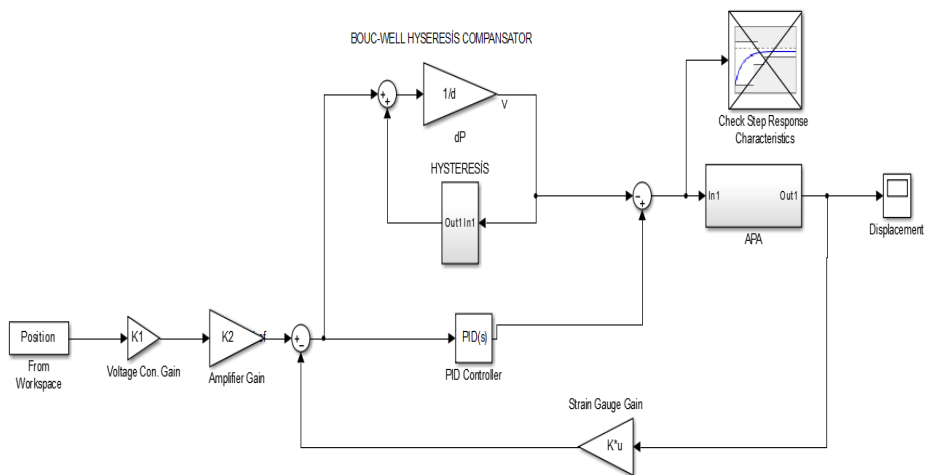


Figure 41: Simulink® Model of the Compensator and Closed Loop Hybrid System

The design criteria such as step response and frequency response characteristics are presented in Table 7 in Section 3.2. These inputs are used in software to designate the desired interval of responses that are shown for time response in

Figure 42 and for limitation of controller parameter K_i which is integral control parameter and K_p which is proportional control parameter due to electronic amplifier are limited. Also, system linearization toolbox is used in MATLAB using the best fit.

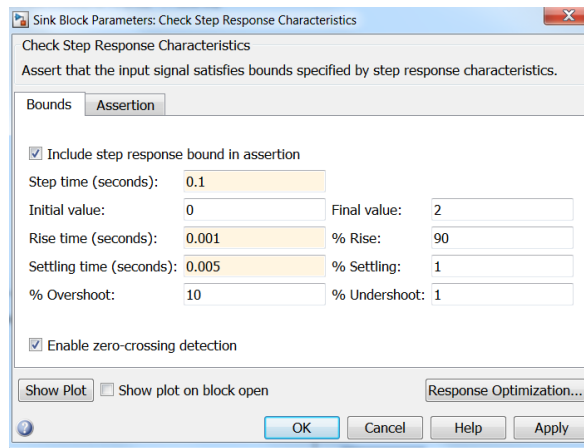


Figure 42: The Target Time Response Characteristics

In order to decrease optimization time, lower bound of the proportional gain is defined as $0.005 \text{ V}/\mu\text{m}$ and upper bound is limited with $0.1 \text{ V}/\mu\text{m}$ and the lower bound of integral gain is taken as $0.01 \text{ V}/\mu\text{m}$ and upper one is as $1000 \text{ V}/\mu\text{m}$. At the end of optimization, the proportional controller gain is found as $1000 \text{ V}/\mu\text{m}$ and $0.011 \text{ V}/\mu\text{m}$ that is illustrated in Figure 43, respectively.

Although the proportional and integral of controller seems to be enough for the time response, the gain found in frequency domain is different to fulfil the system design requirements. Proportional controller's gain is identified as $990 \text{ V}/\mu\text{m}$ and $0.01 \text{ V}/\mu\text{m}$. The bode diagram including these controller gain is simulated in Figure 43. For this optimization, gains are found below as;

$$K_p = 990 \frac{\text{V}}{\mu\text{m}}$$

$$K_i = 0.01 \frac{\text{V}}{\mu\text{m}}$$

According to chirp input signal, 1645 Hz is found as the fundamental natural frequency.

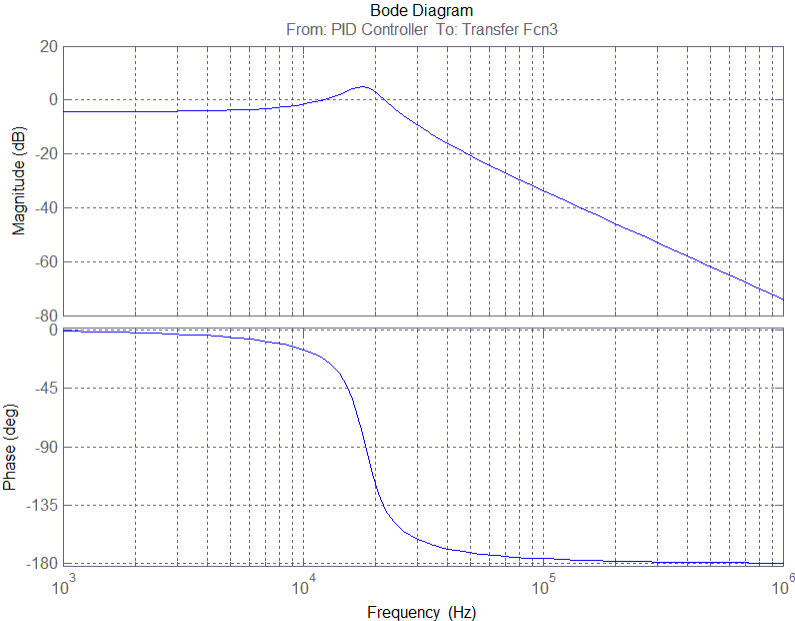


Figure 43: Response Optimization Result in Frequency Domain

Then, with the parameters of controller gain, it is verified whether the time response characteristics are sufficient with this gain or not. As illustrated in Figure 44, the model response should be within the design limitations and the controller parameters are optimized accordingly.

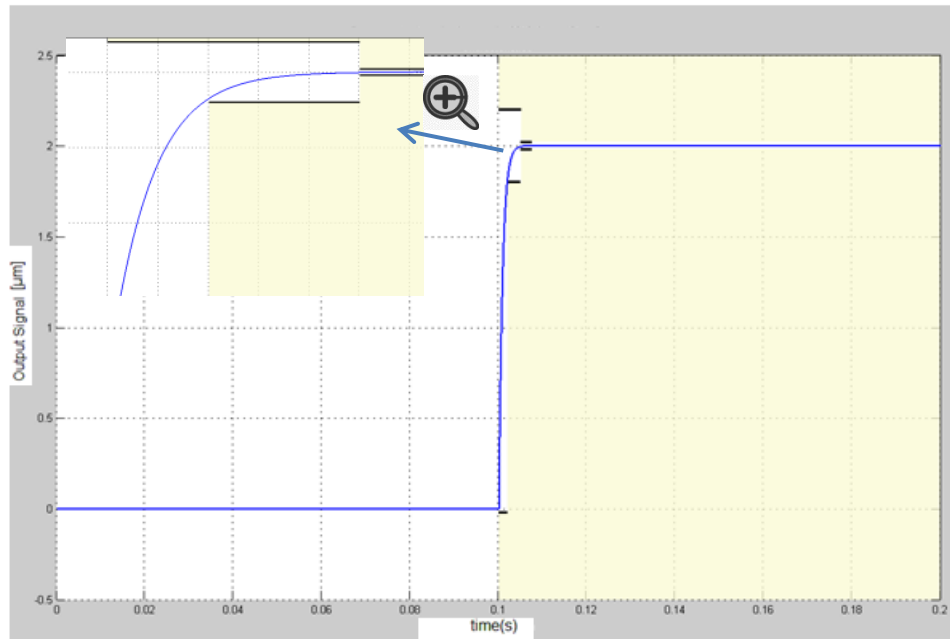


Figure 44: Time Response Result with the Chosen Proportional Controller

3.8 Conclusion

In this chapter, according to system design requirements, the system is designed with piezo actuator. According to the design, Bouc-Wen based mathematical model is set up and system design parameters are then optimized. Also, finite element model is used to evaluate the system displacement and force generation. Displacement of the actuator is calculated as 86 μm from analytical method and 80.9 μm through FEA. The system prototype is then created with sensors and data acquisition system. Then, open loop feedforward and close loop PI controller is designed. Also, PI controller parameters are optimized according to rise time and the system's natural frequency. Following those, the controller parameters are optimized and verified with experimental results and the design criteria for bandwidth and rise time are also provided. All in all, as it can be seen from the results that the whole analytical evaluation and FEA results are compatible with each other. To verify these results, an experimental setup is also established.

CHAPTER 4

PERFORMANCE TESTS OF PIEZO SYSTEM

4.1. Introduction

In this section, experimental tests comprising piezo actuator characterization are performed. System flow diagram for the experimental verification has already given in Figure 38. According to experimental results, mathematical model parameters are verified. Then, the inverse Bouc-Wen model is created in order to decrease the hysteresis error. Completing the open loop and the inverse model compensator tests, PI controller is added to the model. Tests are performed with the PI controller, and then results are compared according to the hysteresis error. The dynamic tests are performed with charge amplifier and the process flow has already been illustrated in Figure 38.

4.2. Piezo Actuator Characterization Tests

In this part of the study, tests conducted to identify the unknown system parameters used in mathematical model are explained. Bouc-Wen model coefficients and the piezo characteristics are the parameters investigated in this part of the study.

The parameters of Bouc-Wen model related to piezo actuator are then calculated. As mentioned in Section 3.3.5, the experimental results are then used in order to optimize the model parameters. The displacement is also changed by altering the

temperature of the surroundings and therefore, the tests are realized at the room temperature. The used Simulink® Model is illustrated in Figure 45.

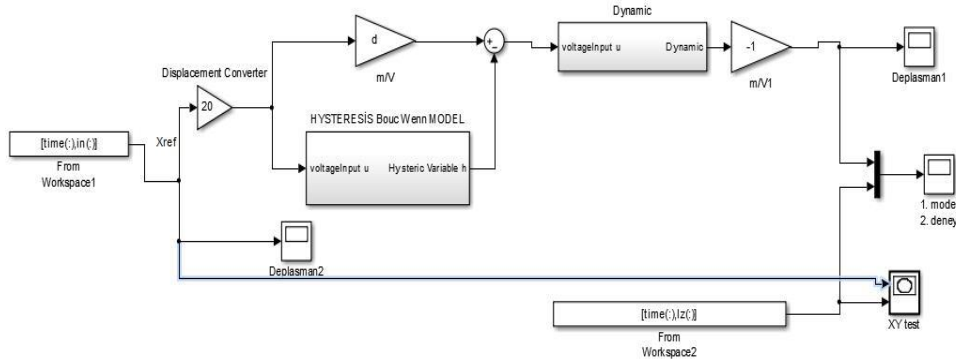


Figure 45: Simulink® Model of Piezo Actuator

The main focus in the experiment is to minimize the hysteresis affect. As the hysteresis is non-linear and depends on the driving frequency; the magnitude of hysteresis can be tested with sine and triangle input signal at various frequencies.

The basic experimental test setup is shown in Figure 46. The piezo actuator is actuated with a voltage controlled electric source, CEDRAT LA75C test equipment, which is explained in Section 3.5. The driving frequency is sent by a computer using LabVIEW programming tool with NI analog input and output modules.

The test set-up consists of a fixture to hold the APA; a mechanical adjustable slide for holding the laser sensor. The input voltage is then applied through a voltage amplifier with a gain of 20 by a power supply (range 0–7.5 V) to the actuator. The APA generates a pulling force and the displacement output is obtained from the oscilloscope and the characteristics are plotted for the forward and reverse direction of the actuator’s displacement.

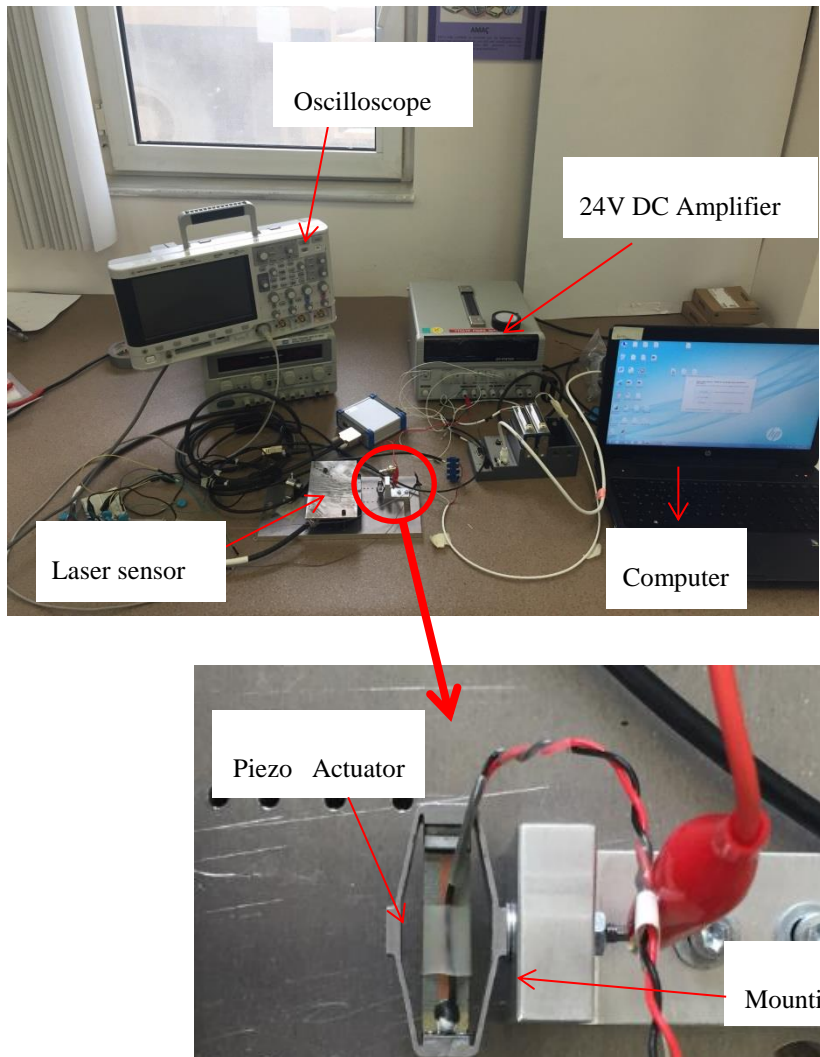


Figure 46: Piezo Actuator Test Setup

The results of the tests are then compared with the simulation presented in Figure 47 and Figure 52 with respect to Table 15 which is calculated by MATLAB Simulink® model of the system. It can be realized that the data taken from the laser displacement sensor is at free condition and the simulation results are also shown in same graph. When simulation and experiment results are investigated, the percentage difference between experimental and simulation results is around up to 3%. Both hysteresis errors are varied by 11% to 14% as illustrated in Table 15.

The error of the hysteresis is obtained from the MATLAB Simulink® model of the system that is shown in Table 15. The Bouc-Wen “A”, “B”, “C” parameters are evaluated. Preliminary characterizations of the used piezoelectric actuator shows that the effect of the creep on the hysteresis curve can be seen with the frequency lower than 0.01 Hz [34].

Table 15: Used Bouc-Wen Parameters

	A	B	C	Hys Error	Hys Error
0.05 Hz Sin	0.3082	0.0405	-1,21E-02	11,76%	N/A
0.05 Hz Tri	0.2394	0.0710	-3,51E-02	N/A	11,68%
0.1 Hz Sin	0.1752	0.0320	-8,00E-03	12,41%	N/A
0.1 Hz Tri	0.1791	0.0406	-1,70E-02	N/A	10,26%
0.5 Hz Sin	0.1969	0.0403	-1,54E-02	13,83%	N/A
0.5 Hz Tri	0.19685	0.0413	-1,52E-02	N/A	12,89%
1 Hz Sin	0.3543	0.0412	4,30E-03	14,97%	N/A
1 Hz Tri	0.2327	0.0175	3,60E-03	N/A	13,84%

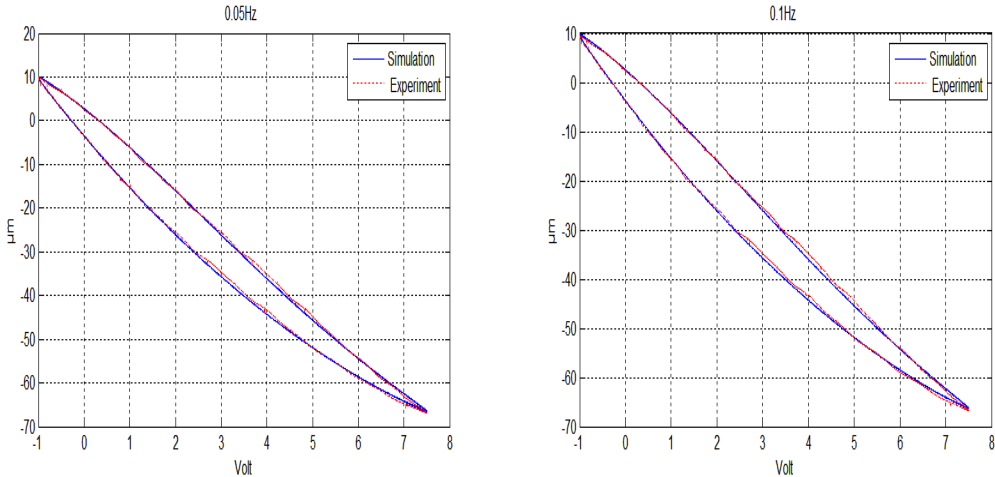


Figure 47: Hysteresis by Simulation & Experiment with Sine Input

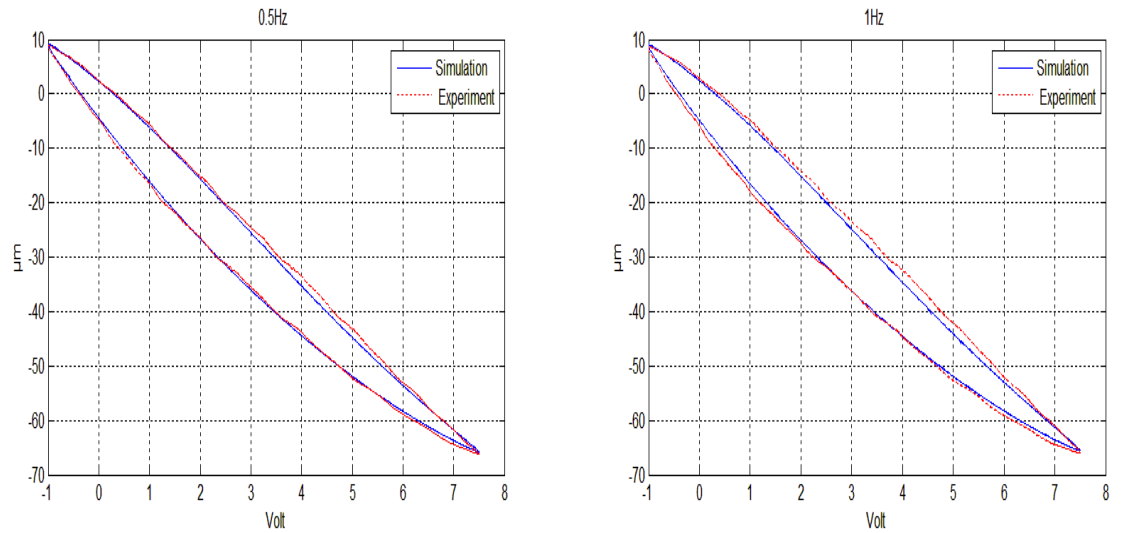


Figure 47: Hysteresis by Simulation & Experiment with Sine Input (Cont.)

The aim here is to verify the theory using only piezo actuator up to 1 Hz. In these tests, sine and triangle input signals are used to drive the piezo actuator in order to see difference of the driving frequency. The first input signal used for the test and the simulation is the sine at four different frequency signals, which are 0.05 Hz, 0.1 Hz, 0.5 Hz and 1 Hz. As seen from the Figure 47, the blue line describes the simulation and the red line describes the experimental results. After some optimization iteration with simplex method followed by trust-region reflective nonlinear least squares method, the parameters are found for desired accuracy.

The difference between the simulation and the experiment for 0.05 Hz is shown in Figure 48. This blue line is changed by the input signal that is volt, and it is clearly seen that, around in the middle of the input signal magnitude, the difference is going to maximum as 1.25 μm . When the full stroke is considered as 80 μm , the percentage difference is 1.6% as it is within our design criteria. The simulation result shows that, in the middle of graph, the difference between simulation and experiment has increased due to model Bouc-Wen model compensator.

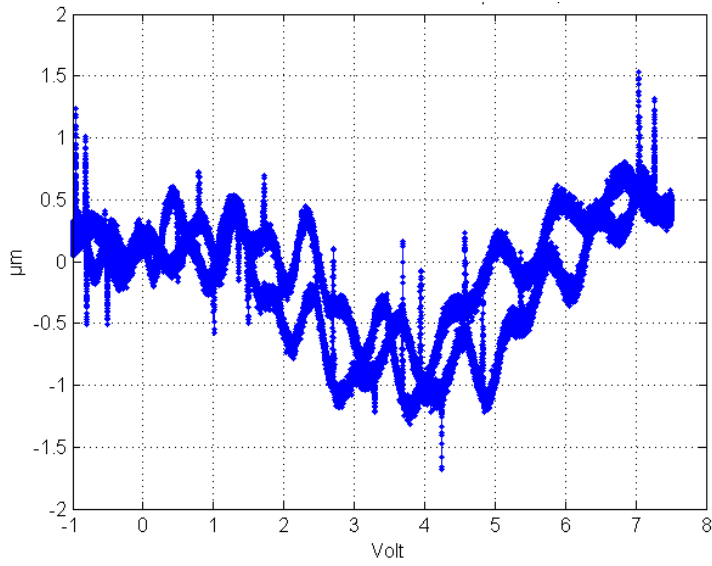


Figure 48: The 0.05 Hz Sine Signal Simulation and Experiment Difference

The difference between simulation and experiment for 0.1 Hz is shown in Figure 49. The maximum difference is 1.38 μm . When the full stroke is considered, 80 μm , the percentage difference is 1.7% and it is within the design criteria.

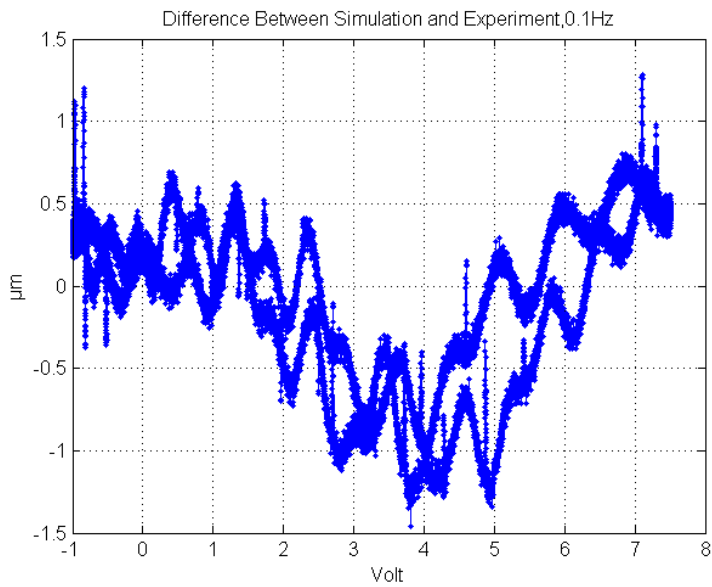


Figure 49: The 0.1 Hz Sine Signal Simulation and Experiment Difference

The difference between simulation and experiment for 0.5 Hz is shown in Figure 50. The maximum difference is 1.83 μm . When the full stroke is considered, 80 μm , the percentage difference is 2.3% and it is within the design criteria.

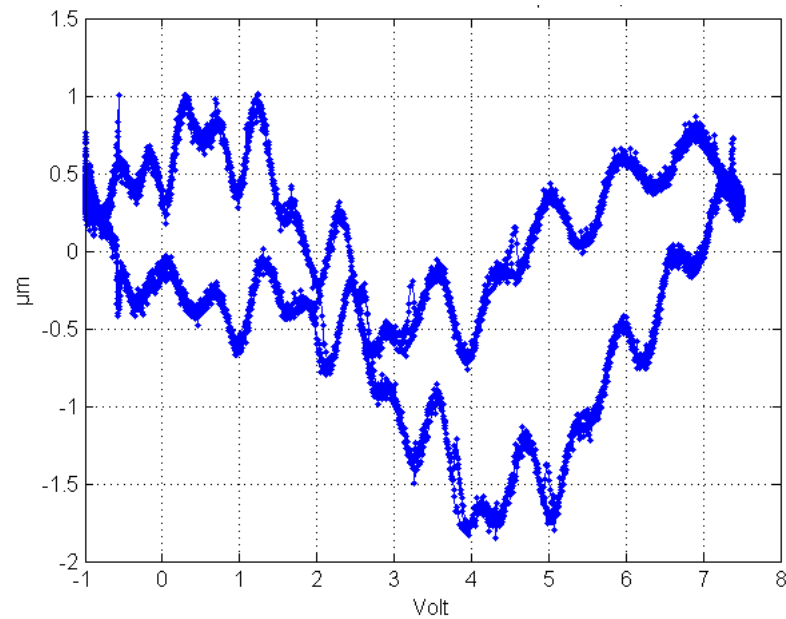


Figure 50: The 0.5 Hz Sine Signal Simulation and Experiment Difference

The difference between simulation and experiment for 0.5 Hz is shown in Figure 51. The maximum difference is found as 2.02 μm . When the full stroke is considered, 80 μm , the percentage difference is 2% and it is within the design criteria.

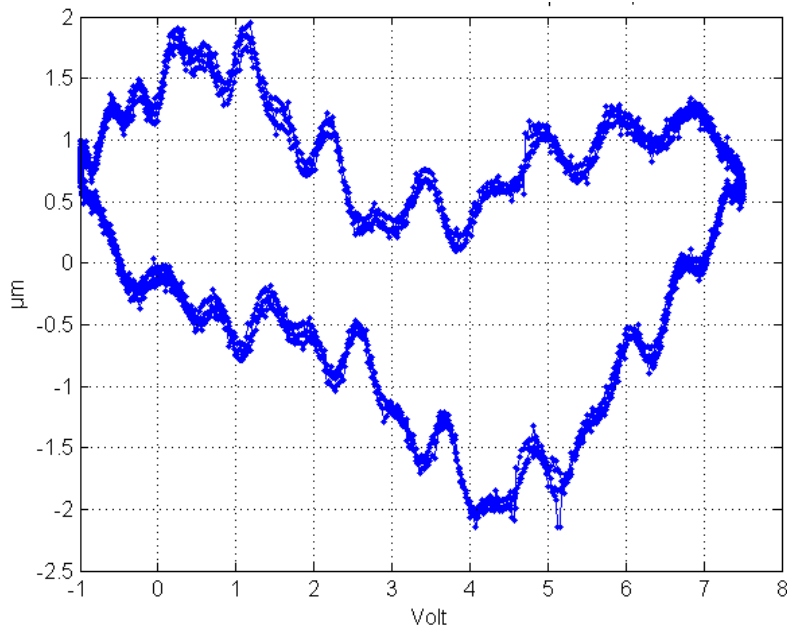


Figure 51: The 1 Hz Sine Signal Simulation and Experiment Difference

The input signal is then increased in frequency and it is observed that the hysteresis difference is also increased. Moreover, with increased frequency, it is seen that the simulation results are getting worse and the percentage difference is increased. The reason for it is that the higher frequency is adding the output more hysteresis and causing more nonlinearity error to the system. The nonlinear system is solved with MATLAB Simulink® Parameter Optimization iteratively with the increasing sensitivity and the parameters are converged to the optimum ones.

The second test is performed by a triangle input signal. Test results are illustrated in Figure 52. When these results are compared with the sine input one, the percentage difference values are better than that of the sine input. This is due to better parameter estimation in triangle input than sine input by MATLAB Simulink® Parameter Optimization.

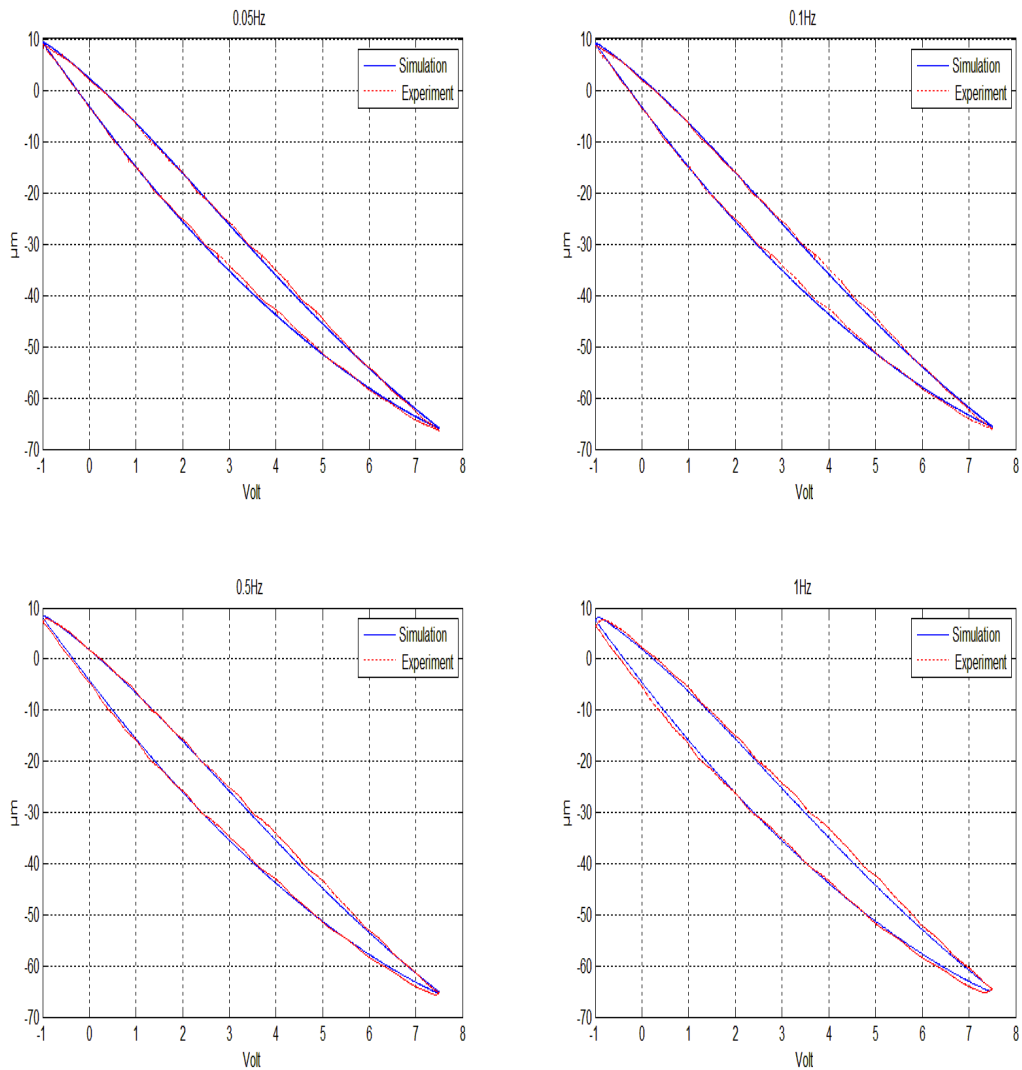


Figure 52: Hysteresis by Simulation & Experiment with Triangle Input

The difference between simulation and experiment for 0.05 Hz is shown in Figure 53. This blue line is changed by the input signal which is volt. It is clearly seen that, at around the middle of the input signal, the difference between simulation and experiment is negative and found as 0.63 μm . When the full stroke is considered, 80 μm , the percentage difference 0.8% is within the required design criteria.

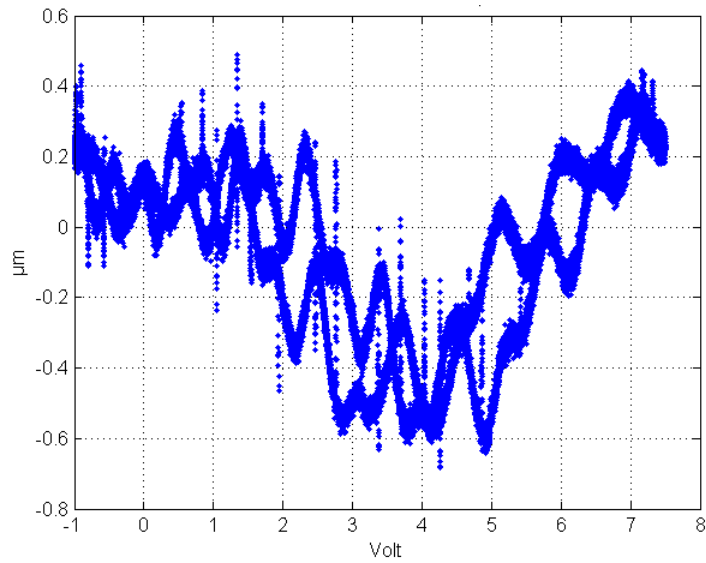


Figure 53: The 0.05 Hz Triangle Signal Simulation and Experiment Difference

The difference between simulation and experiment for 0.1 Hz is shown in Figure 54. The maximum difference is found 0.58 μm . When full stroke is considered, 80 μm , the percentage difference is 0.7% within our design criteria.

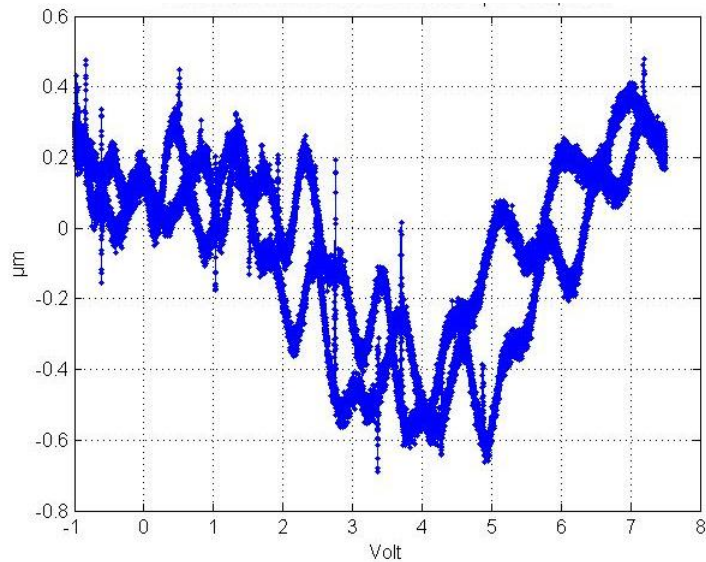


Figure 54: The 0.1 Hz Triangle Signal Simulation and Experiment Difference

The difference between simulation and experiment for 0.5 Hz is shown in Figure 55. The maximum difference for same driven signal is 0.7 μm . When full stroke is considered, 80 μm , the percentage difference 0.9% is within our design criteria.

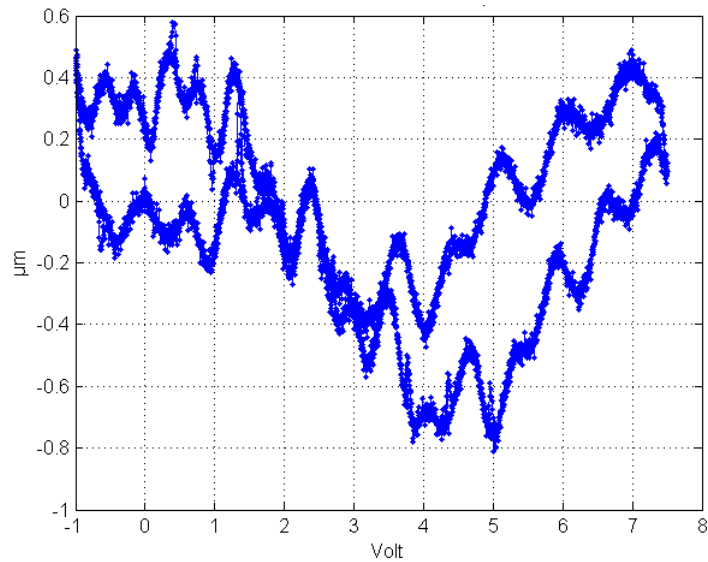


Figure 55: The 0.5 Hz Triangle Signal Simulation and Experiment Difference

The difference between simulation and experiment for 1 Hz is shown in Figure 56. The maximum difference for same driven signal is 0.9 μm . When full stroke is considered, 80 μm , the percentage difference is 1.1% within our design criteria.

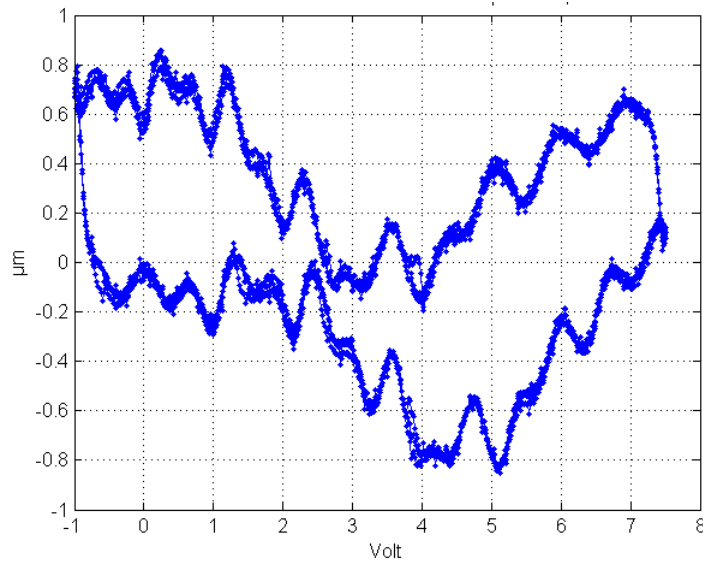


Figure 56: 1 Hz Triangle Signal Simulation and Experiment Difference

There is a difference in the damping characteristics between experimental and simulation model responses. The reason for this difference is the fact that these parameters are iteratively modelled and does not represent the exact values of the system parameters. When the input signal is compared to simulation error, the triangle and sine signals have similar accuracies.

4.3. Position Test with Flapper Mechanism

To check the consistency between the test and the simulation results and validate the mathematical model, open loop performance tests are also performed [40].

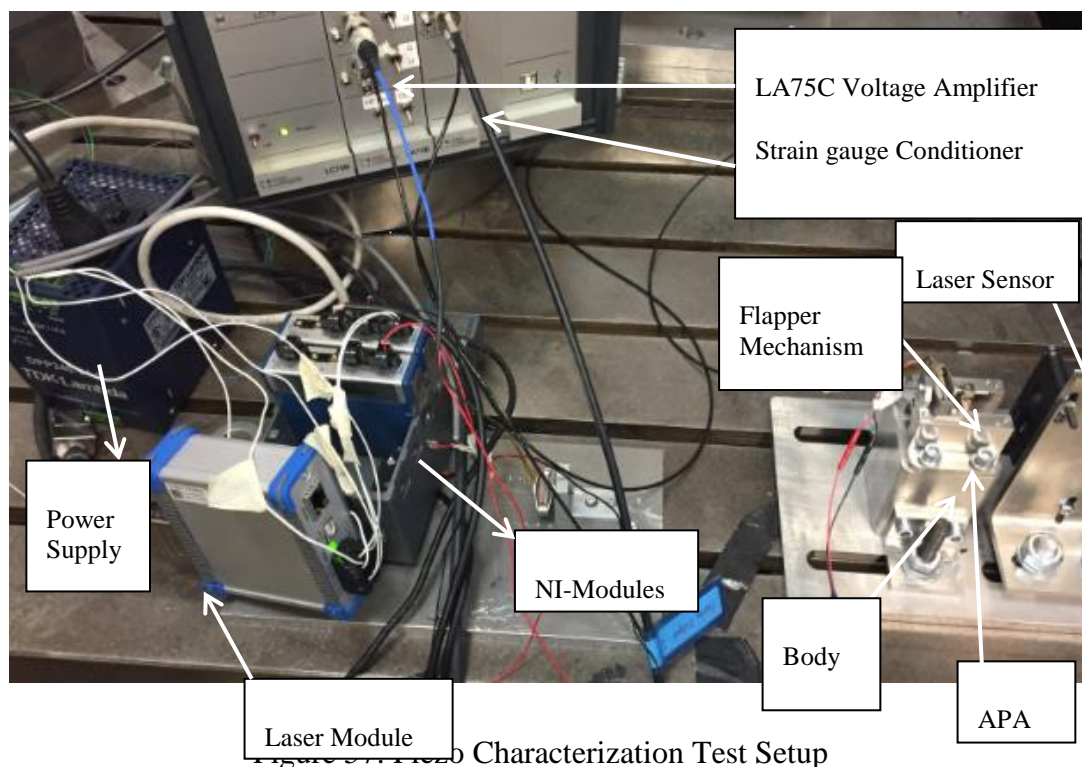
In this test configuration, the input signal is the position command signal to the piezo actuator. The output signals are the signals that are measured by the strain gauge which is applied on piezo and by the laser displacement sensor which is applied on the flapper.

As a test signal, a sine wave voltage is applied to the piezo actuator driver. The different magnitudes of sine wave are applied at the frequencies of 0.1 Hz to 10 Hz.

In these frequency values, the signals do not exceed the maximum allowable stroke of the piezo actuator.

The test duration is taken as 5 cycle for input signal. The first and the last data is not used in the graphical representation and the averaging is used with 5 cycle data.

The main test setup is shown in Figure 57. The test equipment is composed of the laser displacement sensor heads and controllers, the strain gauge conditioning units, the piezoelectric voltage amplifiers, the data acquisition (DAQ) card and the input/output connection blocks with National Instruments (NI) modules and the host computer. In voltage amplifiers, the amplifier gain is given as “20” and that output voltage is amplified by 20 times. The self-hysteresis is also given in its catalog [13].



The assembled test setup is shown in Figure 58. The washers are used in whole assembly and the mounting torque is chosen according to the manufacturer

recommendation. First, the flapper mechanism which is configurable to the test setup is bolted M2.5 nut. Then this structure is assembled with the Piezo actuator made with nut using a preload. Piezo with flapper mechanism is mounted to the piezo mounting part via M2.5 screw. Then the whole structure is placed to the body part and is fixed by M3 screw. The construction is placed to the ground key to the laser displacement sensor.

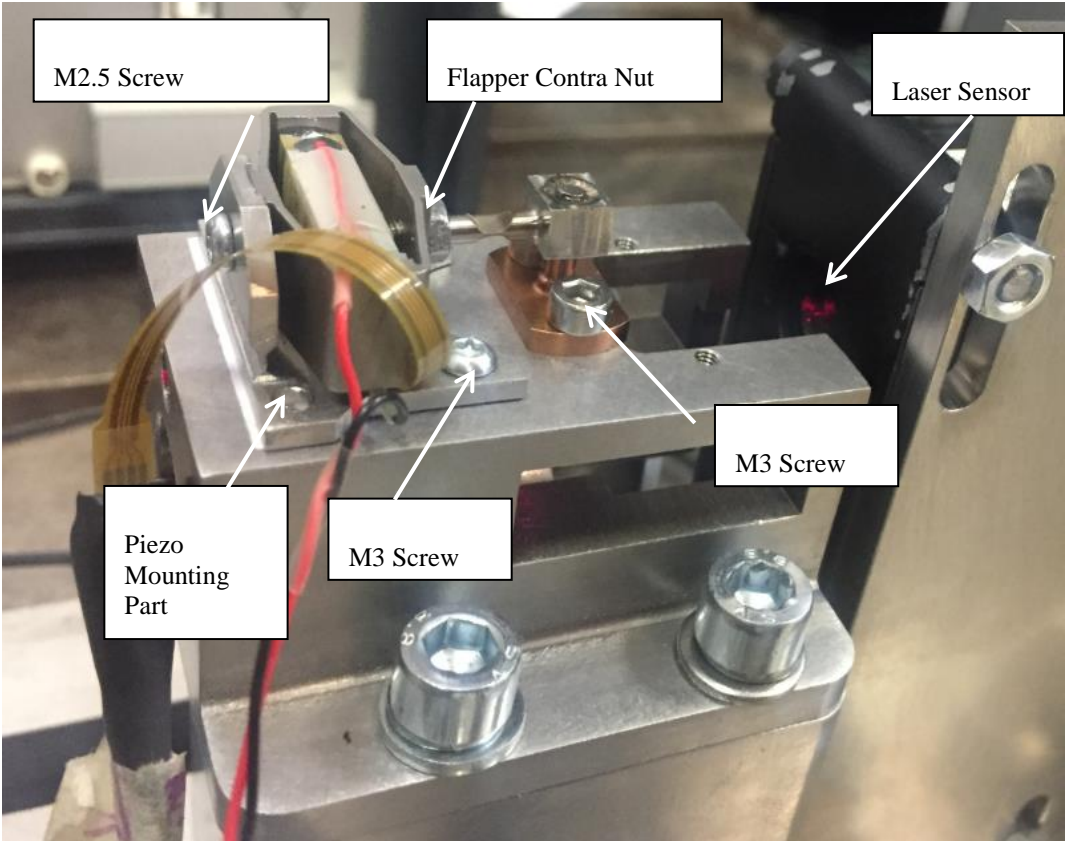


Figure 58: Assembling Structure

Then, the open loop system tests for the flapper itself and actuator are performed. According to the controller designed in Section 3.7, the closed loop performance tests are carried out. The experimental test software and the user interface are then designed to conduct tests and the data acquisition and the real-time control applications, National Instruments LabVIEW® software is used.

At the first test, the ramp voltage is applied and the position of the flapper is measured. The ramp signal is started from 2.5V and moved down to 0V in 10 seconds and then moves up 2.5V in 10 seconds, again. Input signal used is shown in Figure 59,

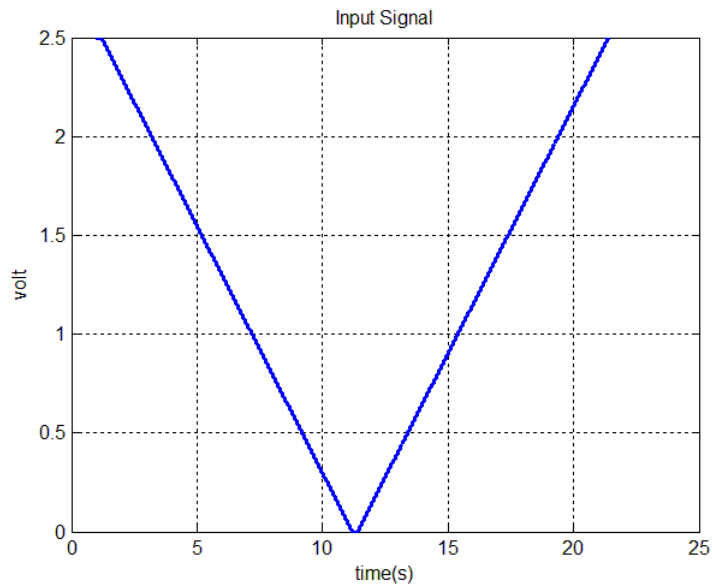


Figure 59: The Input Signal

The Input signal (V) is applied to APA in the open loop (i.e. with no compensator), and with the feedforward Bouc-Wen compensator. The displacement (μm) vs. voltage (volt) results for the open loop and the feedforward Bouc-Wen compensator are illustrated in Figure 60. The hysteresis of the displacement is found as 5.26% and 12.6%, respectively. The feedforward Bouc-Wen compensator decreases the error in hysteresis compared to the open loop system with APA.

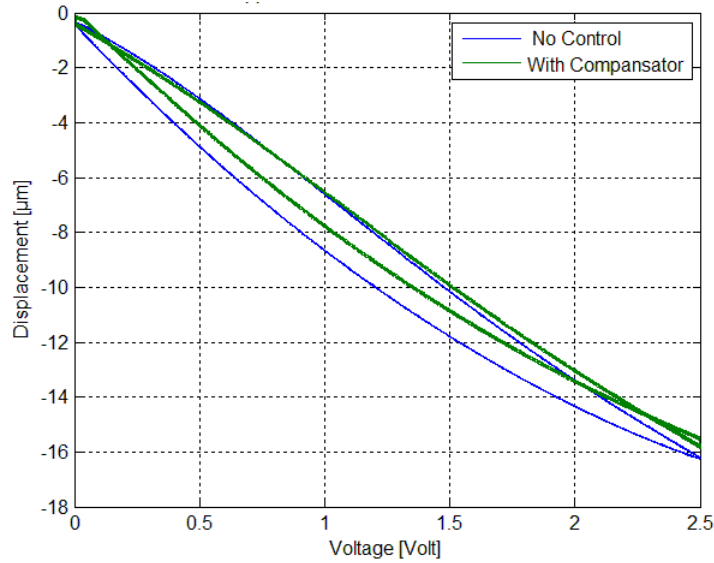


Figure 60: Displacement of Flapper

To control the displacement of the flapper, the PI controller in LabVIEW[®] is used. The controller parameters are set according to Section 3.6. For this experiment, LabVIEW[®] based model is also used which is shown in APPENDIX C. The PI parameters without filter are set to K_p as '0.05' and K_i as '250' $\mu\text{m}/\text{V}$.

During initial performance tests, it is realized that modeling the piezo actuator with a linearized first order transfer function is not sufficient to represent the actual speed response characteristics since the loading force directly affects the displacement output at the peak load value. Also, the dynamics of the piezo driver has an influence on the response of the actuator. Therefore, the controller gain could be optimized to obtain better results. For this purpose, an overall transfer model of the system is linearized with MATLAB Linearization Tools and two poles of the transfer function are calculated in Chapter 3.7. With the transfer function, the controller gains are also optimized experimentally. With test prototype, the flapper is observed to move according to the reference signal shown in Figure 61.

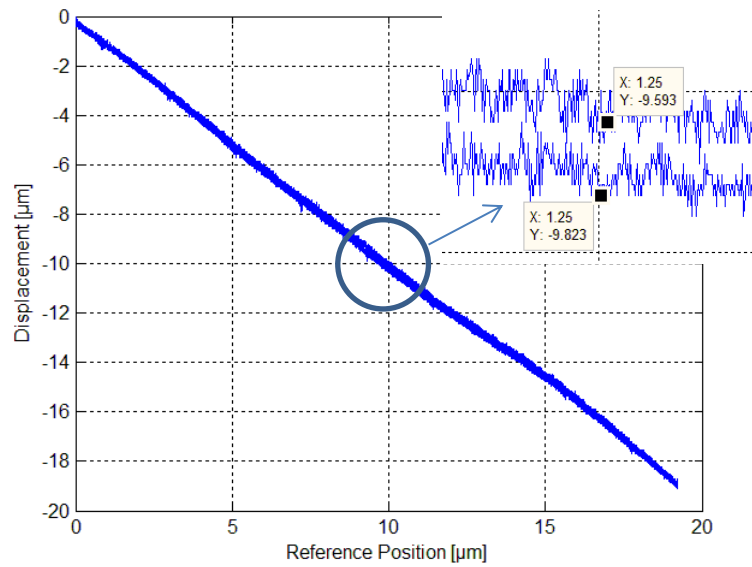


Figure 61: Displacement of Flapper with PI Controller

According to Figure 61, the hysteresis is calculated as:

$$\frac{(9.823 - 9.593)\mu\text{m}}{19\mu\text{m}} 100 = 1.2\%$$

This difference is within the limits of the design requirements. Both simulation model output and experimental result are shown in Figure 62.

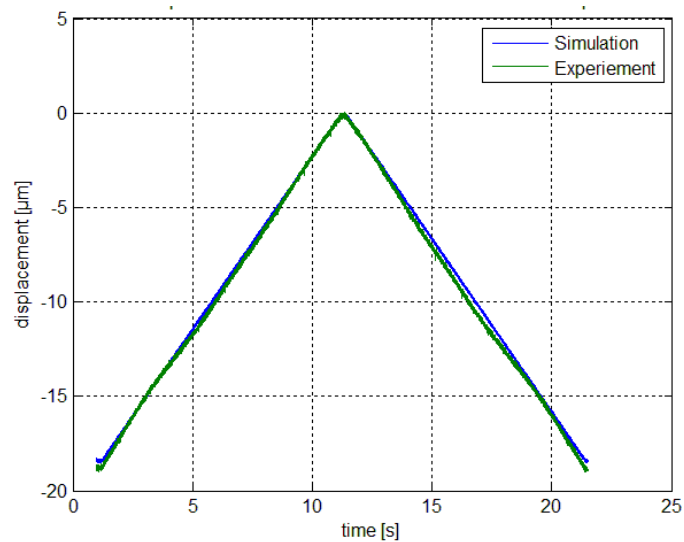


Figure 62: Displacement of the tip of the Flapper with PI Controller

After the position test completed, the hysteresis tests with different frequencies are performed according to design requirements and shown in Table 16. The reference voltage is calculated regarding the formula that the necessary flapper position is given as an input. To find the reference voltage in open loop, 7.5 μm stroke of the flapper is used to prevent a possible damage in the mechanism. As calculated in Section 3.3.3, $K_{flapper}$ has already found by FEA and K_{piezo} is taken from the catalog of the actuator.

$$x_{flapper\,desired} = \frac{(x_{piezo}) \cdot K_{piezo} \frac{V_{ref}}{150}}{K_{flapper} + K_{piezo}} \quad (3.12)$$

$$15\mu m = \frac{80\mu m \cdot 1.264N/\mu m \cdot V_{ref}/170V}{(1.264 + 0.57)N/\mu m} =$$

$$V_{ref} \approx 45V$$

In order to get 15 μm displacement at the flapper, the close loop (CL) control with compensator is also used. The reference displacement is sent to the compensator block and then the model output is send to the controller. To make the flapper pull and push effectively, the assembly operation requires a calibration. Therefore, the piezo actuator is mounted with test setup under applying a 1V. Then, the laser sensor is calibrated according to the flapper to detect displacement at varying frequencies of sinusoidal signal. Various different frequency tests are performed for 5 cycles to use averaging method. The averaging method is applied in order to minimize the spikes and the noise content. After the calibration of the laser, the hysteresis characteristic is tested with the increasing frequency. These close loop (CL) tests are also performed for 5 cycles of sine signal and shown in Table 16.

Table 16: Close Loop Test Scenarios

Test Number	Reference Signal	Type of Controller	Type of Test
1.	0 – 15 μm	PI	0.05 Hz x5 cyc
2.	0 – 15 μm	PI+Compensator	0.05 Hz x5 cyc
3.	0 – 15 μm	PI	1 Hz x5 cyc
4.	0 – 15 μm	PI+Compensator	1 Hz x5 cyc
5.	0 – 15 μm	PI	10 Hz x 5 cyc
6.	0 – 15 μm	PI+Compensator	10 Hz x 5 cyc

The CL test and CL with hysteresis compensator are performed according to different frequency input signal. The reference sine signal is send to system and the response is shown in Figure 63. In this graph, the blue test is performed only with the PI controller and the red test is done with the existence of the hysteresis compensator. The hysteresis error also is found as 1.3% and 1%, respectively. According to the linearity issue, the second test that has a close loop (CL) with compensator provided better results than the first test.

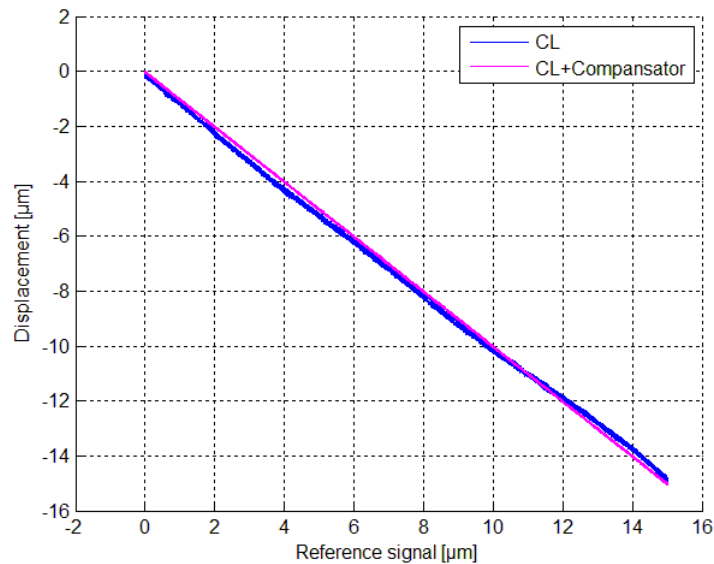


Figure 63: Flapper Test Performed at 0.05 Hz

The second position test is performed at the frequency of 1 Hz and the response is shown in Figure 64 with the hysteresis error of 1.7% and 1.5%, respectively.

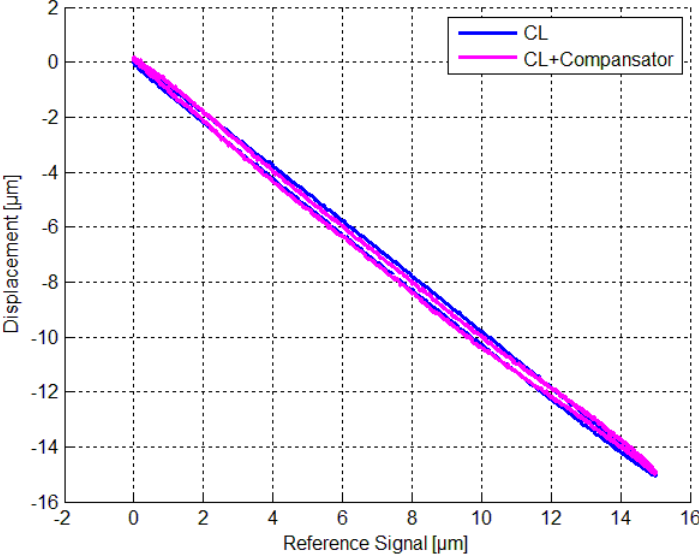


Figure 64: Flapper Test Performed at 1 Hz

The third position test is performed at the frequency of 10 Hz and the response is shown in Figure 65 with the hysteresis error of 7% and 2%, respectively.

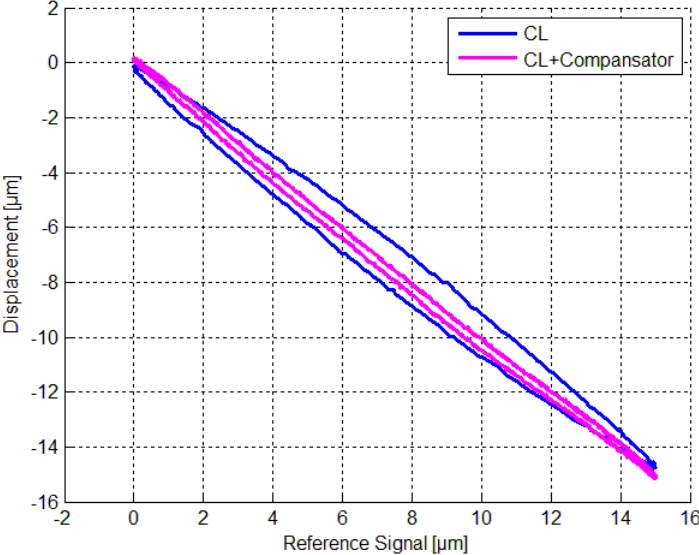


Figure 65: Flapper Test Performed at 10 Hz

It is noticed from the above three figures, the increase in the frequency directly affects the hysteresis error of this system. Up to 1 Hz input signal, PI controller with compensator is a good choice to decrease the hysteresis. Moreover, the charge amplifier is used to perform the dynamic condition which is higher than 10 Hz. These tests are planned according to Table 17. These tests are performed with the charge amplifier and this charge amplifier is designed for 1-100 Hz frequency range and, therefore the test frequencies are selected within the charge amplifier convenient frequency range.

Table 17: Charge Amplifier Test Scenarios

Test Number	Reference Signal	Type of Controller	Type of Test
1. Position	0 – 15 μ m	Charge Amp-Open Loop	1 Hz x5 cyc
2. Position	0 – 15 μ m	Charge Amp-Open Loop	10 Hz x5 cyc
3. Position	0 – 15 μ m	Charge Amp- Open Loop	100 Hz x5 cyc

To begin with the charge amplifier, 1 Hz and 10 Hz reference signals are used to observe the accuracy in the position. The results obtained from the laser sensor for the motion of the flapper are seen in Figure 66 and Figure 67. The hysteresis error is calculated as %3 for 1 Hz and 0.8% for 10 Hz, respectively.

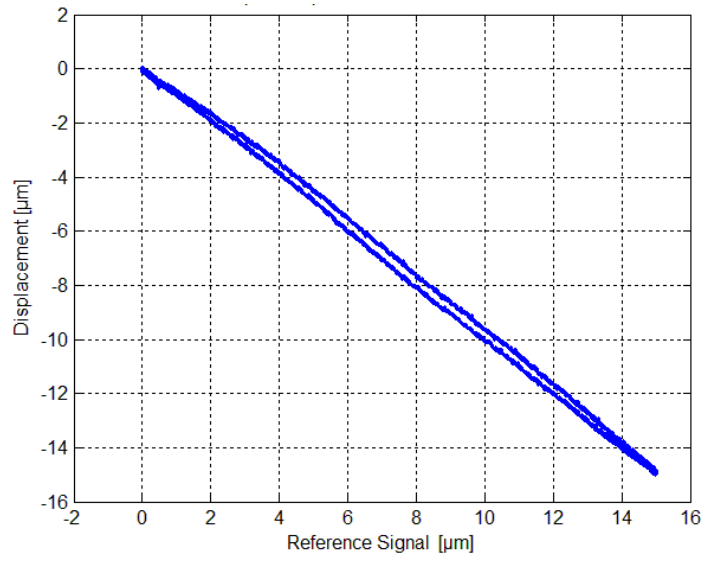


Figure 66: Flapper Test Performed at 1 Hz via Charge Amplifier

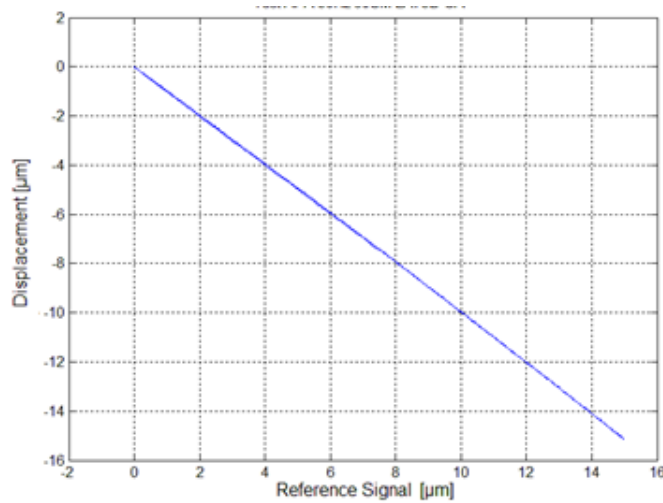


Figure 67: Flapper Test Performed at 10 Hz via Charge Amplifier

The last test, at 100 Hz is performed with the charge amplifier. Laser result of flapper displacement is seen in Figure 68. The hysteresis error is calculated 1.8%.

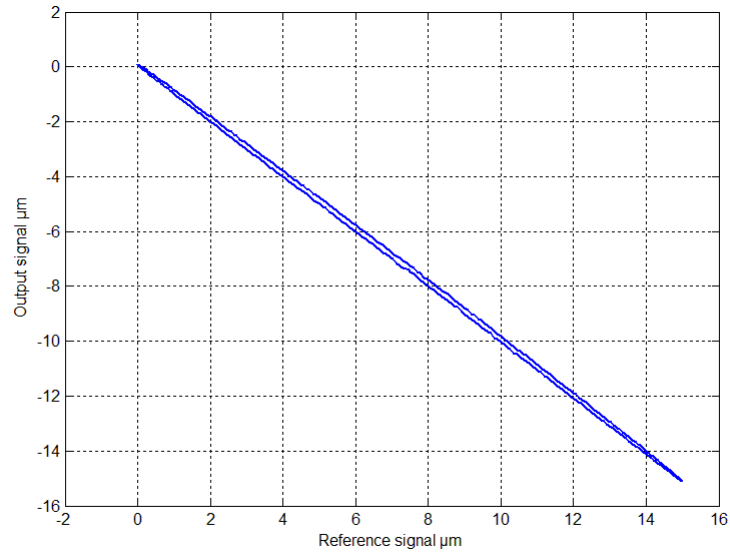


Figure 68: Flapper Test Performed at 100 Hz via Charge Amplifier

4.4. Step and Chirp Tests

In this sub-section, the tests performed on the piezo prototype are explained in details. At first, the open loop system tests for actuator itself and the actuator with an inertial and feedforward model are performed. Then, according to the controller designed in Section 3.7, the closed loop performance tests are carried out.

To conduct these tests and to perform data acquisition and to simulate real-time control applications, National Instruments LabVIEW® software is utilized. Basic test software and a user interface are built for this purpose and the test scenarios are embedded into this particular software.

Step speed commands are given to the actuator and position measurements are obtained from the laser sensor. The investigated parameters are specified within the range provided in Section 3.3.6 and estimated parameters are then investigated iteratively with a cost function and after some iterations, the estimation process is ended. In Figure 69, a comparison between the measurement data and the

reference signal is shown. The data is presented after cleaning the high frequency ripple and noise.

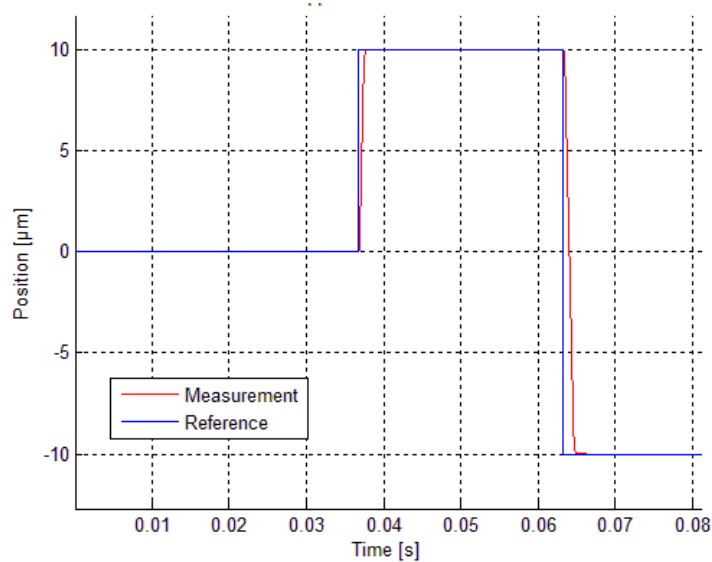


Figure 69: Step Response of the Prototype with $K_p=250$ V/ μm

It is also calculated from the above figure through the MATLAB step response, the rise time is calculated as 1.15 ms.

To observe the frequency response characteristics of the flapper mechanism with APA, the chirp signal from 0.1 Hz to 100 Hz which is limited by amplifier within 100 seconds is applied and shown in Figure 70. It can be seen from the Bode diagram at 100 Hz that the magnitude is still higher than -3 dB. As expected, the phase shifts of the model which is shown in APPENDIX D and the experiments are similar.

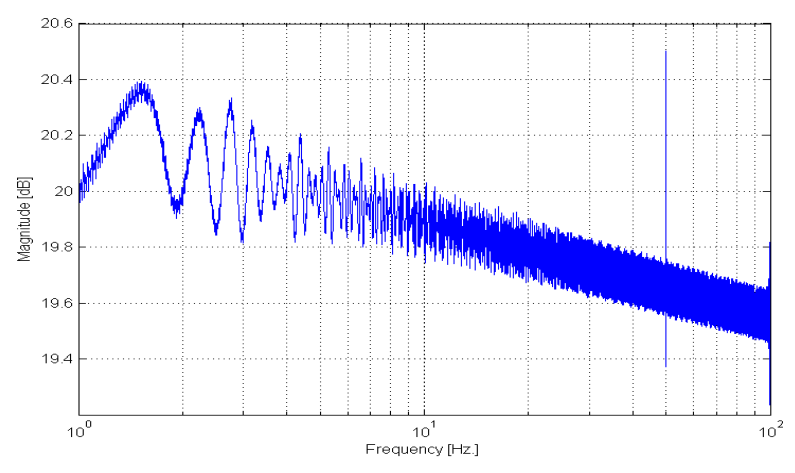
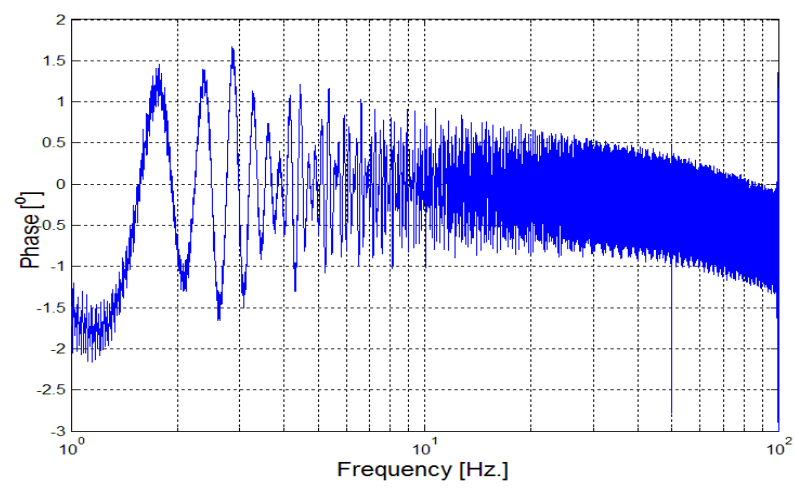
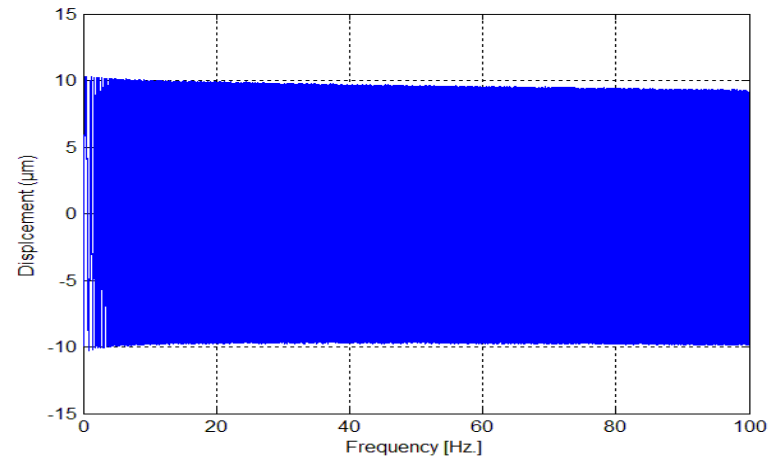


Figure 70: Magnitude and Phase Response of the Flapper with APA

4.5. Conclusion

First of all, only the actuator test is performed in order to verify the mathematical model of the actuator. Then, the feed forward control method which is Bouc-Wen model compensator is used to minimize the hysteresis error of the system. Although this method improves the hysteresis, it is not sufficient to get results such as lower than 3% of hysteresis error. Then, PI controller is used with the voltage amplifier. These controller parameters are optimized with the mathematical model and then an improvement is achieved and it is observed from the experimental results. The results obtained from the piezo demonstrated that, there is no unexpected behavior up to 100 Hz and as the frequency range of interest for this prototype is 100 Hz, it can be concluded that the piezo prototype can be used for the overall system simulation.

CHAPTER 5

SUMMARY AND CONCLUSIONS

5.1 Summary and Discussions

This thesis addresses the modeling, design, and the manufacturing of a Piezo Actuator with the Flapper Mechanism. The design considerations and the operational criteria constitute performance specifications of an on the shelf valve torque motor controlled actuation system.

The mechanical sub-systems suitable to work with piezo actuator are designed considering the performance criteria. Position sensor requirements, sensor placements, electrical circuit of control and data acquisition systems, and electronic components such as amplifiers are selected accordingly.

In order to find out the behavior of the overall system, a mathematical model of the piezo actuator is developed. A flapper mechanism is then added to the model as a sub-system. The overall non-linear model is developed in MATLAB Simulink® Library for further numerical analyses. A prototype system is then designed and manufactured to verify the system mathematical model through the experiments. Before the whole system is assembled, a preliminary test of the actuator is performed in order to eliminate any possible problems solely caused by the actuator. Then, an actuator characterization test is conducted to estimate the physical parameters of the actuator model. The actuator is then tested for its position-voltage characteristics. After assembling the whole mechanism, a series of system position tests are performed to estimate the unknown hysteresis

parameters. Simulation results for the overall system are obtained by MATLAB Simulink® and validated by executing open loop tests with a compensator and close loop tests on the set-up. A proportional controller is used in the controller design of the system employing the feedback information supplied by strain gauge connected to the piezo.

Since a variety of operation requirements are probable, a set of performance tests are performed at various driving frequencies. The APA is then tested alone in order to observe both its time domain and frequency domain characteristics.

In all tests, the magnitude and the frequency of the test signals are selected such that the amplifier will not be saturated and the flapper mechanism will not be damaged. LabVIEW® software is used for the data acquisition and control application purposes in the experiments. A test software is then built to simulate the whole tests in this environment through a software supported by National Instrument's Compact RIO platform.

To sum up, a system is built up with some easy to access components and it is observed to have a remarkably good bandwidth (1500 Hz) and a fairly high positioning accuracy (1 μm) in this particular thesis work.

5.2 General Conclusions

In this study, the APA is modeled and then verified through various tests. Using APA is a very convenient way to replace conventional torque controlled motor in valve technologies as it has a fast response and a high precision. Most of the actuator systems include expensive and complex mechanisms requiring extensive calibration prior to use. Though the replacement of such complex mechanisms with a fairly simple piezo actuator mechanism, both manufacturing and assembling costs can be significantly reduced. Therefore, an actuation system is designed and modelled and the test prototype is produced to verify the system. After the performance of the actuator is examined, in order to minimize the

hysteresis for the driving frequencies between 0.1 Hz and 10 Hz, Bouc-Wen compensator and Proportional-Integral (PI) controller are used. This actuating system is finally observed to be controlled by using different control methods with 1% to 3% displacement hysteresis error.

With this thesis study, it is revealed that the actuation system can be packed as a compact design and as a conclusion, it shows that a designed and an experimentally verified actuation system with a flapper mechanism employing a piezo actuator can be used effectively as a torque motor of servovalves.

5.3 Recommendations for Future Work

Following suggestions may be offered for further improvements of this work:

- The linearity of the flapper mechanism could be affected by the welding process and therefore an alternative solution should be searched instead of the welding.
- In this thesis work, there are two kinds of amplifiers. APA is used with charge amplifier for higher than 10 Hz and is also used with voltage amplifier for lower than 10 Hz. In the experiments, the amplifier is selected manually according to input frequency. Consequently, a superior amplifier which changes voltage and charge mods automatically with respect to the driving signal frequency can be designed and used.
- Since all performance criteria are satisfied by using a basic proportional integral position controller, there is no need to use more complex control algorithms in the tests. However, for further studies aiming better accuracy, different control strategies can be developed and applied such as “H-Infinity”, Adaptive Control” and “Fuzzy Logic Control”.
- Different types of high performance piezo materials such as PMN-PT Piezoelectric Single Crystals can be used.

REFERENCES

- [1] Piezoelectric Technology: A Primer, Designlines Automotive, 2000
- [2] Curie, Jacques; Curie, Pierre (1880). [Development, via compression, of electric polarization in hemihedral crystals with inclined faces]. 90–93.)
- [3] J. Curie, Jacques; Curie, Pierre (1881). [Contractions and expansions produced by voltages in hemihedral crystals with inclined faces]. 93: 1137–1140.)
- [4] Piezo Systems Inc. (2013) History of Piezoelectricity. [Online]. Available from: <http://www.piezo.com/tech4history.html> [Accessed 1st December 2013].
- [5] Haertling, G. H., 1999. Ferroelectric ceramics: His-tory and technology, Journal of the American Ceramic Society, 82, 797)
- [6] Tressler, J. F., ALKOY, S., NEWHAM, R. E., 1995. Piezoelectric sensors and sensor materials, Journal of Electroceramics 2,4, 277-272.
- [7] Jordan, T.L., Ounaies, Z., (2001) Piezoelectric Ceramic Characterization, ICASE Report No. 2001-28.].
- [8] Jordan, T.L., Ounaies, Z., (2001) Piezoelectric Ceramic Characterization, ICASE Report No. 2001-28.].
- [9] CEDRAT TECHNOLOGIES Actuator Solutions. [Online] Available from: <http://www.cedrat-technologies.com/> [Accessed 1st December 2016].
- [10] Piezo Systems Inc. (2013) Introduction to Piezo Transducers. [Online]. Available from: <http://piezo.com/tech2intropiezotrans.html> [Accessed 1st December 2013].

- [11] Sensor Technology Ltd. (2009) Product Overview. Ontario, Canada.]
- [12] Physik Instrumente (PI) GmbH & Co.KG (2013) Piezo Tutorial. [Online]. Available from: http://www.physikinstrumente.com/tutorial/4_28.html[Accessed 1st December 2013].
- [13] La75 - Linear Amplifier for Piezoelectric Actuators - Ca45 Compact Standalone Amplifier Product and Warranty Information, CEDRAT TECHNOLOGIES (4.11.2013)
- [14] Physik Instrumente (PI) GmbH & Co.KG (2013) Piezo Actuator Catalog Site, Piezo Tube Actuators. [Online] Available from: http://www.physikinstrumente.com/tutorial/4_28.html [Accessed 1st December 2013].
- [15] Caner Gençoğlu “Active Vibration Control of Beams and Cylindrical Structures Using Piezoelectric Patches” Ms. Thesis, pp. 18, Middle East Technical University, January 2014
- [16] 3 Hydraulic Servo Systems, Their Control and Modelling, Electronic journal of Vocational Colleges, May 2013.
- [17] Professor Andrew Plummer, Electrohydraulic servovalves – past, present, and future. In: 10th International Fluid Power Conference, IFK2016, 2016-03-08 - 2016-03-10
- [18] R. H. Maskrey W. J. Thayer, ‘A Brief History of Electrohydraulic Servomechanism’ ASME Journal of Dynamic Systems Measurement and Control, June 1978

[19] Servovalve, Hydraulic-Description, Design aerospace LCC. [Online] Available from:

<http://www.daerospace.com/HydraulicSystems/ServovalveDesc.php> [Accessed 1st December 2017].

[20] Bell Aerospace file a patent for a similar design the same year /10 Wolpin, M.P., Smith B., Kistler, W.P. (Bell Aerospace Corp) Flapper valves. Patent US2934765. Filed May 1955, granted Oct 1965.

[21] Johnson, B. A., Hydraulic Servo Control Valves Part 3, WADC Technical Report 55-29, Wright-Patterson Air Force Base, Ohio, 1957

[22] Mehmet Can Karabulut, Design of Hydraulic Valveless Control Actuation System, 2016

[23] CEDRAT Trainee/APA Dynamic Properties Piezo training lecture notes 25.09.2015

[24] MATLAB Simulink Design Optimization, Parameter Estimation Toolbox., www.mathworks.com/help/slido/parameter-estimation.html, last visited on April 2016.

[25] Mcgraw Hill Shigley's Mechanical Engineering Design, 10th Edition

[26] Steel Properties from TS EN 10025-1

[27] https://www.copper.org/resources/properties/144_8/ last visited on December 2017.

[28] <https://www.bossard.com/en/product-solutions/catalog-products.aspx>, Bossard Fastener Catalog, Socket products last visited on December 2017.

[29] CEDRAT TECHNOLOGIES, UC45 controller for digital control of actuators Product and Warranty Information, 25/09/2012

- [30] OptoNCDT-2300 Sensor Data Sheet, <http://www.micro-epsilon.com/download/manuals/man--optoNCDT-2300--en.pdf>, last visited on April 2016.
- [31] National Instruments. The Compact RIO Platform http://www.ni.com/pdf/manuals/376330a_02.pdf, last visited on December 2017.
- [32] R. Bouc, "Forced vibration of mechanical systems with hysteresis", Conference on Nonlinear Oscillation, Prague, 1967.
- [33] Y. K. Wen, "Method for random vibration of hysteresis systems", Journal of the Engineering Mechanics Division, Vol. 102(2), pp.249-263, March/April 1976
- [34] Micky Rakotondra, Bouc-Wen modeling and inverse multiplicative structure to compensate hysteresis nonlinearity in piezoelectric actuators, IEEE Transactions On Automation, Science And Engineering, March 2010.
- [35] Carol Livermore Massachusetts Institute of Technology, last visited on December 2017. <https://ocw.mit.edu/courses/electrical-engineering-and-computer-science/6-777j-design-and-fabrication-of-microelectromechanical-devices-spring-2007/lecture-notes/07lecture21.pdf>
- [36] M. Jouaneh and H. Tian, "Accuracy enhancement of a piezoelectric actuators with hysteresis", ASME Japan/USA Symp. Flexible Automation, pp.631-637, 1992.
- [37] D. Hughes and J. T. Wen, "Preisach modeling of piezoceramic and shape memory alloy hysteresis", Smart Materials and Structures, Vol.4, pp.287- 399, 1997.

- [38] D. Croft, G. Shed and S. Devasia, "Creep, hysteresis and vibration compensation for piezo actuators: atomic force microscopy application", ASME Journal of Dynamic Systems, Measurement and Control, 2001.
- [39] W. T. Ang, P. K. Kholsa and C. N. Riviere, "Feedforward controller with inverse rate-dependent model for piezoelectric actuators in trajectory-tracking applications", IEEE/ASME Transactions on Mechatronics (Tmech), Vol.12(2), pp.134-142, April 2007.
- [40] İ. B. Temeltürk, M. Şahin, "Design optimization, control and experimental characterization of flapper mechanism with amplified piezo actuator" 3rd International Conference on Smart Materials & Structures March 20-22, 2017 Orlando, USA Orlando, ISSN: 2169-0022 JME

APPENDICES

APPENDIX A

Different kinds of actuators are compared in Figure A and Table A. As seen from the figure, piezoelectric material has both high frequency and displacement. The comparison table also shows that, it is convenient for low power and fast switching operation conditions. Therefore, this type of actuator can be used in this kind of valve application.

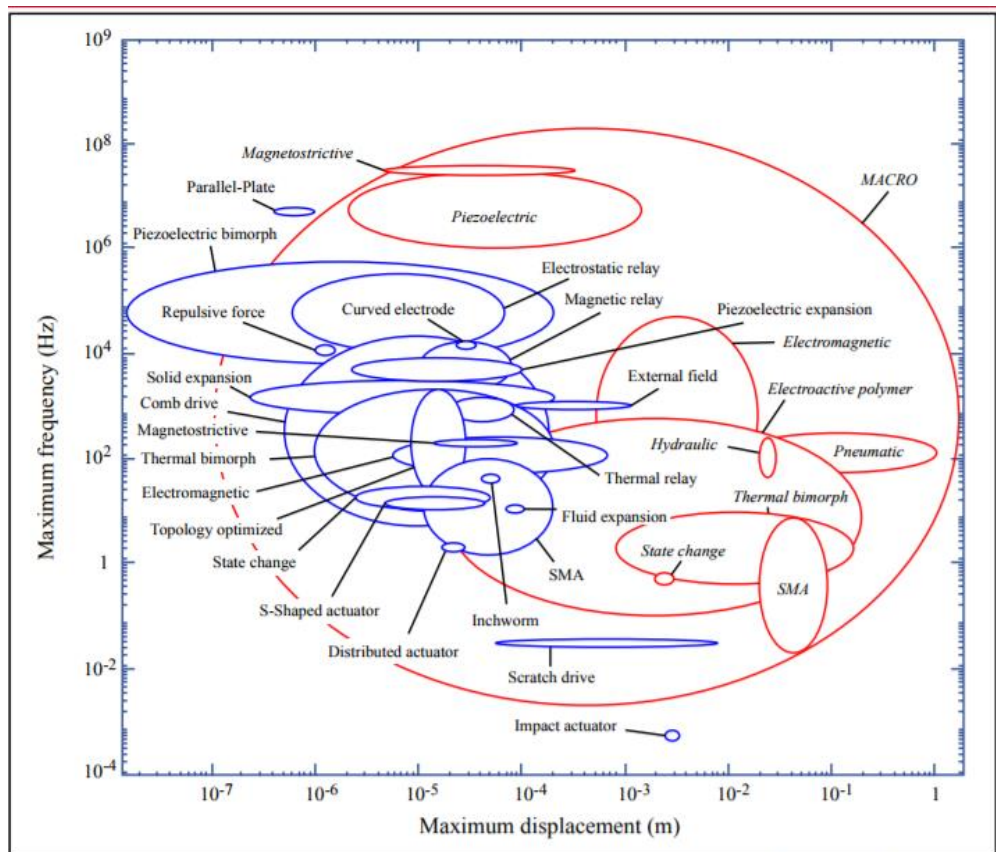


Image by MIT OpenCourseWare.

Figure A: The Schematic Diagram of the System [35]

Advantages of piezo actuators among different types of actuators such as Electrostatic, Thermal and Magnetic are presented in Table A.

Table A: The Schematic Diagram of the Actuators [35]

	Electrostatic	Thermal	Piezo	Magnetic
Low power	✓	✗	✓	✗
Fast switch	✓	~	✓	~
High force	✗	✓	✓	✓
Large travel	✗	✓	~	✓
Simple fab	✓	✓	✗	✗
Low voltage	✗	✓	~	✓
Robustness	~	✓	✓	✓
Sense/actuate	✓	✗	✓	✓

APPENDIX B

Finite Element Modelling

The flapper mechanism is modeled in ABAQUS/CAE® software for static structural analysis. All parts are sketched with the software. The material properties are given in Table B-1 and Table B-2.

Table B-1: Piezo Material Coefficients

	PZT 5H	Unit
Density	7.50E-09	ton/mm ³
d ₃₁	-2.74E-07	mm/V
d ₃₃	5.93E-07	mm/V
d ₁₅	7.41E-07	mm/V
s ^E ₁₁	1.65E-05	mm s ² /ton
s ^E ₃₃	2.07E-05	mm s ² /ton
s ^E ₁₂	-4.78E-06	mm s ² /ton
s ^E ₁₃	-8.45E-06	mm s ² /ton
s ^E ₄₄	4.35E-05	mm s ² /ton
s ^E ₆₆	4.26E-05	mm s ² /ton
e ^T ₁₁ /e ₀	3130	
e ^T ₃₃ /e ₀	3400	
e ₀	8.85E-12	mF/mm

Table B-2: Steel Materials Coefficients

Stainless Steel[26]	
Elastic Modulus [MPa]	210000
Poisson Ratio	0.3
Density [ton/mm ³]	7.80E-09
Yield Strength	355 MPa
Ultimate Tensile Strength	630 MPa
Elongation	20 %
Copper [27]	
Elastic Modulus [MPa]	128000
Poisson Ratio	0.3
Density [ton/mm ³]	8.25E-09
Yield Strength	355 MPa
Ultimate Tensile Strength	630 MPa
Elongation	20 %

The quadratic hexahedral solid elements are used. Boundary conditions, fix surface and monitoring surface shown in Figure B-1 are applied to APA. And also electric field is applied to APA to get displacement. Interaction between mechanical parts such as piezo, spacer and amplified mechanism are set up using “tie” constraints. Tie constraint is connection type which combines two parts. The model is shown in Figure B-1. Blue part is the mechanical amplifier, the red one is the piezo materials and the gray is the spacer.

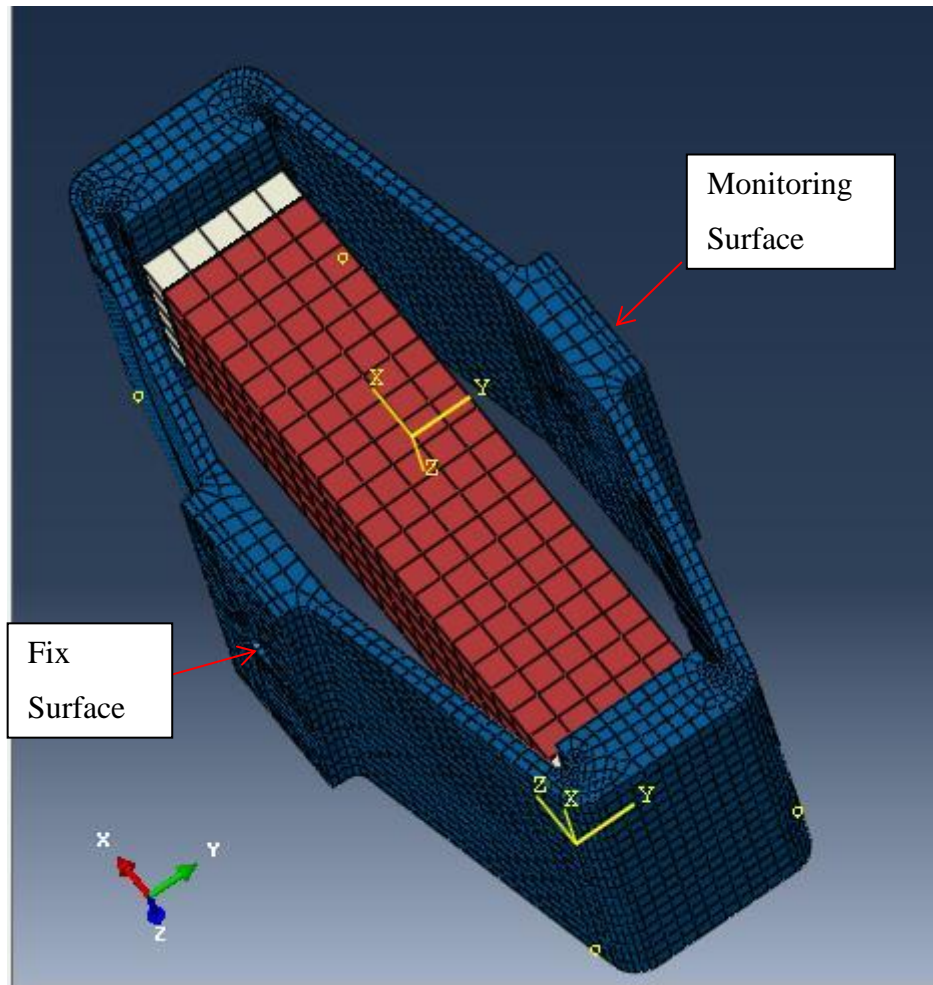


Figure B-1: APA in FEA

Case studies with different mesh densities on the solid models among three kinds of mesh sizes were carried out to show that the results are independent of the mesh assigned. The displacement is obtained from the finite element analysis (FEA) are given in Table B-3.

Table B-3: Mesh Density and the Related Properties

	Coarse Mesh	Fine Mesh	The Finest Mesh
Displacement found from the analyses	0.0805 mm	0.0809 mm	0.08089 mm
Average Element Edge length [mm]	1	0.55	0.1
Number of Elements	921	2959	59289

APPENDIX C

In data acquisition model which is shown in Figure C, are used in four different cases such as: open loop test, inverse Bouc-Wen model test, close loop test, and inverse Bouc-Wen model compensator with close loop test. Output data are collected from the laser sensor and strain gauge sensor. Desired displacement signal and time limitation is designated according to test situation and sent to the simulation model. The inverse Bouc-Wen model calculates the model output with respect to input signal. Whole tests are performed with this model. Moreover, in order to check the controller model, CEDRAT UC45 controller which is based on LabVIEW® is also used. The voltage and the current controller gains are investigated by using the Parameter Estimation Toolbox® of the MATLAB Simulink® Software and are calculated with the Simulink® model parameters. It calibrates the model parameters with respect to the test outputs. The software also puts the estimating parameters into an optimization problem and solves them to find the estimated parameter values.

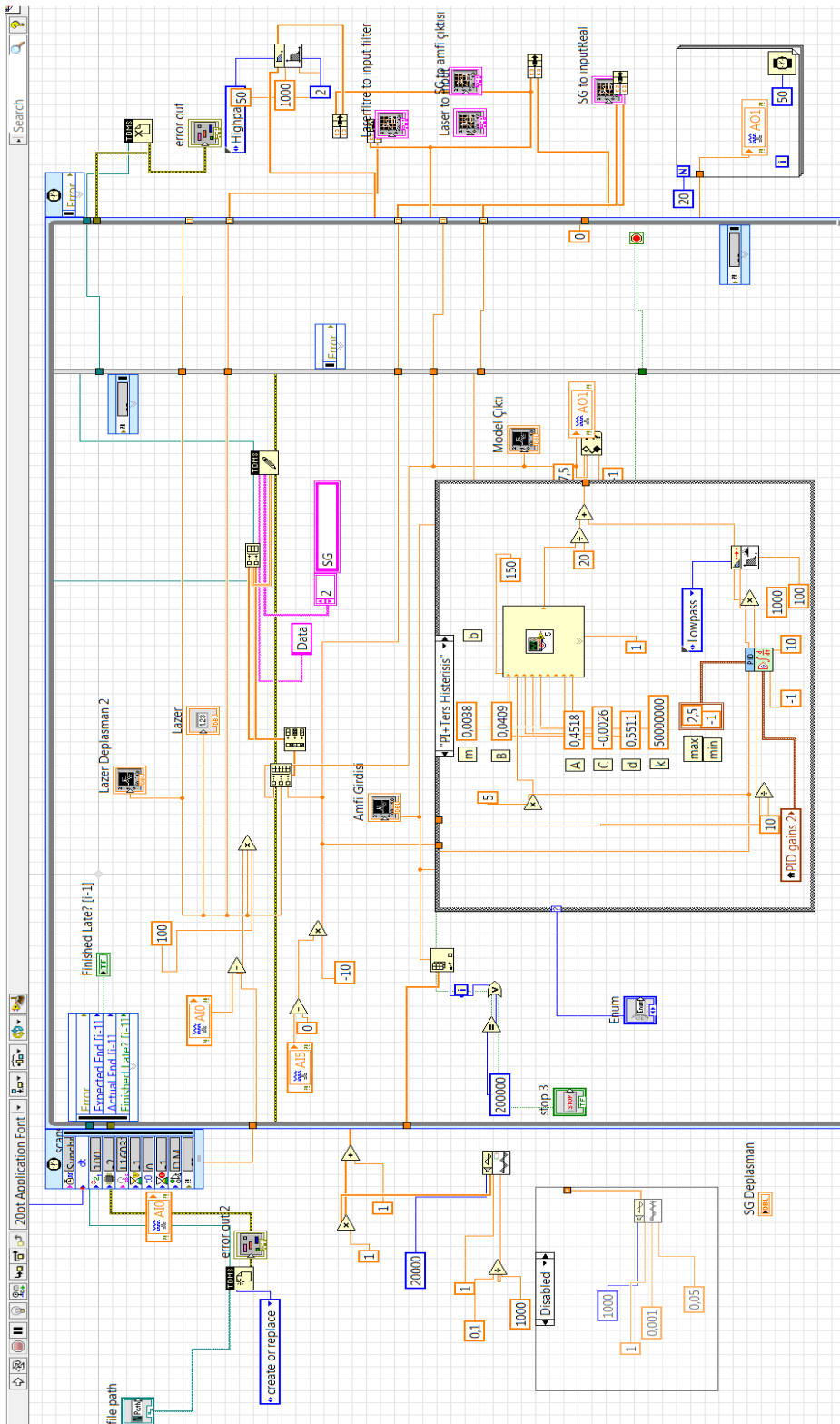


Figure C: LabVIEW® System Full Model

APPENDIX D

In the range of 1-100 Hz chirp, it is needed to get a superior amplifier which has a higher bandwidth frequency. The charge amplifier is limited up to 100 Hz. To observe whole frequency response characteristics, by the help of Simulink model, 20 μm chirp signal from 0.1 Hz to 2000 Hz within 100 seconds is applied and its result is shown in Figure D.

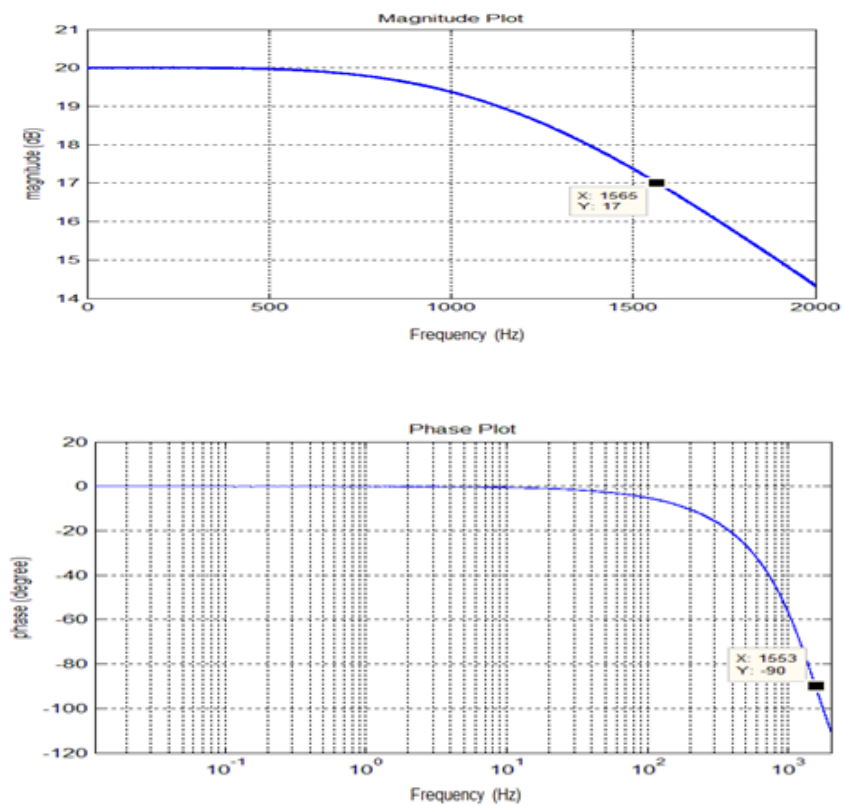


Figure D: Bode Plot of Flapper with APA